3. Energetics: Heat and Temperature

In this chapter we discuss geodynamic processes that may be described with the units of energy or temperature. This general theme is an obvious starting point in geodynamics, as so many properties of rocks that may be observed in the field are a strong function of temperature, for example the formation of metamorphic parageneses or the mechanisms with which rocks deform.

Energy has the unit Joule [J], which is equivalent to mass $\times$ velocity^2 (1 J = 1 kg m^{2}s^{-2}), or volume $\times$ pressure (1 J = 1 m^3 $\times$ Pa = 1 N m, which, because 1 N = 1 kg m s^{-2}, is also 1 kg m^{2}s^{-2}). These conversions give us a first indication that thermal and mechanical energy are often hard to separate. *Thermal* energy may be converted into temperature using heat capacity and density which are parameters that we shall discuss in some detail on the next pages.

The production and redistribution of heat in the lithosphere is done by three fundamentally different processes:

- heat conduction,
- heat advection (or convection) and
- heat production.

The relevance of these three processes for regional metamorphism is summarized at the start of sect. 3.4 in Table 3.4. However, in the first part of this chapter we will present some basic methods how to estimate if and how important each of these three processes may be for the thermal budget of the lithosphere. In this context we also discuss the basics of their mathematical description. The importance of such estimates is enormous: it will enable the reader to critically evaluate in his or her metamorphic study terrain to which degree heat conduction (e. g. because of burial), heat production (e. g. friction heat or radioactivity) or active transport of heat (e. g. by fluid or magma) may have played a role during metamorphism. Thus, the information on the following pages provides a powerful tool for the interpretation of heat sources for field geologists.

3.1 Principles of Heat Conduction

3.1.1 The Heat Conduction Equation

The heat conduction equation - more commonly known as the diffusion equation - is fundamental for the understanding of the transport of heat in the lithosphere. We will also show in other chapters that the very same equation cannot only be applied to the transport of thermal energy, but also to the diffusion of mass. It finds therefore application in many other fields, for example geomorphology, metamorphic petrology or hydrology (s. p. 185; p. 343). Thus, the diffusion equation is the first equation of this book that we will discuss in some detail. The fact that it is a second order partial differential equation should not scare us off. We will show that it is possible to understand it quite intuitively. There is also some explanations on how to read differential equations in section B.1.

Fourier's Law of Heat Conduction. Fourier's 1. law is the basic law underlying the diffusion equation. This law states that the flow of heat q is directly proportional to the temperature gradient (Fourier 1816). This statement can easily be formulated in an equation:

$$q = -k\frac{\mathrm{d}T}{\mathrm{d}z} \quad . \tag{3.1}$$

In this equation q is short for heat flow, T stands for temperature and z for a spatial coordinate, for example depth in the crust. The ratio $\mathrm{d}T/\mathrm{d}z$ is the change of temperature in direction z. We call this ratio the temperature gradient. k is the proportionality constant between the gradient and the flow of heat. In order to understand this law better (and understand the units of k), let us consider a more familiar analogue: the flow of water in a river. The same law applies. In a river the flow of water can be described by the volume of water passing per unit of time and per area of cross section of the river (in SI-units: $\mathrm{m^3\,s^{-1}\,m^{-2}} = \mathrm{m\,s^{-1}}$). This is called the volumetric flow. When normalized only to the width of the river and not to the cross sectional area of the river, the volumetric flow has the units of $\mathrm{m^2\,s^{-1}}$ (sect. 4.5). In contrast, the flow of mass has the units $\mathrm{kg\,s^{-1}\,m^{-2}}$. Fourier's law – applied to our example of water flow – states that the flow of water is proportional to the topographic gradient of the river. This corresponds well to our observations in nature: The steeper a river bed, the faster the flow of water in the river (per square meter of cross sectional area). Fourier's law seems to be a good model description for this observation. This simple example also explains why there is a negative sign in eq. 3.1. The flow is against the gradient: it is *positive* in the *downwards* direction of the gradient.

In the theory of heat conduction, the flow of heat has obviously not the units of volume per time and area, but *energy* per time and area. (in SI units: $\mathrm{J\,s^{-1}\,m^{-2}} = \mathrm{W\,m^{-2}}$). The thermal gradient now replaces the topographic gradient of the river. Because of historical reasons heat flow is sometimes given

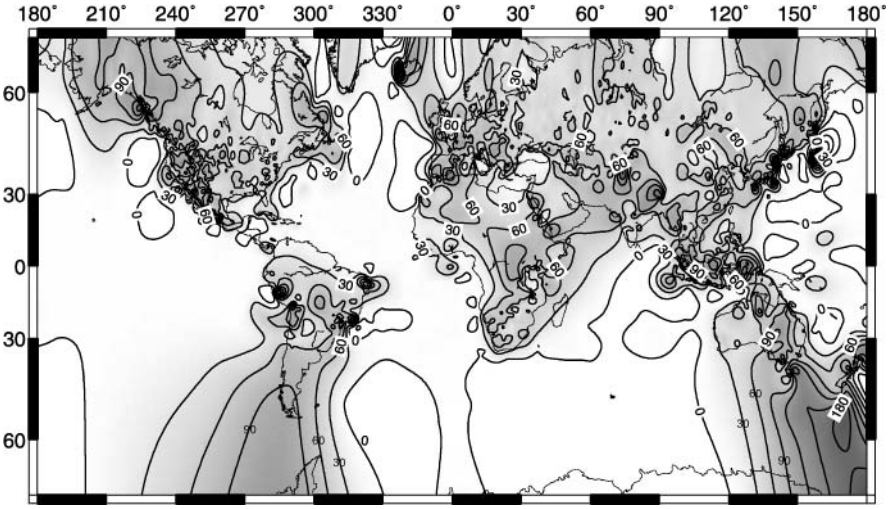


Figure 3.1. Map of global surface heat flow. The map is contoured in milli W m^{-2} and data above 300 mW^{-2} are omitted so that only a conductive response is shown. Nevertheless, because of the highly irregular distribution of the data, the contouring on a global scale is strongly dependent on the contouring algorithm and is associated with large uncertainties in areas of low data density. (made with the Global Heat Flow Data Base of the International Heat Flow Commission, W. Gosnold, Custodian pers. comm. 2006). As a consequence, this map is exclusively a representation of the data base with no consideration of the data distribution, its density or their reliability. As such, it appears (wrongly) that the heat flow on the oceans is lower than that of the continents. For a more considered heat flow map see Pollack et al. (1993) or Wei and Sandwell (2006)

in heat flow units, or hfu. One hfu corresponds to 10^{-6} cal s^{-1} cm^{-2} and can easily be converted into W m^{-2} (s. Problem 3.2, Table D.8). The units of the proportionality constant k, in eq. 3.1, follows now easily from the units of the other components of the equation: Because temperature has the units of K (or °C) and z has the unit m, k must have the units J s^{-1} m^{-1} K^{-1} so that the equation is consistent in its units. The constant k is called *thermal conductivity*. We can now try to read eq. 3.1. We can see that the flow of heat trends to zero if the conductivity is very low, regardless of the thermal gradient. Correspondingly, if the conductivity is very large, the flow of heat becomes large, even if the thermal gradient is very low. The equation may therefore be understood quite intuitively.

Would the thermal gradient be constant everywhere, we could write it as $\Delta T/\Delta z$. However, in geological problems this gradient is never constant. Thus, we use the derivative $\mathrm{d}T/\mathrm{d}z$, which states that we want to be careful and consider our thermal gradient only to be constant within each infinitely small section of the thermal profile. If the gradient changes along the z direction, then eq. 3.1 states that the heat flow must also change.

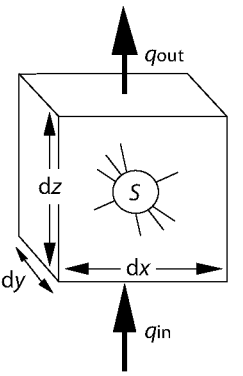


Figure 3.2. The flow of heat in a unity volume of rock. The heat production inside this volume S, is not considered until we discuss eq. 3.23

Energy Balance. The second part of the diffusion equation (often called Fourier's 2. law) describes an energy balance. This energy balance relates heat and temperature and the change of heat flow with change in temperature. This relationship may be established independently from eq. 3.1 and may be written as:

$$\frac{\partial T}{\partial t} \propto -\frac{\partial q}{\partial z} \quad . \tag{3.2}$$

This equation states that the rate of temperature change of a rock must be proportional to the rate with which its heat content changes ($\propto$ is the symbol for "proportional to"). The rate with which the heat content of a rock changes ($\partial q/\partial z$) is given by the difference between the flow of heat *into* the rock and the flow of heat *out of* the rock (Fig. 3.2). If the heat flow into the cube of Fig. 3.2 is larger than the flow of heat out of it, then the heat content of the cube will rise and its temperature will increase. If the heat flow into the volume is just as large as that that flows out, the temperature will remain constant. If more heat flows out of the cube than into it, then its temperature will decrease.

In the last sentences we have begun mixing the terms "temperature" and "heat". However, we have to remain careful no to confuse them as the rate of temperature change is not the same as the rate of heat content change. They relate by:

$$H = T\rho c_p \tag{3.3}$$

where H is the volumetric heat content in J m^{-3} (s. sect. 3.6.4). The rate, with which the temperature will change for a given change in heat content depends on another material specific proportionality constant. This is the *specific heat capacity* c_p. The specific heat capacity or short "*specific heat*" has the units of J kg^{-1} K^{-1} and defines how many Joules are required to heat the mass of one kg of rock by one degree Kelvin. The most common abbreviation for specific heat is c. The subscript p symbolizes the condition that the specific heat is measured at constant pressure (s. sect. 3.2.2). If the

specific heat of a rock is large, we need many Joules to heat the rock and even a rapid increase of its heat content will lead to slow temperature increase and vice versa. Specific heat is formulated in terms of the *mass* that is heated. Considering that the energy balance in eq. 3.2 is formulated in terms of the *spatial* coordinate z, and heat capacity is formulated in terms of *mass*, we need to multiply c_p with the density ρ, so that the relationship between the spatial change of *heat flow* and the temporal change of *temperature* is consistent with the units. We can write the proportionality of eq. 3.2 as:

$$\rho c_p \frac{\partial T}{\partial t} = -\frac{\partial q}{\partial z} \quad . \tag{3.4}$$

It should now be straight forward to understand eq. 3.4 intuitively using Fig. 3.2. The negative sign arises because the temperature *increase* when $\partial q = q_{\text{out}} - q_{\text{in}}$ is negative, that is, more heat flows into the rock volume than out of it. You may have noticed that the step from eq. 3.2 to eq. 3.4 was accompanied by the change from total- to partial differentials. This was necessary, because different parts of this equation are now differentiated with respect to different parameters (s. sect. B.1.1).

The Diffusion Equation. If we substitute Fourier's law of heat conduction (eq. 3.1) into the thermal energy balance of eq. 3.4, we arrive at:

$$\rho c_p \frac{\partial T}{\partial t} = \frac{\partial \left(k \frac{\partial T}{\partial z}\right)}{\partial z} \quad . \tag{3.5}$$

Eq. 3.5 is the general form of the one-dimensional diffusion or heat conduction equation. If k is independent of z (e. g. if we consider heat conduction in an area without lithological contrasts), it is possible to simplify eq. 3.5 significantly. k can then be taken out of the differential and we can write:

$$\rho c_p \frac{\partial T}{\partial t} = k \frac{\partial \partial T}{\partial z \partial z} \qquad \text{or :} \qquad \frac{\partial T}{\partial t} = \kappa \frac{\partial^2 T}{\partial z^2} \quad . \tag{3.6}$$

The constants k, ρ and c_p are now summarized to $\kappa = k/(\rho c_p)$. κ is called thermal diffusivity. Eq. 3.6 can also be understood intuitively, without following the detailed derivation given above. Eq. 3.6 may be formulated in words as:

- *The rate of temperature change is proportional to the spatial curvature of the temperature profile.*

If you do not understand the relationship between this sentence and eq. 3.6, then remember that the first differential of a function describes its slope (or: "gradient", or: "rate") and the second its curvature (s. sect. B.1, Fig. B.3, B.2).

Figure 3.3 illustrates this graphically. In our daily lives we encounter many examples that are described by this equation. Think for example that a piece of toast cools much quicker on its corners than along the edges or in its middle. This is because the *spatial curvature* of the isotherms in the toast

is the largest at the corners! The same is true for the rapid cooling of the tip of a needle, the rapid erosion of ragged mountain tops and countless other examples in nature, all the way down to the rapid chemical equilibration of fine grained rocks in comparison with coarse grained rocks.

If we want to use eq. 3.6 we must solve it. For this we need boundary- and initial conditions. We also need some mathematical knowledge so that we can integrate this equation. Various methods how to go about this are discussed in sect. B.1.1. A large part of this chapter will deal with various solutions of this equation. In this context we will often meet the terms "*boundary conditions*" and "*initial conditions*". Make sure you understand what they mean (s. p. 398).

• *The magnitude of* κ. A quantitative application of eq. 3.6 requires the knowledge of κ and therefore the knowledge of k, ρ and c_p. The specific heat of rocks is about $c_p = 1\,000 - 1\,200\ \mathrm{J\,kg^{-1}\,K^{-1}}$ (Oxburgh 1980). For most rocks c_p does not vary by more than 20 % around this value. Thus, the nice and even value of $c_p = 1\,000\ \mathrm{J\,kg^{-1}\,K^{-1}}$ is a sound assumption that can be used for many thermal problems. The density of many crustal rocks is of the order of $2\,750\ \mathrm{kg\,m^{-3}}$ and varies also not all that much around this value. However, thermal conductivity, varies by the factor 2 or 3 between different rocks types (Table 3.1). Fortunately, it is between 2 and 3 $\mathrm{J\,s^{-1}\,m^{-1}\,K^{-1}}$ for many rock types. For $k = 2.75\ \mathrm{J\,s^{-1}\,m^{-1}\,K^{-1}}$ and the values for specific heat and density from above the diffusivity is: $\kappa = 10^{-6}\ \mathrm{m^2\,s^{-1}}$. Because this value is easy to remember it is commonly used in the literature. Note, however, that κ may also be twice- or half as large if the thermal conductivity of rocks is twice or half as large.

Heat Refraction. If rocks of different thermal conductivity are in contact, the phenomenon of *heat refraction* may occur. What this is, is easily explained with eq. 3.1. In thermal equilibrium, the flow of heat in two adjacent rocks must be equal. Following from eq. 3.1 we can formulate:

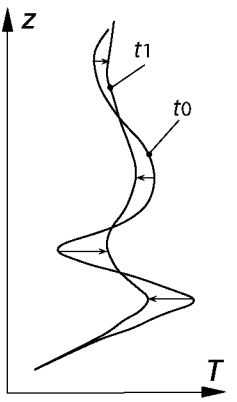


Figure 3.3. The thermal equilibration of a random temperature profile. The temperature profile is drawn at two different time steps t_0 and t_1. Note that the largest change in temperature between the two time steps has occurred in those places of the profile where the curvature of the profile is the largest (s. eq. 3.4). Where the curvature of the profile is zero (at the inflection points) the temperature does not change at all

$$-q = k_1 \frac{\Delta T_1}{\Delta z} = k_2 \frac{\Delta T_2}{\Delta z} \quad , \tag{3.7}$$

where the subscripts $_1$ and $_2$ denote two different rocks as shown in Fig. 3.4. We can see in this equation that, if the conductivities k_1 and k_2 are different, the temperature gradient in the rock with the higher conductivity must be lower and vice versa (Fig. 3.4). This is called heat refraction. Eq. 3.7 can also be written in differential form. This means, the temperature gradient must not change abruptly, but can also change continuously, if there are continuous changes in thermal conductivity.

Let us illustrate the phenomenon with an example. A rock with extremely high thermal conductivity, for example an iron ore body, will be practically isothermal, even if it stretches over many vertical kilometers in the crust. Its high conductivity will cause it to adapt some average temperature. Thus, the upper part the body may have a significantly higher temperature than its surroundings while its lowest part is colder than its surroundings. As a consequence, it is conceivable that the process of heat refraction will even leads to some kind of contact metamorphism (s. Problem 3.3).

Jaupart and Provost (1985) have noticed that there are some important differences in thermal conductivity between the sediments of the Tethys zone and the high Himalayan crystalline complex. They suggested that the process of heat refraction may have been of relevance in connection with the melting of the Himalayan leucogranites. The process has also been discussed as the cause for high grade metamorphism in several Australian provinces (e.g. Mildren and Sandiford 1995) and as the trigger for a range of tectonic processes (Sandiford 1999). In fact, several exploration companies currently explore for geothermal energy sources in Australia by looking for regions where rocks of low thermal conductivity insulate underlying rocks of high thermal conductivity (Hillis et al. 2004).

If we want to describe the process of heat refraction quantitatively, we can not assume the simplification that we have made in going from eq. 3.5 to eq. 3.6. We must stick with eq. 3.5 to describe conductive equilibration. If we form the derivative of the right side of eq. 3.5 using the rules of differentiation of products (Table C.1) we get:

Table 3.1. Thermal conductivities and heat capacities of some rocks and common materials. k is given in J s^{-1} $m^{-1}K^{-1}$ and c_p in J $kg^{-1}K^{-1}$. The change of thermal conductivity as a function of pressure and temperature are negligible at geologically relevant temperatures in the crust (Cull 1976; Schatz and Simmons 1972). Nevertheless, the numbers given here are only approximate

rock type	k	c_p
sandstone	1.5-4.2	920
gneiss	2.1-4.2	800
amphibolite	2.5-3.8	840
granite	2.4-3.8	790
ice	2.2	1 800
water	0.58	4 200
salt	5.4-7.2	880
iron	73	460

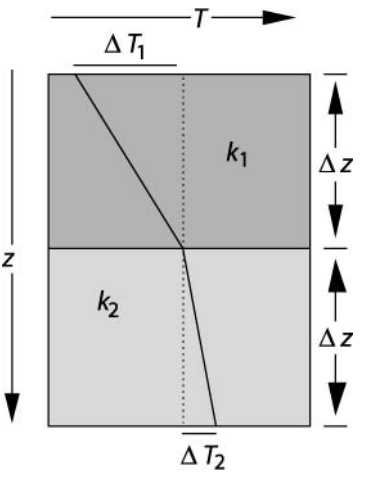


Figure 3.4. Illustration of the process of heat refraction. The flow of heat in the dark and the light shaded bodies is the same. However, the temperature gradient in the dark shaded body is larger, because its thermal conductivity k_1 is smaller. The subscripts $_1$ and $_2$ denote the dark and the light shaded body, respectively

$$\rho c_p \frac{\partial T}{\partial t} = \frac{\partial \left(k \frac{\partial T}{\partial z}\right)}{\partial z} = \frac{\partial k}{\partial z}\frac{\partial T}{\partial z} + k\frac{\partial^2 T}{\partial z^2} \quad . \tag{3.8}$$

In this form the heat conduction equation can be used for the description of many problems with variable conductivity.

Heat Conduction in Several Spatial Dimensions. Eq. 3.6 is a linear differential equation (s. p. 396). This means that heat conduction in two or three dimensions can be described by the sum of heat conduction in the individual directional components. In general, we can write:

$$\frac{\partial T}{\partial t} = \kappa \left(\frac{\partial^2 T}{\partial x^2} + \frac{\partial^2 T}{\partial y^2} + \frac{\partial^2 T}{\partial z^2} \right) \tag{3.9}$$

if the thermal diffusivity is the same in all three spatial directions. In the literature eq. 3.9 is often written as:

$$\frac{\partial T}{\partial t} = \kappa \nabla^2 T \tag{3.10}$$

The symbol ∇ is called the "Nabla-" or: "Del"-operator and is defined in eq. B.32. ∇^2 describes the same thing for the second partial derivative (s. sect. B.3). Partial differentials (or derivatives) are discussed in detail in section B.1.1. An important property of the diffusion equation is that it contains an energy balance. This means that no energy can be gained or lost by diffusion processes. If a rock cools by conduction, then it is by heat loss at the model boundaries, not because of the conduction itself.

• *Complicated geometries.* The diffusion equation we presented above is linear in temperature if all the material constants are independent of temperature and time. Therefore, it is possible to describe diffusion problems of complicated geometries simply by a linear superposition of the solutions for

more simple problems. We will use this approach extensively when we describe the cooling history of intrusions in sect. 3.6. For the same reason is it possible to describe time dependent problems by a superposition of a steady state solution and a time dependent component.

Heat Conduction in Polar Coordinates. Many heat conduction problems in the earth sciences are much better described in cylindrical or spherical coordinates. In *cylindrical* coordinates, eq. 3.6 adapts the form:

$$\frac{\partial T}{\partial t} = \kappa \left(\frac{\partial^2 T}{\partial r^2} + \frac{1}{r} \frac{\partial T}{\partial r} \right) \quad . \tag{3.11}$$

If we consider heat conduction in *spherical* coordinates (and restrict ourselves to heat flow in the radial direction), then the heat conduction equation adapts the form:

$$\frac{\partial T}{\partial t} = \kappa \left(\frac{\partial^2 T}{\partial r^2} + \frac{2}{r} \frac{\partial T}{\partial r} \right) \quad . \tag{3.12}$$

In eqs. 3.11 and 3.12 r is the distance from the coordinate origin on the cylinder axis or at the sphere center, respectively. Detailed derivations of these equations will not be described here, but they can be found - among many others – by Carslaw and Jaeger (1959); Crank (1975) or Smith (1985). Examples for spherical conduction problems that can be described with eq. 3.12 are the Kelvin model for the cooling of the earth or the chemical diffusion of elements in garnet crystals. Note that eqs. 3.11 and 3.12 are one-dimensional and their results can therefore be directly compared with eq. 3.6 (e.g. Fig. 3.32 and 3.37).

The Kelvin Model for the Cooling of Earth. The most famous example for the application of the heat conduction equation is the estimate of the age of the earth by Lord Kelvin (1864). However, we note that very similar estimates were already performed by Fourier himself in 1820. Both physicists realized that - in principle - one could estimate the age of the earth from the present day thermal gradient at the surface (surface heat flow, s. Table D.3) if the following assumptions are made (Fig. 3.5): 1. The whole earth was at the time of its formation of constant temperature (which was assumed by Kelvin to be 4 000 °C); 2. the surface temperature has remained constant ever since and 3. heat conduction is the principle process of cooling. Using eq. 3.12, Kelvin concluded that the earth must be around 100 my old (he used a very similar solution to the one we introduce in sect. 3.6.1). Today we know that his calculation was wrong for two important reasons. The first (and most quoted) reason is that there are heat producing elements in the crust that prolong the cooling of earth. Radioactivity was unknown at Kelvin's time. The second reason is that convection in the upper mantle rises the isotherms. While this process actually leads to a faster cooling of earth, both *radioactivity* and *convection* cause the present day geothermal gradient in the lithosphere to be steeper than it would be without these two processes.

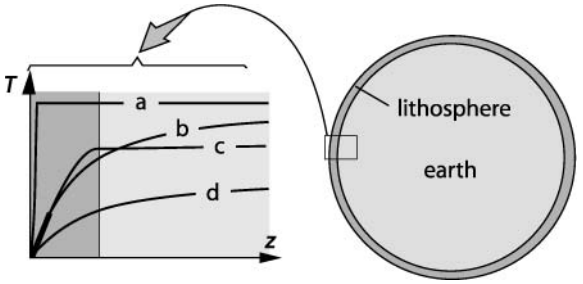


Figure 3.5. Schematic illustration of the model of Lord Kelvin for the estimation of the age of earth. The small T-z-diagram is an enlarged section of outer 300 km of the globe. The shaded area is the lithosphere. a is the initial thermal profile of the earth at the time of its formation. b is the present day thermal profile that was calculated by Kelvin based on the measured surface heat flow q_s (thick drawn part on the thermal profile) and on a spherical heat conduction model. However, because of radioactivity (unbeknown to Kelvin), the lower lithosphere is much hotter than Kelvin thought possible. Moreover, in the asthenosphere convection destroys a conductive thermal gradient, which is very low in this part of earth. (convection was know at Kelvin's time but ignored in his estimates). d is the thermal profile that we should measure today, if the earth had only cooled by conduction since its formation at $\approx 4.5 \cdot 10^9$ y. The surface heat flow would be much lower than what we measure today

This leads to a massive underestimate of the age of earth. Interestingly, the error that is caused in Kelvin's estimate by him neglecting convection is much larger than that caused by neglecting radioactivity. In 1895 John Perry improved Kelvin's estimates drastically, by assuming a "convective mantle conductivity" which he assumed to be ten times larger than the conductivity of the crust (s. p. V). With this assumption he arrived at an almost correct age.

Why Kelvin ignored convection in the mantle, although it had been known for some time, we do not know. However, in defense of his estimate it should be said that he *did* mention in his discussion that heat production, for example by chemical reaction, was not considered in his model but might change the results. The model of Kelvin remains a fantastic example for a conduction model that turned out to be completely wrong because other heat transport mechanisms were not considered. It should serve us as a reminder when interpreting the heat sources of a metamorphic terrain.

3.1.2 The Laplace Equation

Equations 3.6 and 3.10 describe the evolution of temperature as a function of time. Thus, we can use them to describe heating and cooling curves of rocks. However, for many geological questions we are not all this interested in the *temporal* changes of the temperature, but rather in the steady state shape of a temperature profile, for example the shape of a stable continental

geotherm. For all those problems, where it is reasonable to assume that there is *no* temporal change of a temperature profile, we can write:

$$\frac{\partial T}{\partial t} = 0 \quad . \tag{3.13}$$

Any geological situation where this equation applies is called the *steady state.* When we make this assumption, κ can be cancelled out of eq. 3.6 and eq. 3.10. We are left with:

$$\nabla^2 T = 0 \quad . \tag{3.14}$$

Eq. 3.14 is called Laplace-equation. Just like the diffusion equation, it is an extremely important equation for many geological problems. In this chapter we will need it when we consider stable geotherms, but it also has applications in many other branches of the earth sciences.

3.1.3 The Error Function

If we want to use eq. 3.6 to describe a time dependent conduction problem, we must solve it for a given set of boundary- and initial conditions. If we try this, we would quickly realize that this is only possible for a very few boundary- and initial conditions. Periodic problems are some of those for which there are "real" solutions of this equation (sect. 3.7.1). For most problems there are simply no solutions of eq. 3.6 possible. For example, for many geological problems we will see that it is useful to assume that the boundary conditions lie at infinity (at distances that are far away compared to the scale of the problem). In all such problems, the results of integrating eq. 3.6 will contain a term of the form:

$$\frac{2}{\sqrt{\pi}} \int_0^n \mathrm{e}^{-n^2} \mathrm{d}n = \mathrm{erf}\,(n) \tag{3.15}$$

This integral cannot be solved. However, because it occurs so often in solutions of the heat flow equation, it has its own name: the *error function.* The values of the error function for different values of n have been determined numerically and can be looked up on tables, or it can be calculated with some numerical approximation (s. Table C.9). Fig. 3.6 shows the shape of the error function. In many solutions of eq. 3.6 the variable n from eq. 3.15 has the form $n = z/\sqrt{4\kappa t}$. There, time t, and distance z are inside the error function and they are in a quadratic relationship to each other. Most solutions that we will use for the description of contact metamorphism contain error functions of this form (sect. 3.6). We will need the term $n = z/\sqrt{4\kappa t}$ in sect. 3.1.4, 4.4.1 and others. The *complementary* error function erfc is defined as:

$$\mathrm{erfc}\,(n) = 1 - \mathrm{erf}\,(n) \quad . \tag{3.16}$$

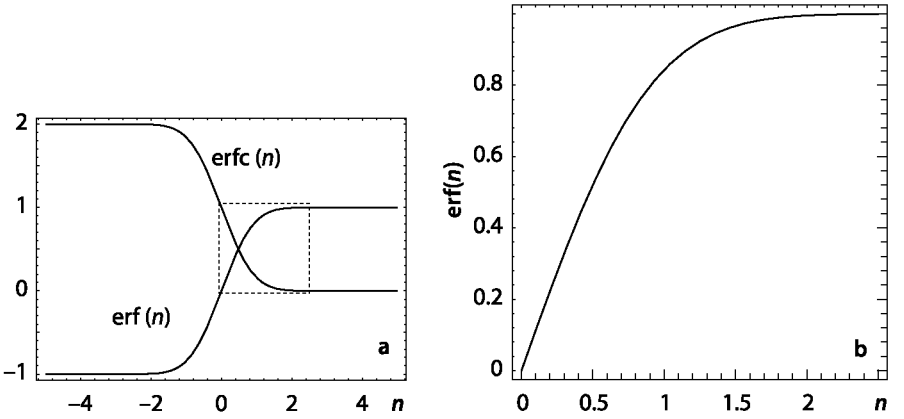


Figure 3.6. The error function and the complementary error function. The dashed frame in **a** shows the part of erf(n) that is shown enlarged in **b**

3.1.4 Time Scales of Diffusion

In the last sections we have seen that heat conduction approaches thermal equilibrium asymptotically. Even after a very long time the new equilibrium is not reached a 100 % and isotherms will still be curved, even if ever so slightly. Thus, if we want to define a duration of thermal equilibration we need to define some arbitrary point along the equilibration curve which we use as a time scale, for example when half or 90 % or 99 % of the new equilibrium is reached. We call such a number along an asymptotically evolving process *characteristic time scale*, in this case: *time scale of diffusion* or: *thermal time constant*, t_{eq}. We can use t_{eq} as a scaling factor for the duration of a thermal event. It is a fantastic aid for an enormous number of estimates, even when in the field. It can be used to estimate the width of contact aureoles, the duration of metamorphic events, the chemical zoning profile of crystals and much more (s. Problem 7.8). The thermal time constant t_{eq} is given by the relationship

$$t_{eq} \propto \left(\frac{l^2}{\kappa}\right) \quad . \tag{3.17}$$

There, l is the spatial size, or: *characteristic length scale* of a thermal event (e. g. the diameter of an intrusion, of a hydrothermal vein or a metamorphic terrain). κ is the thermal diffusivity and $\propto$ means "proportional to". Eq. 3.17 tells us that the duration of diffusive equilibration is proportional to the square of the size of the equilibrating body. In other words, if for example there are two granitic plutons with one being *twice* the size of the other, then the duration of cooling will be *four* times longer for the larger body. The proportional relationship from eq. 3.17 adapts various forms, depending on

the problem solved and on how exactly we want to define the thermal time constant. Usually it is defined as:

$$t_{eq} = \left(\frac{l^2}{2\kappa}\right) \qquad \text{or :} \qquad t_{eq} = \left(\frac{l^2}{(2.32)^2\kappa}\right) \quad . \tag{3.18}$$

The different formulations are based on different assumptions about the magnitude of the scaling factor for t_{eq}. In eq. 3.20 we will discuss this in some more detail. Table 3.2 shows some numerical values for different sizes of cooling bodies.

The value of t_{eq} can be used either way. It can be used to estimate the duration of a diffusion process *or* it can be used to estimate the length scale of a thermally influenced region after a given time scale. We should try to remember that the typical duration of thermal equilibration of length scales of 10 m, 100 m, 1 km, 10 km and 100 km is of the order of 1 y, 100 y, 10 000 y, 1 my and 100 my, respectively. Table 3.2 gives a number of examples of thermal time constants for different length scales.

The Meaning of the "Time Scale" of Diffusion. We now want to define a bit more clearly what is meant by the terms "length scale" and "time scale" which we have introduced in the last section. For this, we have to use some information from sect. 3.6. There, we shall see that many solutions of the heat conduction equation contain an error function of the form: erf $\left(l/\sqrt{4\kappa t}\right)$. For example, the solutions discussed on page p. 111 or in eq. 3.80 are all of the form:

$$T(t) = a + b\left(\text{erf}\left(\frac{l}{\sqrt{4\kappa t}}\right)\right) \tag{3.19}$$

where a and b are constants. In eq. 3.19 the expression $(l/\sqrt{4\kappa t})$ corresponds to the variable n from eq. 3.15. The length scale l and time t are both contained within the error function and do not appear elsewhere in the solution. The shape of the error function in Fig. 3.6 shows that it reaches asymptotically 1 as n get very large. Correspondingly, from eq. 3.19, the term inside

Table 3.2. Different values of the thermal time constant t_{eq} for a series of geologically relevant length scales l, and calculated for one of the two proportionalities given in eq. 3.18 as well as for one used much later in this book (p. 279) for the same purpose

l	$t_{eq} = l^2/2\kappa$	$t_{eq} = l^2/\pi^2\kappa$
10 m	$5 \cdot 10^7$ s $\approx$ 1.58 y $\approx 10^0$ y	$1.01 \cdot 10^7$ s $\approx$ 16 weeks $\approx 10^{-1}$ y
100 m	$5 \cdot 10^9$ s $\approx$ 158 y $\approx 10^2$ y	$1.01 \cdot 10^9$ s $\approx$ 32 y $\approx 10^1$ y
1 km	$5 \cdot 10^{11}$ s $\approx$ 15 000 y $\approx 10^4$ y	$1.01 \cdot 10^{11}$ s $\approx$ 3 200 y $\approx 10^3$ y
10 km	$5 \cdot 10^{13}$ s $\approx$ 1.5 my $\approx 10^6$ y	$1.01 \cdot 10^{13}$ s $\approx$ 320 000 y $\approx 10^5$ y
100 km	$5 \cdot 10^{15}$ s $\approx$ 158 my $\approx 10^8$ y	$1.01 \cdot 10^{15}$ s $\approx$ 32 my $\approx 10^7$ y

the brackets will always remain 1 for very large l (regardless of t), or for very small t (regardless of l). We can also see that – because time is in the denominator inside the error function – *complete* equilibrium is reached only after infinite time (when the term inside the brackets asymptotically approaches zero). In order to define a "duration of equilibration" we may want to arbitrarily choose a point in the equilibration process where the argument of the error function (for which we use n in eq. 3.15) is 1. This means that:

$$\left(\frac{l}{\sqrt{4\kappa t}}\right) = 1 \qquad \text{or:} \qquad t = \frac{l^2}{2\kappa} = t_{eq} \quad . \tag{3.20}$$

Figure 3.6 illustrates that for the argument to be 1 (where $t = l^2/(2\kappa)$), the thermal equilibration is 84.3 % complete. Just for simplicity, this arbitrary value is often chosen as a scaling factor for the equilibration history where it may be said that the diffusive equilibration is "largely complete".

As the value of 84.3 % seems a bit arbitrary, thermal time constants are sometimes formulated using the reverse consideration: What is the thickness of a layer, which has equilibrated to 90 % within a given time? From Fig. 3.6 we can see that $\mathrm{erf}(n) = 0.9$, for $n \approx 1.16$ or $l \approx 2.32\sqrt{\kappa t}$. This expression for thickness is also used for the thermal definition of the lithosphere (sect. 3.4). It is what is sometimes called the *thermal boundary layer.*

Both formulations discussed above are chosen in an arbitrary way, and either can be used depending whether one wants a slightly simpler formulation of t_{eq}, or the value of the percent of thermal equilibration. It is important to note that t_{eq} gives an approximation of the time it will take for most of the thermal equilibration to take place. In summary, it will be sufficient for most purposes to remember the basic message of eq. 3.17:

- During conductive processes the duration of thermal equilibration increases with the square of the length scale of the equilibrating body.
- For geologically realistic thermal diffusivities, the characteristic time scale of equilibration of a 10^3 m length scale is of the order of 10^4 y. On the scale of the lithosphere (10^8 m), the time scale of equilibration is of the order of 10^8 y.

This means that regional metamorphism of nappe piles that are several tens of kilometers thick should last of the order of several tens of my. We shall discuss the implications of this in much more detail in sect. 6.2.1.

3.2 Principles of Heat Production

We discern three fundamentally different geological mechanisms that produce heat:

- radioactive heat production,

– chemical heat production,
– mechanical heat production.

In the next sections we derive the basic equations that are needed to describe these three mechanism and we discuss their respective geological relevance. In general, the rate of temperature change due to heat production may be described by:

$$\frac{\mathrm{d}T}{\mathrm{d}t} = \frac{S}{\rho c_p} \quad . \tag{3.21}$$

There, T, t, ρ and c_p correspond to temperature, time, density and heat capacity as discussed on p. 53 and S is the volumetric rate of heat production in $\mathrm{J\,s^{-1}\,m^{-3}} = \mathrm{W\,m^{-3}}$. Heat production rate must be divided by density and specific heat to convert the volumetric heat production rate into a rate of temperature change, just as we have done with heat flow in section 3.1.1. If S is positive, heat is produced, $\mathrm{d}T/\mathrm{d}t$ is positive and rocks heat up. If S is negative, heat is consumed, $\mathrm{d}T/\mathrm{d}t$ is negative and rocks cool. The heat production rate S can be of radioactive, chemical or mechanical origin so that we can write:

$$S = S_{\mathrm{rad}} + S_{\mathrm{chem}} + S_{\mathrm{mec}} \quad . \tag{3.22}$$

All three of these components may have a significant influence on the thermal evolution of rocks depending on the circumstances and all three have different characteristics that require different methods of description.

Production or Conduction? From section 3.1 we remember that the rate of temperature change due to conduction is proportional to the difference between heat flow into and out of a unit rock volume $(q_{\mathrm{in}} - q_{\mathrm{out}})$. However, we now learn that the rate of temperature change also depends on the amount of heat that is produced *inside* this unit volume (Fig. 3.2). This value must be added to the difference $q_{\mathrm{in}} - q_{\mathrm{out}}$. Thus, if we adapt eq. 3.6 to formulate a thermal energy balance considering conduction *and* production, we can write:

$$\frac{\partial T}{\partial t} = \kappa \frac{\partial^2 T}{\partial z^2} + \left(\frac{S}{\rho c_p}\right) \quad . \tag{3.23}$$

Note that we now need to use partial derivatives. Whether or not we need to consider eq. 3.23 to model a given thermal problem, or if we can use the simpler form of eq. 3.21 (neglecting heat production) or eq. 3.21 (neglecting heat conduction) depends on the magnitude and relative rates of heat production and heat conduction. Some heat production rates are very rapid (e.g. friction heat production during an earthquake), others are very slow (e.g. reaction heat production during retrograde metamorphism) but it really is on their rate *relative* to conduction that is critical to consider. A comparison between the diffusion and the heat production term on the right hand side of eq. 3.23

element	U	Th	K
mean mantle concentration (kg/kg)	31×10^{-9}	124×10^{-9}	31×10^{-5}
mean crustal concentration	1.24×10^{-6}	5.6×10^{-6}	1.43×10^{-2}
mantle heat production (W/kg)	3×10^{-12}	3.2×10^{-12}	1.1×10^{-12}
crustal heat production (W/kg)	1.4×10^{-10}	1.5×10^{-10}	0.5×10^{-10}

Table 3.3. Concentrations of heat producing elements in the crust and undepleted mantle (after Turcotte and Schubert 2002). In granites, the heat production is about 2–3 times higher than the values listed here. The heat productions are per kg of rock, i.e. the values come from concentrations given in the first two rows multiplied with the heat productions given in the text

can help us to judge if one of the two processes is much smaller than the other and can therefore be neglected in the problem that is being considered. Such a comparison could be made two ways:

1. *Comparison.* The characteristic time scale of diffusion t_{eq} of diffusion may be compared with the duration of heat production. If t_{eq} is much larger than the duration of heat production, then conduction can be neglected and heat production will dominate the temperature change. However, if t_{eq} is much smaller than the duration of heat production, then all heat that is produced will be conducted away at a much faster rate than it is being produced. Even large amounts of heat production will have a comparably small influence on the temperature and it may be possible to neglect the production term. If heat production- and conduction occur on similar time scales, then the following comparison may be of value.
2. *Comparison.* Consider the case of stable temperature where $\mathrm{d}T/\mathrm{d}t = 0$. Then we can see from eq. 3.23 and eq. 3.6 that: $-S/k = \mathrm{d}^2T/\mathrm{d}x^2$. In words: if the ratio S/k corresponds to the curvature of the temperature profile, then the rate of heat production is balanced by the rate of heat conduction. An important example for such a balance is given by the steady state shape of isotherms in subduction zones (p. 107) and a corresponding example in the theory of mass transfer is discussed on p. 192.

However, for this chapter, let us remain with the case where heat production is much more important than heat conduction and we neglect any diffusion processes in the first instance.

3.2.1 Radioactive Heat Production

Radioactive (or: radiogenic) heat is produced in the earth predominantly by the naturally occurring radioactive isotopes ^{238}U, ^{235}U, ^{232}Th and ^{40}K. Of the two naturally occurring uranium isotopes 99.28% is ^{238}U and only 0.72% is ^{235}U. All of the naturally occurring thorium is ^{232}Th and only 0.0119% of

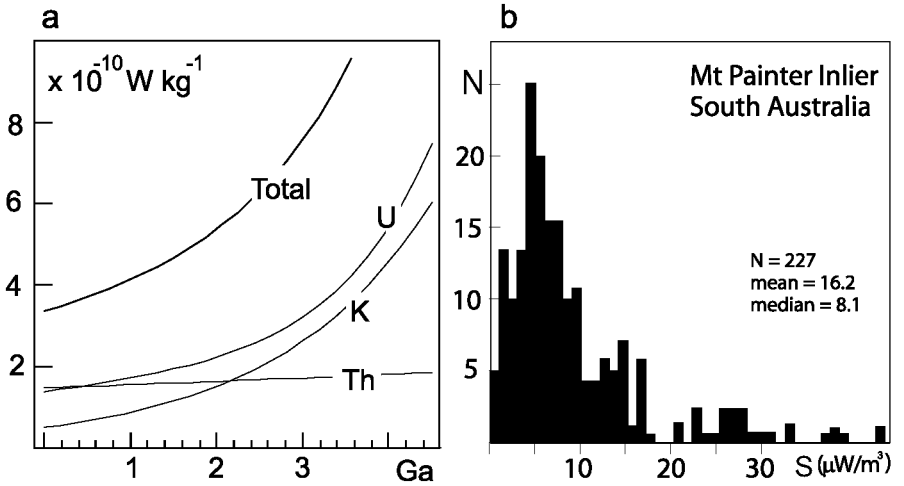


Figure 3.7. **a** Radioactive heat production in the crust through time. Note that the heat production in the Archaean 3 Ga ago was about twice as high as today. Also note that U and Th are the primary heat producing elements today, but it was U an K in the past. **b** Rates of radiogenic heat production in granites from the Mt Painter province, a low-pressure high-temperature metamorphic terrain in Australia (after Sandiford and Hand 1998b). Heat production rates in other Proterozoic terrains of Australia are similar. N is the number of data points

the natural potassium is ^{40}K (Turcotte and Schubert 2002). As pure metals, these 4 isotopes produce the following amounts of heat: $^{238}\mathrm{U} = 9.46 \times 10^{-5}\mathrm{W\ kg^{-1}}$; $^{235}\mathrm{U} = 5.69 \times 10^{-4}\mathrm{W\ kg^{-1}}$; $^{232}\mathrm{Th} = 2.64 \times 10^{-5}\mathrm{W\ kg^{-1}}$ and $^{40}\mathrm{K} = 2.92 \times 10^{-5}\mathrm{W\ kg^{-1}}$. Fortunately, the concentrations of these elements in rocks are quite low so that substantially less heat is produced per cubic meter of rock. Table 3.3 lists some average concentrations of the heat producing elements in the continental crust and in the mantle. We can see that the earth's mantle (oceanic crust has comparable values) contains about 2 orders of magnitude less radioactive elements than the crust. These concentrations are still important when considering problems related to cooling of earth as a whole or when thinking about the vigor of mantle convection in the Archaean, but for considerations of the heat budget of the Phanerozoic crust we need not consider radioactivity in the mantle. However, the crustal heat production is significant: The sum of the values listed in this table is about $3.4 \times 10^{-10}\ \mathrm{W\,kg^{-1}}$, which corresponds roughly to a heat production rate of about one $\mu\mathrm{W\,m^{-3}}$. Using typical values for heat capacity and density of crustal rocks and eq. 3.21, $S = 1\ \mu\mathrm{W\,m^{-3}}$ converts to a heating rate of of about 10°C per million years (s. Problem 3.6). So the burial of highly radiogenic bodies by deformation can cause significant heating ! In fact, most granites have substantially higher heat productions than those listed in Table 3.3 and there are many terrains around the world where radiogenic heat

production rates is significantly higher than some $\mu W\,m^{-3}$ (Fig. 3.7b; Sandiford and Hand 1998b). Radiogenic heat production in the continental crust is responsible for about half of the heat flow that we can measure at the surface of the earth (Chapter 2, Fig. 2.18). However, in total, about 80 % of the cooling of earth is related to radioactive decay because even the low radioactivity in the mantle has an important influence on enhancing convective motion in the mantle and therefore on the heat that flows from the mantle into the lithosphere. Radioactive heat production is an important contributor to the heat budget of the crust as a whole (Chamberlain and Sonder 1990; MacLaren et al. 1999; Sandiford et al. 1998).

Radioactivity in Space and Time. We know that heat producing elements are not homogeneously distributed across the crust, but that the bulk of the heat producing elements is concentrated in the upper crust. This is because all of the important radiogenic elements occur in granite and the intrusion of granites has been the principle agent of fractionating and redistributing matter from the earth's interior towards the surface. Uranium and thorium are very large atoms and are therefore incompatible and thus contained in granitic melts. Potassium is less radioactive, but there is so much of it in potassium feldspar so that it also has a significant contribution. Over time, granitic melts have transported those elements into the upper crust. Nevertheless, the vertical distribution of heat producing elements in the crust may be extremely variable (e. g. Haack 1983; Lachenbruch and Bunker 1971). In the section on the calculation of geotherms we will spend some time to discuss the influence of the vertical distribution of these elements on the temperature profile of the lithosphere (sect. 3.4.2, see also p. 289).

The temporal variation of radioactivity in the earth's crust through time has been a topic of significant debate, as it is intimately connected to the question if plate tectonics is a modern feature or if it occurred in the Archaean as well. The half lives of the four important radioactive isotopes are known to us. They are: ^{238}U = 4.47 Ga; ^{235}U =0.704 Ga; ^{232}Th = 14 Ga and ^{40}K = 1.25 Ga. As such, the half lives are comparable to the age of earth and it is easy to estimate the radioactivity in the past. Fig. 3.7a shows that the heat production in the Archaean was about twice as high as today. Of course this is true for the mantle as well. A series of authors have discussed the influence of higher heat production in the Archaean for secular changes observed in the style of ore deposits (Groves et al. 2005), the style of metamorphism (Sandiford 1989) and the style of continent formation in general (Abbott and Hoffman 1984).

3.2.2 Mechanical Heat Production

The forces that deform rocks can be viewed as mechanical energy that is added to the rock. The work done on the system is the product of force applied to the system times the distance over which it is deformed. This

energy will be taken up by a variety of *mechanical energy sinks*. A part of this energy will be transformed into potential energy (s. sect. 5.3.1), some into dislocation energy in crystal lattices, some in noise and other forms of energy. However, most authors agree that the majority of this mechanically produced energy will be transformed into friction heat. Frictional heating is also often referred to as *shear heating* (because it is produced when rocks are sheared) or *viscous dissipation* (because momentum is dissipated, see details in sect. 5.1.1). We abbreviate this mechanical heat production with S_{mec}. The rate of mechanical heat production S_{mec} is given by the product of deviatoric stress τ and strain rate $\dot{\epsilon}$. Stress has the units of Pascal. One Pascal is one Joule per cubic meter ($1\ \mathrm{Pa} = 1\ \mathrm{J\,m^{-3}}$). Thus, stress can be expressed as energy per volume and energy is stress *times* volume. These conversions between the different units should be straight forward, remembering the well-known relationships:

$$\text{force} = \text{mass} \times \text{acceleration} \quad \text{and} \quad \text{stress} = \frac{\text{force}}{\text{area}} \ .$$

The units of acceleration are $\mathrm{m\,s^{-2}}$ and those of force are therefore: $\mathrm{kg\,m\,s^{-2}}$. Stress and pressure therefore have the units of $\mathrm{kg\,m\,s^{-2}\,m^{-2}}$ or $\mathrm{Pa} = \mathrm{kg\,m^{-1}\,s^{-2}}$ and energy has the units of $\mathrm{J} = \mathrm{kg\,m^2\,s^{-2}}$. Accordingly, if high deviatoric stresses are required to deform a rock, a lot work is done on the system and the mechanical energy production rate is high, and vice versa. We notice that when we rub our hands together: The harder we press and the faster we rub, the warmer they get. Both deviatoric stress and strain rate are tensors and the rate of mechanical heat production is therefore given by a tensor product. Considering tangential and normal components in three dimensions, friction heat is given by:

$$S_{\mathrm{mec}} = \tau_{xx}\dot{\epsilon}_{xx} + \tau_{yy}\dot{\epsilon}_{yy} + \tau_{zz}\dot{\epsilon}_{zz} + 2\left(\tau_{xy}\dot{\epsilon}_{xy} + \tau_{xz}\dot{\epsilon}_{xz} + \tau_{yz}\dot{\epsilon}_{yz}\right) \tag{3.24}$$

(see e.g. Burg and Gerya 2005). The subscripts and notation of the components of deviatoric stress and strain rate should not worry us here and will be discussed in some detail in sect. 5.1.1. For now, we consider only the one-dimensional case (and only normal components, i.e. we neglect shear stresses and shear strain rates). Then we can view the mechanical heat production rate as the simple scalar product:

$$S_{\mathrm{mec}} = \tau\dot{\epsilon} \ . \tag{3.25}$$

Some of the implicit assumptions in this simplification are discussed in sect. 5.1.1 and 6.2.2. In order to write the temperature change that arises from frictional heating we can write in analogy to eq. 3.21:

$$\frac{\mathrm{d}T}{\mathrm{d}t} = \frac{\tau\dot{\epsilon}}{\rho c_p} \ . \tag{3.26}$$

Note that eq. 3.26 is independent of the deformation mechanism. Both brittle and ductile deformation mechanisms will produce the same amount of friction

heat if they support the same deviatoric stresses. We only may need to be careful with the units: Brittle faults do not have a *strain rate* (in s^{-1}) but a *slip rate* in meters per second. The product of slip rate and deviatoric stress does not have the units of heat production per cubic meter, but the units of heat flow (i.e. $J\,s^{-1}\,m^{-2}$ normal to the fault surface) which can be converted into a heating rate using the laws of heat conduction discussed in previous sections.

Temperature Dependent Strength. In chapter 5 (p. 231) we will show that the deviatoric stresses that rocks can support during viscous deformation are a strong function of temperature. Thus, eq. 3.26 should strictly have been written as:

$$\frac{dT}{dt} = \frac{\tau(T)\dot{\epsilon}}{\rho c_p} \quad . \tag{3.27}$$

We can see from this equation that the temperature increase that may occur due to shear heating is in itself a function of temperature. There is a negative feedback between shear heat production and thermal weakening so that any incremental amount of shear heating will instantaneously soften the rocks and subsequent heating becomes more and more difficult as temperature gets higher. Shear heating is self limiting.

For some assumptions about the deformation mechanism it is possible to integrate eq. 3.27, even though temperature occurs both on the left and right hand sides of the equation. For example, for the deformation law described by eq. 5.46, it is possible to integrate eq. 3.27 (Stüwe 1998a). While this analytical solution will not be repeated here, a graph of this solution is shown in Fig. 3.8 for the rheological parameters of quartz and olivine. It may be seen that – if rocks are very soft (e.g. at very high temperatures) – there is no shear heating and temperatures before and after deformation are the same. However, at temperatures below about 600°C shear heating may be quite significant. Due to the self limiting nature of shear heating, curves become parallel to the vertical axis at even colder temperatures.

Note that Fig. 3.8 can only be used to evaluate the effects of shear heating if conduction of heat may be neglected. The time scale of conductive equilibration of the lithosphere is of the order of hundreds of my, while the duration of continental deformation processes is only 1–10 my. Thus, on the scale of the lithosphere, the duration of mechanical heat production is at least one order of magnitude less than the duration of heat conduction. Thus, conduction of heat may be neglected if shear heating is considered on the scale of the lithosphere (s. comparison on p. 66). Also note that Fig. 3.8 was calculated assuming that the strain rate remains constant. While this describes some geological scenarios, there are many others where *stress* is a constant and the strain rate changes in order to balance it (s. p. 246).

Shear Zones of Finite Width. If we consider problems on a small scale, for example shear heating around a small shear zone, then the influence of conduction during heat production needs to be considered. For the solution

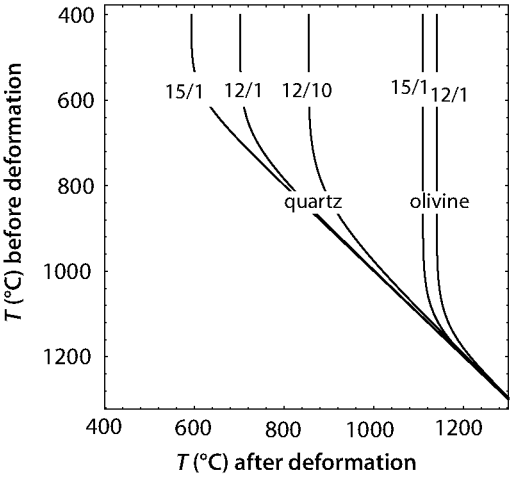


Figure 3.8. Temperature of rocks at the start of deformation, plotted against the temperature at the end of deformation. Mechanical heat production is assumed to be the only heating process and heat conduction is neglected. The diagram was calculated with the solution presented by Stüwe (1998a), which was derived from eq. 3.27 and eq. 5.46. The various curves are labeled according to the following syntax: before the dash: ${}_{10}\mathrm{Log}(\dot{\epsilon})$ between $\dot{\epsilon} = 10^{-12}$ and 10^{-15} s^{-1}; after the dash: elongation from 1–10. Obviously, the increase in temperature is larger for larger strains. However, during crustal shortening, a stretch of 2–3 is rarely exceeded. Thus, the effects of shear heating are likely to be much larger in strike slip regimes where much larger strains are possible than during crustal thickening. Rheological assumptions for quartz are: $Q = 1.9 \cdot 10^5$ $\mathrm{J\,mol^{-1}}$, $A = 5 \cdot 10^{-6}$ $\mathrm{MPa^{-3}\,s^{-1}}$, $n = 3$. Rheological assumptions for olivine are: $Q = 5.2{\cdot}10^5$ $\mathrm{J\,mol^{-1}}$, $A = 7{\cdot}10^4$ $\mathrm{MPa^{-3}\,s^{-1}}$, $n = 3$

of such problems, eq. 3.26 must be enlarged by a term that describes diffusion. The equation we must solve is eq. 3.23, subject to initial and boundary conditions that describe the shear zone geometry. Fortunately, many shear zones have reasonably simple planar geometries that may be described with simple initial and boundary conditions. If we define the width of a shear zone to be $2l$ and assume a one-dimensional spatial coordinate z that extends normal to the shear zone and has its origin in the shear zone center, then the boundary conditions for a planar shear zone of constant width may be formulated as follows:

- $T = 0$ at the time $t = 0$ in the half space $z > 0$.
- For all $t > 0$ there is heat production in the region $0 < z < l$ at a constant rate S.
- For all $t > 0$ the thermal gradient at $z = 0$ is: $\mathrm{d}T/\mathrm{d}z = 0$.
- At $z = \pm\infty$ the temperature stays at $T = 0$ at all times.

You can visualize yourself these initial and boundary conditions by sketching them into a diagram where z is plotted against T. Using these initial and boundary conditions it is possible to find solutions of eq. 3.23 that describe the

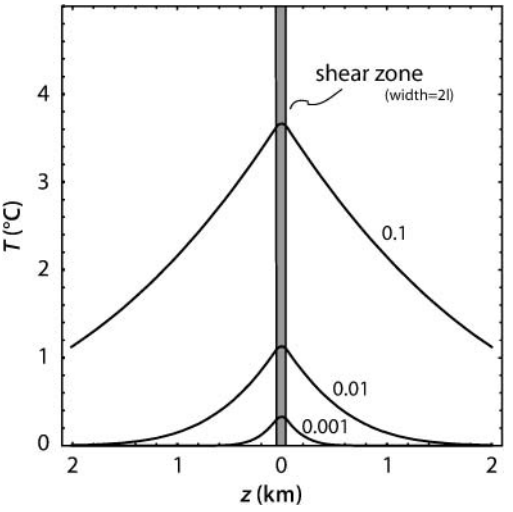


Figure 3.9. Temperature profile across a shear zone of the width $2l = 50$ m at three different time steps labeled in my. The heat production rate in the shear zone is 10^{-4} W m^{-3}; the thermal conductivity k is 2.7 J s^{-1} m^{-1} K^{-1}. The figure was calculated with equations given in the 1st edition of this book. For another example where the same model may apply see p. 201

temperatures in and around the shear zone. This and many other solutions of the heat flow equation are discussed by Carslaw and Jaeger (1959) and can be looked up therein. Fig. 3.9 shows a graph of the relevant solution (given in the first edition of this book). The largest error in this figure is introduced by the assumption that the mechanical energy production rate was assumed to be constant. In reality, there is a feed back mechanism between heating and softening in the shear zone. Carslaw and Jaeger (1959) present for this problem some solutions in which the heat production rate can be varied as a function of time. However, for most realistic problems, where shear heat production feeds back on the rheology of the rock (e. g. in Fig. 3.8) it is wiser to use a numerical solution of eq. 3.23.

Geological Relevance of Shear Heat Production. A range of authors have discussed the importance of shear heating on a geologically significant scale (e. g. Burg and Gerya 2005; Nabelek and Liu 1999; Brun and Cobbold 1980; Lachenbruch 1980; Scholz 1980; Barton and England 1979; Graham and England 1976). Nevertheless, its importance in many tectonic and metamorphic processes remains contentious. This is because both, deviatoric stresses and strain rates on the scale of the crust are not very well constrained and are among the most discussed geological parameters. We can constrain shear heating to a certain degree using eq. 3.26 to estimate the temperature increase a rock might experience for some realistic deviatoric stresses and strain rates. For this, we neglect heat conduction away from the site of mechanical heat production in the first instance. Our estimates are therefore an upper constraint but may be quite appropriate if the length scale of shear heat production is very large (e.g. deforming nappe piles of several tens of kilometers) and the time scale of heat production is short (e.g. less than a few millions of years).

Methods to measure geological strain rates show an upper limit of $\dot{\epsilon} = 10^{-12}$ to 10^{-14} s^{-1}. These numbers imply that deformation doubles the thickness of a rock package (strain of about 100 %) within 1–10 my. The magnitude of deviatoric stresses is much less constrained. Stress determination experiments are performed at strain rates of $\dot{\epsilon} = 10^{-6}$ s^{-1} and must be extrapolated by six to eight orders of magnitude of strain rate. The relevance of such experimental results remains therefore debated. Moreover, deviatoric stress is strongly temperature dependent. Nevertheless, we know that the order of magnitude of plate tectonic driving forces is between 10^{12} and 10^{13} N m^{-1} (s. sect. 5.3) and we will show on p. 300 that this implies a rock strength of 50–100 MPa, averaged over the thickness of the lithosphere. However, the vertical distribution of this strength in the lithosphere is largely unclear. In fact, in section 6.3.5 and 5.2.1 we will see that the middle crust may exceed those values dramatically. In problem 3.7 we use some number to estimate the arising heating rates.

An estimate for total heating can be arrived at even easier: During orogenesis, the crust typically changes its thickness by a factor of two (it doubles in collisional orogens and halves its thickness in many extensional settings). Remember that a stretch of 2 corresponds to a longitudinal strain (or elongation) of 1 ($\dot{\epsilon} \cdot t = \epsilon = 1$; s. eq. 4.1). Assuming all else being constant, it is easy to integrate eq. 3.26. The temperature at the end of deformation for a longitudinal strain of 1 can simply be estimated with: $T = \tau/(\rho c_p)$. Using standard values for the density and specific heat ($\rho = 2\,700$ kg m^{-3} and $c_p = 1\,000$ J kg^{-1} K^{-1}) we can see that a rock that has a shear strength of 100 MPa will be heated by about 37 °C. If rocks are twice as strong, then the temperature increase is twice as high. As the strength of rocks may be several hundreds of MPa under some circumstances, we must conclude that viscous dissipation may be of significant importance to the thermal energy budget of the lithosphere.

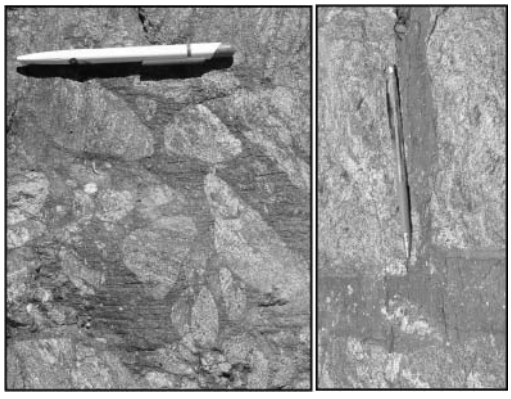


Figure 3.10. Field photographs of pseudotachylites. The left photo shows network typical of many pseudotachylites, the right photo shows a pseudotachylite with chilled margin and recrystallised center. Both photos are 550 my old pseudotachylites from the Woodroffe Thrust system, Central Australia (Camacho et al. 1995)

Examples where friction heat production has a significant influence on the temperature of rocks are well-known to us from pseudotachylites from all crustal levels (Camacho et al. 1995; 2001; Austrheim et al. 1996) (Fig. 3.10). In those, friction heat was sufficient to even melt the rock. Pseudotachylites form during seismic events where extremely rapid deformation occurred on a very local scale. They are therefore not very appropriate to estimate the influence of friction heat on the thermal evolution of the entire crust where we have to deal with averaged strain rates and averaged stresses (e. g. Kincaid and Silver 1996; Stüwe 1998a). Regardless, even significant amounts of friction heat need not be reflected in significantly increased temperatures. Whether or not shear heating actually becomes geologically significant on a crustal scale depends largely on 2 factors:

- 1. It depends on the relationship between the *length scale* of heat production (which determines how rapidly heat may be conducted away from the site of production) and the *time scale* of heat production. The same considerations that we discussed on p. 66 apply. For example, if a 100 m thick shear zone is active for 1 my, then eq. 3.18 tells us that the characteristic time scale of diffusion of this shear zone is of the order of only 1 000 y. Thus, shear heat produced over a time interval of 1 my will be largely conducted away as it is produced. In contrast, if a 15 km nappe pile deforms under the same conditions, then its thermal time constant will be tens of my and all heat produced within 1 my will be largely retained in the pile.
- 2. It depends on the feedback between heating and softening of rocks.

In summary we can say that shear heating *is* a potential candidate for significant heating of rocks and that every argument for or against shear heating should be reduced to an argument about one of the following three points:

- What is the strength of the rocks under consideration?
- What is the strain rate?
- What is the relationship between the *duration* of deformation and the *size* of the deforming rock body?

We can also conclude from the active discussion in the literature that the question is partly open and that it is unwise to take sides without some valued consideration of the problem.

Adiabatic Processes. "Adiabatic" means: "without change in heat content" or: "without change in enthalpy". If a rock is buried, the pressure rises because of the weight of the increasing overburden. The rock is compressed and there is work done to change its volume. The energy of the rock increases by the product of the applied lithostatic force and the distance of shortening during the volume change. It is a type of mechanically produced energy. If no change of the heat content of the system is allowed, then the rock must get warmer. The rock heats *adiabatically*. Correspondingly, an adiabatically heated rock will cool and expand when it is decompressed. We can observe

adiabatic cooling on gas bottles that freeze on their surface when they are opened and adiabatic heating on bicycle tires that warm up when they are pumped up. Rocks are compressible enough so that adiabatic processes is a geologically relevant process, in particular in the earths mantle. For the consideration of adiabatic processes we define the *isothermal compressibility* β as the relative volume change, ∂V, per increment of pressure change, ∂P, at constant temperature. This has the units of Pa^{-1} (sect. 5.1.2):

$$\beta = -\frac{1}{V}\left(\frac{\partial V}{\partial P}\right)_T \quad . \tag{3.28}$$

We discuss the compressibility in sect. 5.1.2. More commonly we will encounter the thermal expansion coefficient α. Corresponding to the isothermal compressibility, α is given by the relative volume change per increment of temperature change at constant pressure. This is given by:

$$\alpha = -\frac{1}{V}\left(\frac{\partial V}{\partial T}\right)_P \quad . \tag{3.29}$$

Rocks have typical values of $\alpha \approx 3 \cdot 10^{-5}$ K^{-1} and $\beta \approx 10^{-11}$ Pa^{-1}. When discussing adiabatic heating processes we need yet another parameter, which is the *adiabatic compressibility* (which is different from the compressibility at constant temperature). This is given by the change in density with change in pressure at constant entropy and should not be confused with the isothermal compressibility discussed in eq. 3.28. The adiabatic compressibility is smaller than the isothermal compressibility.

Whatever the case may be, to the geologist it is relevant to remember that part of the temperature increase with depth in the earth is due to an adiabatic temperature gradient. Without going into the derivation in any detail we state here that this gradient is given by:

$$\frac{\mathrm{d}T}{\mathrm{d}z} = \frac{\alpha g T}{c_p} \quad . \tag{3.30}$$

The constant g is the gravitational acceleration, T is temperature and c_p is the specific heat. Without further explanation we also want to remember that this gradient is understood to be at constant entropy. Detailed derivations of eq. 3.30 are given by Turcotte and Schubert (1982) and in many other geophysical teaching texts. If we insert realistic numbers we see that the adiabatic temperature gradient in the mantle is about 0.3–0.5 °C km^{-1}. In other words, the adiabatic temperature change between the surface and the base of a 100 km thick lithosphere is about 50 °C. For most geological processes within the crust this is negligible. However, for geodynamic processes that require the consideration of large vertical length scales in the mantle, the process is of relevance. It is particularly important for melting processes in the upper mantle (Fig. 3.11). In fact, because convection in the asthenosphere is rapid enough to equalize most conductive gradients, the adiabatic gradient is often the only temperature change with depth that there is.

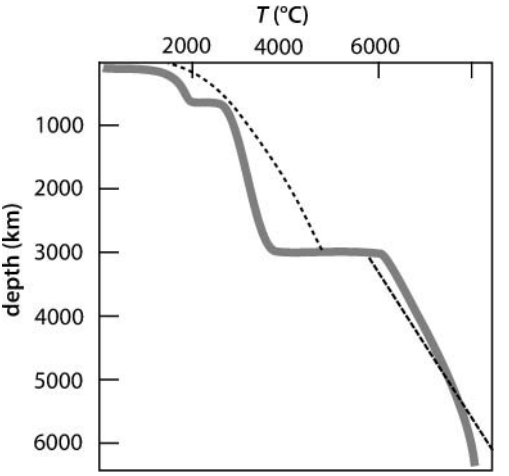


Figure 3.11. The temperature profile (thick line) and the melting curve (dashed line) between the earth's surface and the center of the earth in 6 300 km depth (after Jeanloz and Richter 1979; Jeanloz 1988). See Fig. 2.16 for scaling of this figure. In the mantle, the temperature increase is given by the adiabatic temperature gradient (eq. 3.30). The steps in the temperature profile arise from exothermic and endothermic reactions during phase transitions. Note that only the outer core is liquid according to this diagram. However, rapid exhumation of the upper mantle may lead to a cross over of the two curves above 500 km depth and therefore to partial melting. This is what happens underneath mid oceanic ridges or during continental extension

3.2.3 Chemical Heat Production

Different rocks are characterized by different internal heat contents defined by the strength of bonding of the atoms in the crystal lattices in the rock-forming minerals. During chemical reaction, the difference in heat content between reactants and products is released or consumed as *latent heat of reaction.* We abbreviate this chemically produced or consumed heat with S_{chem}. By far the largest majority of chemical reactions are *endothermic* when the temperature increases. Because of this, temperature rise of rocks may be buffered by the phase transition. Correspondingly, most reactions are exothermic when crossed down temperature. However, most chemical reactions have a positive slope in a pressure-temperature diagram. Thus exothermal reaction can not only be triggered by a *decrease* in temperature, but also by an *increase* in pressure (at constant temperature). In very general terms, we can chemical reactions that produce heat into three groups. In decreasing order of importance these are:

- **Phase transitions:** The chemically produced heat of reactions involving phase transitions is significant to the thermal budget of rocks.

- **Dehydration reactions:** In the solid state, dehydration reactions are the most important producer of reaction heat (Connolly and Thompson 1989; Peacock 1989). In the greenschist facies they produce of the order of $4 \cdot 10^6$ J per kg of released water. However, rocks contain only of the order of 4 % H_2O and this water is being released over quite a large temperature interval. Thus, the heat of reaction is fairly insignificant during regional metamorphism. Connolly and Thompson (1989) estimated that metamorphic reaction produce of the order of $5\text{–}10 \cdot 10^{-14}$ W cm^{-3}.
- **Solid - solid reactions:** The chemical heat production of solid – solid reaction is negligible for geological problems.

The geologically most important reactions that involve phase transitions are the melting reactions where the *latent heat of fusion* is released or the *latent heat of melting* is consumed. As a consequence, it is important to consider reaction heat when dealing with the thermal energy budget of migmatites and intrusions. A commonly used value for the latent heat of melting of rocks is $L = 320\,000$ J kg^{-1}. Evaporation and condensation reactions are also strongly exothermic and endothermic respectively, but they are not very important in the geodynamics of the lithosphere.

Quantitative Description of Chemical Heat Production. The rate of reaction heat production S_{chem} has the same units as any other heat production rate: W m^{-3}. It can be described by:

$$S_{\text{chem}} = L\rho \frac{\mathrm{d}V}{\mathrm{d}t} \quad . \tag{3.31}$$

In this equation L is the latent heat of reaction in J kg^{-1}. Since we think of the chemical heat production rate as a *volumetric* heat production rate, it is necessary to multiply L by the density ρ to convert it into a volumetric heat content. The expression $\mathrm{d}V/\mathrm{d}t$ is the volumetric proportion of the reaction that occurs per unit time (in s^{-1}). Note that V has the units of percent and not cubic meters. Thus, the equation determines the part of L that is freed in every time step of the reaction. Substituting eq. 3.31 into eq. 3.21 we can now formulate the temperature change during chemical heat production to be:

$$\frac{\partial T}{\partial t} = \frac{L}{c_p} \frac{\partial V}{\partial t} \quad . \tag{3.32}$$

If we consider one dimensional diffusion of heat in direction z as well, but neglect other heat sources we can write:

$$\frac{\partial T}{\partial t} = \kappa \frac{\partial^2 T}{\partial z^2} + \frac{L}{c_p} \frac{\partial V}{\partial t} \quad , \tag{3.33}$$

where the first term on the right side is the diffusion term discussed at length in eq. 3.6. You will recall from there that $\kappa = k/\rho c_p$. In this form of the

equation we also have neglected differences in density between the reactants and the products. It may help you to understand eq. 3.33 by formulating it in terms of energy rather than in terms of temperature. It then takes the form:

$$\frac{\partial H}{\partial t} = k\frac{\partial^2 T}{\partial z^2} + L\rho\frac{\partial V}{\partial t} \quad . \tag{3.34}$$

There, H is the heat content in $\mathrm{J\,m^{-3}}$. The conversion between heat and temperature is illustrated in Fig. 3.12 and was briefly discussed in eq. 3.3. In principle, it is possible to implement the heat of reaction quantitatively and describe the evolution of PT paths under consideration of buffering processes. However, the estimates of Thompson and England (1984), Connolly and Thompson (1989), Peacock (1989), Barr and Dahlen (1989) and others shows that the magnitude of reaction heat does not justify to implement such a model in great detail and that it is only important to consider latent heat when rocks melt. Then, reaction heat has indeed quite a significant effect on the thermal evolution of rocks and we will now discuss how to describe it.

Thermally Buffered Melting. Melting during prograde metamorphism in the upper amphibolite and granulite facies is a strongly endothermic process. Thus, the rate with which temperature increases during metamorphism at this grade will be buffered by the melting reactions. At univariant melting reactions, the temperature will remain constant until the phase transition from solid reactants to liquid products is complete. It is the very same reason why we have so much snow slush on our roads in spring: ice and water will both have a temperature of 0 °C, until all ice has melted, even if the air temperature has been above freezing for quite some time. For the same reason water will boil at a constant temperature of 100 °C, regardless of the heat added by the stove, until it all has evaporated. In the buffering interval, the amount of heat added to the rock from the outside is exactly balanced by the amount of heat consumed by the phase transition.

Most rocks consist of many chemical components in complicated chemical systems. As a consequence, they do not melt at a single temperature, but over a melting interval between their solidus (where the first melt appear during temperature increase) and liquidus (where the last remaining piece of rock melts). If we want to describe such rocks, we must find a formulation that allows us to release (or consume) the latent heat over a large temperature interval. For this it is useful to reformulate the rate of volume change from one phase to another from eq. 3.31 into:

$$\frac{\partial V}{\partial t} = \frac{\partial V}{\partial T}\frac{\partial T}{\partial t} \quad . \tag{3.35}$$

In this form it is easier to add the heat of reaction to the time derivative on the left side of eq. 3.33. This reads then as:

$$\left(c_p - L\frac{\partial V}{\partial T}\right)\frac{\partial T}{\partial t} = \frac{k}{\rho}\frac{\partial^2 T}{\partial z^2} \tag{3.36}$$

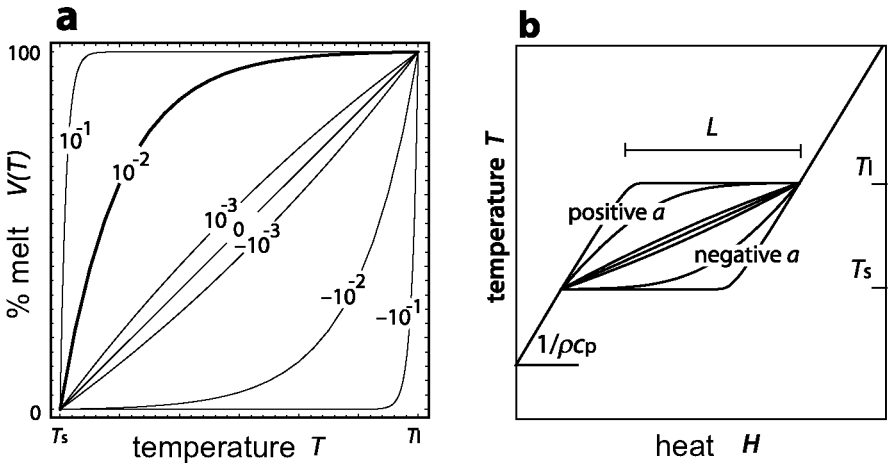


Figure 3.12. a A schematic model for the description of the relationship between melt volume and temperature. The curves are labeled for different values of the constant a in eq. 3.38. For $a = 0$, eq. 3.38 simplifies to the linear relationship $V(T) = T/(T_l - T_s)$. The thick drawn line is probably the most realistic curve for the melting of hydrated metapelitic rocks. **b** The relationship between heat content and temperature in the melting interval of a melting rock (shown between solidus temperature T_s and liquidus temperature T_l. The slope of the curves within the melting interval are for five different assumptions of the melting process according to eq. 3.38; after Stüwe 1995)

or:

$$\frac{\partial T}{\partial t} = \kappa_{\text{mod}} \frac{\partial^2 T}{\partial z^2} \quad . \tag{3.37}$$

There, $\kappa_{\text{mod}} = k/(\rho c_{\text{mod}})$ is the modified diffusivity and c_{mod} is a modified heat capacity: $c_{\text{mod}} = c_p - L\rho(\partial V/\partial T)$. We wrote down these equations to illustrate that chemical buffering of thermal processes can be described by modifying the diffusivity. The numerical problems that can arise when doing this were first described by Price and Slack (1954).

How Do Rocks Melt? Many migmatite terrains have equilibrated around 700°C, although their peak pressures vary considerably from terrain to terrain. This leads one to suspect that this common peak temperature may be unrelated to the burial depth of the terrain and has other causes. The proximity of 700°C to the solidus temperature of rocks suggests that thermal buffering by the effects of latent heat is a conceivable cause of this common phenomenon (Stüwe 1995). In order to explore this hypothesis, it is necessary to know the amount of melt that is formed at or around 700°C, because only eutectic melts form at the solidus. Petrogenetic studies have rapidly advanced over the last five years and can – in principle – be used to determine the relationship between melt volume and temperature in the melting inter-

val (White et al. 2001; Riesco et al. 2004; Kelsey et al. 2005). However, for a ball park estimate, a useful relationship may be:

$$V(T) = \frac{e^{aT} - e^{aT_s}}{e^{aT_l} - e^{aT_s}} \tag{3.38}$$

In this freely invented equation, a can be adjusted to explore different relationships (i.e. different melting models) between melt proportion, $V(T)$ and temperature T between the solidus temperature T_s and the liquidus temperature T_l (Fig. 3.12). If a has a large positive value, then most of the rock melts near the solidus. If a adapts large negative values, then most of the melting occurs near the liquidus. For values of $a \rightarrow$ zero, melting becomes linear in temperature. Many rocks contain hydrated phases at the onset of melting. As water is a great catalyst for melting processes, it is likely that more melting will occur near the solidus than near the liquidus. Realistic values for a are therefore likely to be positive and possibly around $a = 0.01$. If we accept eq. 3.38 as a melting model, then the change of melt volume with temperature dV/dT can be derived from eq. 3.36 to be the following:

$$\frac{dV}{dT} = \left(\frac{a}{e^{aT_l} - e^{aT_s}}\right) e^{aT} \quad . \tag{3.39}$$

This relationship can be used directly to estimate the influence of melting on the thermal evolution of rocks. Stüwe (1995) showed that it may be large enough to account for the equilibration of parageneses in the low-pressure high-temperature metamorphic environment.

3.3 Principles of Heat Advection

Heat can be transported *actively* by the motion of warm rocks. We discern between *advection* and *convection* of heat. *Advection* is generally used if the active transport of heat is only in one direction, for example the transport of heat by an intrusion that moves in the vertical direction. *Convection* is generally used when referring to material transport in a closed loop, for example the convection of mantle material in the asthenosphere, or that of fluids in a hydrothermal system. In this book, we only deal with advection. One-dimensional active transport of heat (for example in the vertical direction z), relative to the z direction may be described by:

$$\frac{\partial T}{\partial t} = u\frac{\partial T}{\partial z} \quad . \tag{3.40}$$

In eq. 3.40, u is the transport velocity; the derivative $\partial T/\partial z$ describes the thermal gradient and $\partial T/\partial t$ is the change of temperature with time. For positive u, eq. 3.40 describes transport *against* the spatial coordinate z: transport is from high z towards lower z (Fig. B.7 illustrates the sign of u). Eq. 3.40 is

also called the transport equation and is equally applicable to the transport of mass, for example during advection of concentration profiles through a crystal lattice. In three dimensions, the heat advection equation is:

$$\frac{\partial T}{\partial t} = u_x \frac{\partial T}{\partial x} + u_y \frac{\partial T}{\partial y} + u_z \frac{\partial T}{\partial z} \quad . \tag{3.41}$$

Although we shall discuss below some examples where eq. 3.40 may be solved analytically, the vast majority of geological problems require numerical solutions of eq. 3.40. Indeed, although eq. 3.40 looks much simpler to solve than eq. 3.6 it is much more complicated to solve it. In numerical solutions of advection problems we are often faced by the problem of *numerical diffusion* (sect. B.2.3, B.2.3). One way to avoid problems with numerical diffusion is by converting the problem from an advection problem into one where there is no advection, but moving boundary conditions; i.e. we describe the problem in a Lagrangian, rather than a Eulerian reference frame (sect. 4.2.2). In Lagrangian descriptions the material is transported through the coordinate system. Eulerian reference frames move with the material.

There are three different important mechanisms by which heat is advected in the lithosphere that require different methods of description. These three mechanisms are:

- advection of heat by magmas, e. g. magmatic intrusion;
- advection of heat by solid rock motion, e. g. erosion or deformation;
- advection of heat by fluids, e. g. during infiltration events.

The difference between these three processes in terms of their mathematical description arises mainly from the relative rates of advective and diffusive processes. These three processes will therefore now be discussed separately.

3.3.1 Heat Advection by Magma

During intrusion of magma from deeper into shallower levels in the crust, the heat of the magma is transported to higher crustal levels by the motion of the magma itself. The process of magmatic intrusion is - in general - much faster than most other geological processes, for example the thermal equilibration during contact metamorphism. It is therefore usually not necessary to describe the intrusion process itself by an advection equation. For questions related to the *thermal* evolution of contact metamorphism is usually suffices to assume that intrusion is infinitely rapid and can be described by *instantaneous heating problems* (s. sect. 3.6). Simple examples for good model assumptions to describe intrusions into the crust are given by Jaeger (1964) and for intrusion at the Moho (under plating) are given by Wells (1980) and Huppert and Sparks 1988). Thermal processes related to intrusion will be discussed at length in sect. 3.6. Nevertheless, we want to note that country rocks that heated during contact metamorphism are often referred to as being

"advectively heated". Strictly speaking this is not correct as it is *conduction* from the intrusion into the country rocks, not *advection* itself that causes contact metamorphism (s. sect. 6.3.3).

3.3.2 Heat Advection by Solid Rock

Any movement and deformation of rocks will carry the heat it contains with it. for example, during exhumation of rocks by erosion, the lithosphere (and its heat) are moved vertically upwards (s. sect. 4.3.4). The column is moved *through* a surface of constant temperature - the surface of earth. Erosion is therefore a heat advection process. In a similar way, any other motion of rocks, for example during thrusting or folding may be interpreted as an advective process (if viewed in an externally fixed Eulerian reference frame, s. p. 144). Here we will only discuss one-dimensional, vertical advection of heat to and from the earth's surface. The time scale of continental denudation processes is comparable to the time scale of thermal equilibration on the scale of the crust and we can therefore not neglect to consider both processes at the same time. If we want to describe advection and diffusion of heat simultaneously, then we must expand eq. 3.40 by the diffusion term from eq. 3.6. The equation that must be solved becomes:

$$\frac{\partial T}{\partial t} = \kappa \frac{\partial^2 T}{\partial z^2} + u \frac{\partial T}{\partial z} \quad . \tag{3.42}$$

A schematic illustration how the two processes interact to shape a geotherm during erosion is shown in Fig. 3.13. You may also want to consider to expand this equation by yet another term describing heat production (e.g. the term in eq. 3.21). Then, we would have a complete thermal energy balance to describe any thermal problem. However, it is strongly recommended to perform a careful evaluation of the relative importance of heat conduction, advection and production for a given problem to decide which terms must be considered and which not. Such a comparison may be done similar to that we have shown on p. 66. Here we consider only diffusion and advection.

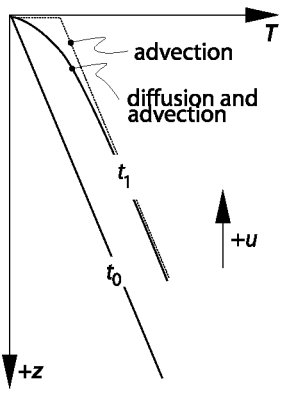


Figure 3.13. Schematic illustration of one-dimensional advection of heat by erosion. The coordinate system is fixed with $z = 0$ at the earth's surface. Temperature profiles through the crust are shown for two times: at the onset of erosion t_0, at which a linear geotherm is assumed and a later time t_1. The advection rate u is positive upwards. In the shown time interval the erosion process *advects* the geotherm by $u \times t_1$ meters upwards. Simultaneous *diffusion* causes the curvature of the temperature profile

Geotherms During Erosion and Sedimentation. Eq. 3.42 can be used to describe the evolution of a crustal geotherm that is advected through the earth's surface, for example during erosion (upwards advection) or sedimentation (downwards advection) (Benfield 1949) or – on a smaller scale – the evolution of temperature profiles in soil during accumulation or ablation of snow. For simple assumptions about advection rate (e.g. that this is constant) and boundary conditions, analytical solutions of eq. 3.42 may be found. In the following we present some examples of useful boundary conditions for both steady state and time dependent scenarios.

• *Steady state geotherms during erosion.* For fixed boundary conditions a thermal steady state will be reached by geotherms during erosion if the upwards advection of heat is exactly balanced by conductive cooling from the surface. Then, there is no temperature change with time (i.e. $\partial T/\partial t = 0$) and eq. 3.42 simplifies to:

$$\frac{\partial}{\partial z}\left(\frac{\partial T}{\partial z}\right) = -\frac{u}{\kappa}\frac{\partial T}{\partial z} \quad . \tag{3.43}$$

(Spiegel 1968, Mancktelow and Grasemann 1997). Using $\lambda = u/\kappa$ and $v = \partial T/\partial z$ this can also be written as: $v'(z) = -\lambda v(z)$. This is a very common differential equation and its solution is: $v(z) = v(0)\exp(-\lambda z)$. Written in full:

$$\frac{\partial T}{\partial z} = -\frac{\partial T}{\partial z}|_{(z=0)} \mathrm{e}^{-(uz/\kappa)} \quad . \tag{3.44}$$

The derivation is explained in the appendix on p. 416. There are three geologically relevant boundary conditions with which this equation can be easily integrated a 2nd time to give a closed solution for steady state thermal profiles during advection. In all three examples we assume that one of the two required boundary conditions is given by zero surface temperature ($T_{(z=0)} = 0$), but any surface temperature can simply be added to the given solutions.

• 1. If the other boundary conditions is defined by the mean geothermal gradient g at $z = 0$, then this boundary condition can be directly inserted into eq. 3.44 and integrated a 2nd time. The solution is:

$$T = \frac{g\kappa}{u}\left(1 - \mathrm{e}^{-(uz/\kappa)}\right) \quad . \tag{3.45}$$

• 2. If the lower boundary is fixed with the temperature T_∞ as the depth goes to infinity ($T_{(z\to\infty)} = T_\infty$) then a steady state solution of eq. 3.42 is:

$$T = T_\infty\left(1 - \mathrm{e}^{-(uz/\kappa)}\right) \quad . \tag{3.46}$$

• 3. If the lower boundary is fixed at the temperature $T = T_L$ at a fixed depth $z = L$, a steady state the temperature is described by the solution:

$$T = T_L\left(\frac{1 - \mathrm{e}^{-(uz/\kappa)}}{1 - \mathrm{e}^{-(uL/\kappa)}}\right) \quad . \tag{3.47}$$

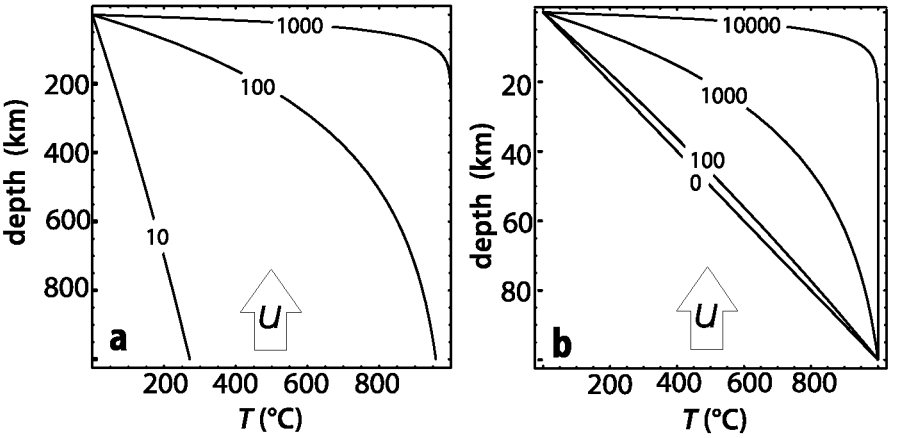


Figure 3.14. Examples of steady state geotherms during simultaneous upwards advection and diffusion. **a** Geotherms fixed at the surface with $T = 0$ and at infinite depth at temperature $T_\infty = 1000°\mathrm{C}$ (calculated with eq. 3.46). **b** Geotherms fixed at the surface with $T = 0$ and at depth $L = 100\,000$ with $T_L = 1000°\mathrm{C}$ (calculated with eq. 3.47). Contours are for different advection rates u labeled in meters per million years and $\kappa = 10^{-6}\mathrm{m}^2\mathrm{s}^{-1}$

This latter case is quite a realistic scenario for the lithosphere where is may be fair to assume that the temperature at its base is constant (Stüwe et al. 1993b) (Fig. 3.14). More refined solutions for a range of other problems including variably erosion rate and erosion of a heat producing crust are discussed by Mancktelow and Grasemann (1997) as well as Batt and Braun (1997).

• *Time dependent evolutions and cooling paths.* Time dependent solutions may also be found for the two problems discussed above (Mancktelow and Grasemann 1997). Here we present a time dependent evolution for yet another scenario, namely one where there is no lower boundary condition, i.e. the advection of a semi-infinite half space with a constant thermal gradient g through the surface. For that, a solution of eq. 3.42 is:

$$T = gz - gut + \frac{g}{2}\left((z+ut)\mathrm{e}^{uz/\kappa}\mathrm{erfc}\left(\frac{z+ut}{\sqrt{4\kappa t}}\right) + (ut-z)\mathrm{erfc}\left(\frac{z-ut}{\sqrt{4\kappa t}}\right)\right) \quad (3.48)$$

(Benfield 1949; Carslaw and Jaeger 1959, chapter XV; Mancktelow and Grasemann 1997). While this equation may be used to calculate time dependent geotherms, most geologist do actually not want to know temperatures as a function of depth but the temporal evolution of a given rock. In other words, the evolution of temperature in a Lagrangian reference frame instead of the Eulerian description given by the equations above (s. sect. 4.2.2). Within the reference frames of the geotherm descriptions, rocks move (are advected) through the coordinate system at the rate u. Thus, if they were at the initial depth z_i at the onset of erosion, they change their depth to:

$$z = z_i - ut \tag{3.49}$$

at time t. Thus, if we want to calculate cooling histories of a given rock that are due to its exhumation by erosion, we can simply use eqs. 3.46, 3.47 or 3.48 and substitute eq. 3.49 for z. Cooling curves that were calculated with this approach and eq. 3.48 are shown in Fig. 3.15.

3.3.3 Heat Advection by Fluids

Heat may also be advected by fluids that circulate through rocks. Heating of rocks due to fluid advection is different from the previous examples, because only part of the rock volume is being advected, namely the fluids that fill the pore volume. Thus, when formulating an advective term in an advection-diffusion equation, we need to take care so that we describe only the advection of a fraction of the total rock volume. In a general one-dimensional form eq. 3.40 can be written as:

$$\frac{\partial T}{\partial t} = \phi v_f \left(\frac{\rho_f c_{pf}}{\rho c_p} \right) \frac{\partial T}{\partial z} \quad , \tag{3.50}$$

(McKenzie 1984). There, ϕ is the porosity of the rock (s. sect. 6.1.3) and v_f is the fluid flux in $m^3m^{-2}s^{-1}$. The product ϕv_f is the fluid volume that is transported per unit time and per unit area through the rock. This product has the units of $m\,s^{-1}$, which corresponds to the standard definition of fluxes (sect. 4.5.3). It is called the *volumetric fluid flux*. ρ and ρ_f are the densities and c_p as well as c_{pf} are the specific heat capacities, both of the rock and the fluid, respectively. The term inside the brackets is the ratio of the volumetric heat capacities (volumetric heat capacity = heat capacity × density) of the fluid to that of the rock.

Eq. 3.50 may be used to describe the thermal effects of fluid advection. However, in many geological processes heat advection by fluids occurs on similar time scales as heat conduction. Thus, it is usually necessary to expand

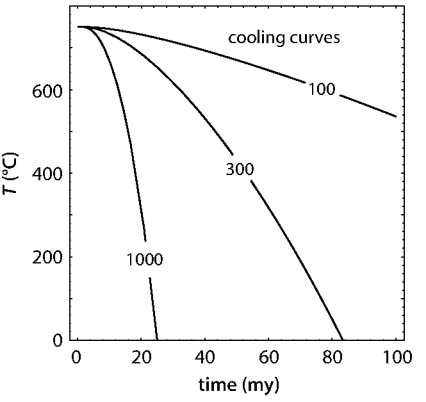


Figure 3.15. Cooling curves of rocks that cool as the consequence of exhumation only. The three curves are for three different erosion rates in $m\,my^{-1}$. Calculated with eqs. 3.48 and 3.49. Other assumptions are: $g = 30°C\ km^{-1}$ and $\kappa = 10^{-6}m^2s^{-1}$. An important feature of the cooling curves is that the cooling rate increases with decreasing temperature. This relationship is opposite to cooling following contact metamorphism

eq. 3.50 by a term describing diffusion as we did in eq. 3.50. The importance of the transport of heat by fluids for the thermal evolution of the crust was discussed by Bickle and McKenzie (1987), Connolly and Thompson (1989) as well as Peacock (1989). These authors agree that the fluid flux that may be caused by metamorphic dehydration reactions is less than about 1 kg fluid per square meter and per year. This is not enough to transport heat very efficiently by fluids. Peacock (1989) estimated that the thermal evolution of rocks can only be influenced by fluids if these are focused into narrow zones from regions as wide as 10 km. We can conclude that heat advection by fluids is insignificant at least when we are interested in thermal budgets of the crust as a whole. Clearly, in special geological settings, for example hydrothermal cells, heat advection by fluids may be the controlling process. Note also that equations similar to eq. 3.50 may be used to describe advection of fluids through rocks in general and are among the important equations governing fluid flow through fractured media.

3.3.4 The Peclet Number

In many geological processes the diffusion rates and advection rates are of the same order of magnitude. This is true for fluid infiltration processes, for erosion that occurs during thermal equilibration of the crust, thermal profiles around moving faults and many more (sect. 3.7.4). In such processes the Peclet number Pe is a useful parameter which can be used to estimate the relative influence of diffusive and advective processes. The Peclet number is defined as:

$$Pe = \frac{ul}{\kappa} = \frac{ul\rho c_p}{k} \tag{3.51}$$

where u is the rate of advection, κ the diffusivity and l the characteristic length scale of the advection process. The second way to write the Peclet number is only inserted above to remind us that the diffusivity is the ratio of conductivity k, density ρ and heat capacity c_p. If Pe is about 1, then diffusion and advection are of similar importance to a process. If Pe is much larger than 1, advection dominates the process. If Pe is much smaller than 1, then diffusion dominates the process. Eq. 3.51 can be used to derive advection rates. For example, on Fig. 3.16 isotherms have been displaced by a thrust. Consider the 400°C isotherm. On any length scale that is larger than l_2, this isotherms is simply displaced by the material advection of the hanging wall (i.e. $Pe > 1$). On the length scale of l_1 (dark shaped region) both diffusion and advection have played a role in shaping the curved isotherm (i.e. $Pe = 1$). On the length scale l_1 (light shaded region), diffusion has dominated and the isotherm appears not displaced across the fault (i.e. $Pe < 1$).

Aside from its importance for the description of thermal processes, the Peclet number finds many other application. For example, Bickle and McKenzie (1987) have used the Peclet number for some fundamental interpretations about the relative importance of diffusive and advective processes during

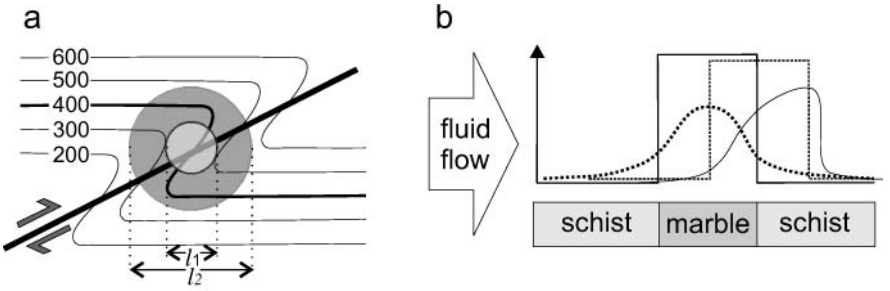


Figure 3.16. a Schematic cartoon showing the displacement of isotherms during thrusting. Note that – within the length scale l_1 – diffusion has eliminated any displacement of isotherms across the fault, while above length scale l_2 only displacement, but no curvature is visible. **b** Diffusion and advection of isotopes from a layered sequence. The vertical axis is isotope concentration, the horizontal axis is a profile across the three rock types shown. The continuous step shaped line shows the concentrations at the time of formation. The dotted line after subsequent diffusion ($Pe < 1$), the dashed line after fluid infiltration ($Pe > 1$), but without diffusion ($Pe = 1$). The asymmetric line during both ($Pe = 1$)

fluid infiltration of rocks (Fig. 3.16 and Sandiford (2002) has used the Peclet number to argue about the stability of orogens.

3.4 Heat in the Continental Lithosphere

In the past sections we have discussed the three fundamental processes that produce and redistribute heat in the lithosphere: *conduction*, *production* and *advection*. In summary from above we can conclude that a full one-dimensional description of the thermal energy balance for the lithosphere has the form:

$$\frac{\partial T}{\partial t} = \left(\frac{k}{\rho c_p}\right)\frac{\partial^2 T}{\partial z^2} + u\frac{\partial T}{\partial z} + \left(\frac{S}{\rho c_p}\right) \quad , \tag{3.52}$$

where the diffusivity is the ratio of conductivity and density × heat capacity: $\kappa = k/\rho c_p$ and the heat production S may have mechanical, chemical and radioactive contributions (s. eq. 3.22). In this section we will apply our knowledge from the last sections and describe aspects of the thermal structure of the continental lithosphere. For this, not all of the terms in eq. 3.52 may be relevant. Table 3.4 shows (as a summary from the last sections), which thermal energy parameters may be relevant to thermal estimates on the scale of the lithosphere. In order to set the scene, we begin with a brief explanation how the lithosphere may be defined thermally and what "geotherms" actually are.

Table 3.4. Summary of possible heat transfer mechanisms in the crust and their potential relevance for the heat budget of metamorphic terrains. The column "*relevance*" makes some very crude suggestions whether the processes listed in the 1st and 2nd column can be of relevance for terrain scale metamorphism. The relationships shown in the 4th column are the key relationships that should be considered when estimating the relevance of a given transfer mechanism in a given terrain. *Conduction* is only relevant if the time scale of conduction, t_{eq}, is comparable to the ratio of the square of length scale l and thermal diffusivity κ. *Advection* is only relevant if the Peclet number, Pe, is larger than 1, where u is the advection rate, l length scale of the advective process and κ the diffusivity. *Heat production* is only relevant if the heat production rate S times its duration t produces significant amounts of thermal energy (which may then be converted into temperature rise using density and heat capacity). For *radioactivity* this product is generally large on geological time scales, for *chemical* heat production this product is only large for melting reactions and for *mechanical* heat production it is given by the product of stress and strain rate. Both stress and strain rate are not well known and the relevance of mechanical heat production to metamorphism remains a much debated topic in earth sciences. Acronyms for selected key references are: ER77 = England and Richardson (1977); ET84 = England and Thompson (1984); HS88 = Huppert and Sparks (1988); BM87 = Bickle and McKenzie (1987); J64 = Jaeger (1964); L86 = Lux et al. (1986); L70 = Lachenbruch (1970); S98 = Sandiford et al. (1998); C90 = Chamberlain and Sonder (1990); ME90 = Molnar and England (1990a); S98 = Stüwe (1998a); S95 = Stüwe (1995); P89 = Peacock (1989); CT89 = Connolly and Thompson (1989)

transfer mechanism	geological process		geol. relevance	relationship to consider	key ref.
conduction			large	$t_{eq} = l^2/\kappa$	ER77; ET84
advection	by fluids		rare		BM87
	by magma	- intrusion	large		J64; L86
		- underplating	large	$Pe = ul/\kappa$	HS88
	by rock	- erosion	large		
		- deformation	large		
production	radioactive		large		L70; S98; C90
	mechanical		unknown		ME90; S98
	chemical	- melting	large	$S \times t$	S95
		- dehydration	small		P89; CT89
		- solid-solid	negligible		P89

Thermal Definition of the Lithosphere. The lithosphere may be defined thermally or mechanically (s. sect. 2.4.1). According to the thermal definition, the lithosphere is the outer shell of the earth, in which heat is transported primarily by conduction. In contrast, in the asthenosphere, heat

is transported primarily by convection. Thus, the lithosphere itself is nothing but a *thermal boundary layer* of the earth, although we defined thermal boundary layer somewhat differently in Fig. 2.19 . This boundary layer looses heat at all times through the earth's surface into the atmosphere and further – by radiation – into space. The average heat flow through the surface of the continents is 0.065 $\mathrm{W\,m^{-2}}$. The total surface area of the continents is about $A_c = 2 \cdot 10^8$ $\mathrm{km^2}$. Thus, the total heat loss of earth from the continents is $1.3 \cdot 10^{13}$ $\mathrm{J\,s^{-1}}$. This heat loss is balanced by radioactive heat production within the lithosphere and by heat flow into the lithosphere from the asthenosphere, so that this thermal boundary layer has a largely constant temperature profile, if it is not disturbed by orogenesis. Thermally stabilized lithosphere has a thickness between 100 and 200 km (Pollack and Chapman 1977).

Definition of Geotherms. The function that describes temperature in the lithosphere as a function of depth is what we call a *geotherm*. We discern:

– stable or steady state geotherms,
– transient geotherms.

• *Stable geotherms.* Stable or *steady state* geotherms form by long term thermal equilibration of the lithosphere (sect. 3.4.1). In general, this is understood that the term "steady state" refers to a geotherm in a stationary lithosphere and we shall use it in this way in this section. However, in other reference frames, steady state geotherms may also occur in a moving lithosphere (for example a lithosphere that moves upwards relative to the surface during erosion, s. p. 82). In sect. 3.7.3 and 3.5.2 we discuss examples of steady state geotherms in Eulerian reference frames.

In most geological situations, the temperatures of steady state geotherms increase steadily with depth. Stable geotherms are only found in regions that have had at least about 100 my time for equilibration and have not changed in thickness during this time. The origin of this number is discussed in sect. 3.1.4. Thus, active orogens are *not* characterized by stable geotherms. Regardless, the calculation of steady state geotherms in orogens may help us to estimate the maximum or minimum temperatures that can be attained during an orogenic process at a given depth. This maximum or minimum possible temperature is often called *potential temperature* (e.g. Sandiford and Powell 1990).

• *Transient geotherms.* Transient geotherms are only valid for a particular point in time. In some geological situations, transient geotherms do *not* increase steadily with depth and the change of the geotherm with time can be different in different depths. For example, after rapid stacking of nappes, rocks may simultaneously heat above a major thrust, but cool below it (sect. 7.4.2). In principle it is possible to document such relationships of transient geotherms in space and time with careful observation in the field.

If they can be documented, then such information is invaluable for the interpretation of the nature of a tectonometamorphic process (s. sect. 7.4.2). We discuss the transient evolution of geotherms during orogenic processes in several other chapters (e. g. sect. 3.6 and 6.2.1).

In this section we calculate the quantitative shape of stable continental geotherms as shown schematically in Fig. 2.18.

3.4.1 Stable Geotherms: The Relevant Equation

For the stable or steady state case, the heat conduction equation (eq. 3.6) or the full thermal energy balance (eq. 3.52) can be simplified enough so that it is possible to find simple analytical solutions that provide useful tools to understand the thermal structure of the lithosphere, even without a lot of mathematical knowledge. This is therefore a good example to familiarize ourselves with the involved thought process. The equation we must solve is the now familiar heat conduction equation with a heat production term:

$$\frac{\partial T}{\partial t} = \left(\frac{k}{\rho c_p}\right) \frac{\partial^2 T}{\partial z^2} + \frac{S}{\rho c_p} \quad . \tag{3.53}$$

We need the heat production term to account for radioactivity, which is of substantial importance to stable geotherms. However, we can neglect advective terms as we consider only steady state. For *steady state* geotherms, there is no change of the temperature with time (s. sect. 3.1.2). This means:

$$\frac{\partial T}{\partial t} = 0 \quad .$$

Eq. 3.53 simplifies to:

$$\left(\frac{k}{\rho c_p}\right) \frac{\mathrm{d}^2 T}{\mathrm{d}z^2} + \frac{S}{\rho c_p} = 0 \quad . \tag{3.54}$$

Note that eq. 3.54 is no *partial* differential equation anymore. By canceling out of the constants we get:

$$k \frac{\mathrm{d}^2 T}{\mathrm{d}z^2} = -S \quad . \tag{3.55}$$

The integration of this equation forms the basis for all calculations of stable geotherms.

Geotherms Without Radioactivity. Equation 3.55 may be integrated the easiest, if we neglect radioactive heat production all together. Although we have shown in chap. 2 and sect. 3.2.1 how important radioactivity is for the temperature profiles of the lithosphere (e. g. Fig. 2.18) we can easiest understand the integration of eq. 3.55 by assuming the heat production is negligible: $S = 0$. Eq. 3.55 then simplifies to:

$$k\frac{\mathrm{d}^2T}{\mathrm{d}z^2} = 0 \qquad \text{or even:} \qquad \frac{\mathrm{d}^2T}{\mathrm{d}z^2} = 0 \quad . \tag{3.56}$$

As this still is a differential equation of the second order, me must integrate it twice to solve it. A first integration gives:

$$\frac{\mathrm{d}T}{\mathrm{d}z} = C_1 \tag{3.57}$$

and a second:

$$T = C_1 z + C_2 \quad . \tag{3.58}$$

The two integration constants C_1 and C_2 must be determined by the geological boundary conditions (s. sect. B.1.1). For example, we can assume that we know that the temperature at the surface of earth (at $z = 0$) is constant and has the value $T = 0$. Then, for eq. 3.58 to hold, C_2 must be zero so that the temperature is zero at $z = 0$. It we assume a thermal definition of the lithosphere, then we can determine the other constant with the assumption that $T = T_\mathrm{l}$ at depth $z = z_\mathrm{l}$ where T_l and z_l are the temperature and the depth of the base of the lithosphere. With this assumption C_1 must have the value $C_1 = T_\mathrm{l}/z_\mathrm{l}$. The temperature as a function of depth is therefore described by:

$$T = z\frac{T_\mathrm{l}}{z_\mathrm{l}} \quad . \tag{3.59}$$

Equation 3.59 describes a linear temperature profile between the surface and the base of the lithosphere. This is not very surprising as we have assumed no heat production and no other reasons why the temperature profile should be anything else but a straight line between the assumptions at the boundaries. With a thermal conductivity of $k = 2$–$3\ \mathrm{W\,m^{-1}\,°C^{-1}}$, and $T_\mathrm{l} = 1\,200\,°\mathrm{C}$ as well as a lithospheric thickness of $z_\mathrm{l} = 100\ \mathrm{km}$, our equation describes a surface heat flow of 0.024–0.036 $\mathrm{W\,m^{-2}}$. This value is much lower than the average surface heat flow of the continents which is between 0.04 and 0.08 $\mathrm{W\,m^{-2}}$. This is one of the proofs of the existence of radioactivity in the lithosphere. We can easily conclude that eq. 3.56 is not a very good model description and that it is wiser to integrate eq. 3.55 using a meaningful function that describes S as a function of depth. When we do so, we will always assume that $S = S_\mathrm{rad}$, i.e. there is no other heat production sources but the radiogenic ones. In the steady state mechanical or chemical heat production sources are irrelevant.

3.4.2 The Contribution of Radioactivity

The radioactive heat production rate of rocks is of the order of some microwatts per cubic meter (s. Table 3.3). However, unusually high heat productions have been reported from a series of locations around the world, in particular from Australia (McLaren et al. 1999) (Fig. 3.7). A typical value measured from samples at the earth's surface is: $S = 2-5\mu\mathrm{W\,m^{-3}} \equiv 2-5\cdot10^{-6}\ \mathrm{W\,m^{-3}}$. The contribution of this value to the surface heat flow is simply the heat production times its depth extent. For example, if the heat production were constant in the entire crust of 30 km thickness ($z_c = 30$ km) then the surface heat flow caused by radioactivity is:

$$q = q_s = S \cdot z_c = 0.03\mathrm{Wm^{-2}} \quad . \tag{3.60}$$

This can be converted into a temperature gradient using eq. 3.1 where we have seen that the thermal gradient has the units of heat flow divided by the thermal conductivity. If the thermal conductivity is $k = 3\ \mathrm{W\,m^{-1}\,K^{-1}}$, then the assumptions from above indicate: $\mathrm{d}T/\mathrm{d}z = q/k = 0.05\,^{\circ}\mathrm{C\,m^{-1}} = 50\,^{\circ}\mathrm{C\,km^{-1}}$. This geothermal gradient of 50 °C per kilometer is only due to the contribution of radioactivity. The mantle heat flow would have to be added to this. Since the resulting thermal gradient would be much higher than just about all thermal gradients measured on earth, we can conclude that the radioactivity of rocks measured at the earth's surface must be higher than that of the rest of the crust (for more information on the radioactive heat flow contribution see p. 289).

The Distribution of Heat Production. The considerations above have shown that the radioactive heat production of the crust is unlikely to be that of the surface in the entire crust. Various studies have therefore explored the vertical distribution of heat producing elements (e.g. Cermak and Rybach 1989; Pinet and Jaupart 1987; Pribnow and Hurter 1998; Heier and Brown 1978). The most simple model for a heat source distribution is that the heat production is constant to the depth z_{rad} and zero below that. This model depth, to which the crust produces radioactive heat at the same rate as on the surface, has been elegantly determined using the relationship of two independent sets of data that can be measured at the surface: The surface heat flow and the heat production rate at the surface, S_0. Roy et al. (1968) explored this relationship in the eastern US and its significance was described by Lachenbruch (1968; 1970; 1971). They found a roughly linear relationship between these two parameters (Fig. 3.17). The straight line that fits these data has the form:

$$q_s = q_m + q_{rad} = q_m + z_{rad} S_0 \quad . \tag{3.61}$$

In this equation, q_s is the surface heat flow, q_m is the mantle heat flow, q_{rad} the radiogenically produced heat flow and z_{rad} is the thickness of a hypothetical layer in which radioactive heat is produced at the same rate as on the surface. q_m can be measured from the intersection of the line with the heat flow axis

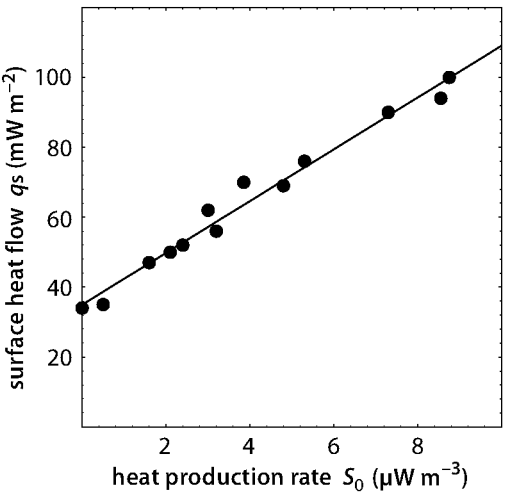


Figure 3.17. Measured data of surface heat flow q_s and surface heat production S_0 in the eastern US. The best line that fits the data is described by the equation $q_s = 0.035 + 7\,413 S_0$. Accordingly, the thickness of the layer that produces heat at a rate S is 7 413 m thick and the contribution of mantle heat flow to the total heat flow is 0.035 W m^{-2} (after Roy et al. 1968)

and the value of z_{rad} is given by its slope. The data of Roy et al. (1968) show that z_{rad} is about 7 km in the eastern US. Similar considerations in other areas indicate thicknesses of 10–15 km. Of course, the crust does not produce heat constantly in this layer and no heat at all below it, but the relationship is useful to estimate the total heat production in the crust. This is given by the product $z_{rad} S_0$. This product corresponds to the area underneath the different model curves in Fig. 3.18.

For the calculation of geotherms in the following sections we will use different model assumptions about the distribution of radioactivity with depth (Fig. 3.18). We will see that these different assumptions have important different implications for the temperatures in both the crust and the mantle part of the lithosphere. So we want to remember that both the *magnitude* and the *distribution* of radioactive heat production are important for the thermal budget of the crust (Sandiford et al. 1998; 2002; Chamberlain and Sonder 1990).

3.4.3 Geotherms with Heat Flow Boundary Condition

We begin our calculations of stable geotherms by integrating eq. 3.55 by assuming a somewhat different boundary condition at the base than what we have used to derive eq. 3.59. We will assume as boundary condition that the *heat flow* at the Moho is constant, instead of assuming the *temperature* at the base of the lithosphere. We do this for three reasons: Firstly, because this boundary condition has been the assumption of England and Thompson (1984). Their model has become the classical model to describe Barrovian metamorphism and is therefore the obvious starting point. Secondly – following the argument of England and Richardson (1977) – we want to argue that we know the heat flow at the Moho much better than the temperature

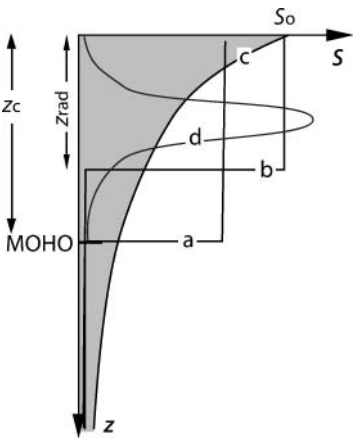


Figure 3.18. Four simple models describing the distribution of heat production with depth in the crust (s. Haack 1983). The total heat production of the crust is given by the area underneath the model curves. It is the same for all four models and is shaded for model *c*. *a* Constant concentration in the entire crust and no heat production in the mantle. *b* Constant concentration in the upper crust in a layer with the thickness z_{rad} and no heat production below that. *c* Exponential drop off of the heat production with depth. *d* Heat production peaking in the middle crust. Such a situation may occur if a crust with heat source distribution *c* is buried underneath a low heat producing sedimentary pile. Note that the surface heat production is different in the different models, while the total heat production is the same

or depth of the base of the lithosphere. Thirdly, we assume this boundary condition because the integration of eq. 3.55 is quite easy with this boundary condition.

Constant Heat Production. If the heat production is independent of depth, S is a constant. Integration of eq. 3.55 results in:

$$k\frac{\mathrm{d}T}{\mathrm{d}z} = -Sz + C_1 \quad . \tag{3.62}$$

The left side of this equation has the units of heat flow. The constant of integration C_1 must be derived from the boundary conditions. If we know the mantle heat flow at the Moho, and assume that it is constant through time, we can describe this condition as: q_{m}=constant at $z = z_{\mathrm{c}}$. If no details are known about the changes of the heat flow at this depth, then this is the most simple assumption and corresponds therefore with the idea of a good model (sect. 1.1). With this assumption, the constant of integration must be:

$$C_1 = Sz_{\mathrm{c}} + q_{\mathrm{m}} \quad ,$$

so that at the depth $z = z_{\mathrm{c}}$ (z_{c} is the crustal thickness) we get: $k\left(\frac{\mathrm{d}T}{\mathrm{d}z}\right) = q_{\mathrm{m}}$. After inserting C_1 into eq. 3.62 and integrating a second time we get:

$$kT = -\frac{Sz^2}{2} + Sz_{\mathrm{c}}z + q_{\mathrm{m}}z + C_2 \quad . \tag{3.63}$$

The most meaningful assumption for the second boundary is that the temperature at the surface at $z = 0$ has the value $T = 0$. This gives us that $C_2 = 0$. After some simplification we get the following expression:

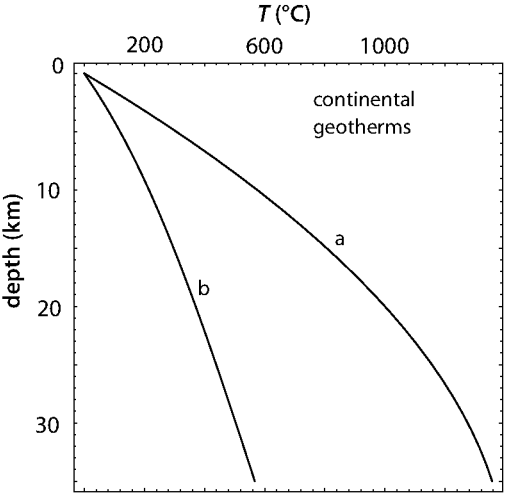


Figure 3.19. Two calculated continental geotherm. It was assumed that the mantle heat flow has the value $q_m = 0.025\ \mathrm{W\,m^{-2}}$. Curve *a* was calculated assuming that the entire crust has a constant heat production. It was calculated with eq. 3.64. Curve *b* was calculated with eq. 3.70 assuming that the heat production decreases exponentially with depth ($h_r = 10$ km). For *a* and *b* following other assumptions were made: $z_c = 35$ km; $S = 3 \cdot 10^{-6}\ \mathrm{W\,m^{-3}}$ (= S_0 in eq. 3.70); $k = 2\ \mathrm{J\,s^{-1}\,m^{-1}\,K^{-1}}$

$$T = \frac{Sz}{k}\left(z_c - \frac{z}{2}\right) + \frac{q_m z}{k} \quad . \tag{3.64}$$

Equation 3.64 describes the temperature as a function of depth in the crust. It is an *analytical solution* of the differential equation eq. 3.55. An analysis of the units can be used to confirm the internal consistency of this equation. A geotherm calculated with eq. 3.64 is shown in Fig. 3.19a. It is immediately obvious that the temperatures are much too high, although we made meaningful assumptions for mantle heat flow, crustal thickness and surface heat production. However, we also made the incorrect assumption that the heat production is constant in the whole crust and has everywhere the same value as that measured on the surface. This assumption is in contrast to what we argued on p. 93, where we discussed the distribution of heat production with depth. The *real* distribution of the heat producing elements in the crust is not very well known, but we can help ourselves with one of the models from Fig. 3.18. If we make the assumption *b* from that figure (heat is only produced at a constant rate down to the depth z_{rad}), then there is a discontinuity in the heat production with depth. As a consequence, we can integrate eq. 3.55 only to the depth $z = z_{rad}$. We get a result that is very similar to eq. 3.64:

$$T = \frac{Sz}{k}\left(z_{rad} - \frac{z}{2}\right) + \frac{q_m z}{k} \quad \text{in the region:} \quad z < z_{rad} \quad . \tag{3.65}$$

For larger depths we can help ourselves with the knowledge that the geothermal gradient must be a straight line (i.e. the heat flow must be constant and is q_m) because there is no disturbing influence or heat production anymore (s. eq. 3.59). The temperature at the base of the heat producing layer may be found by evaluating eq. 3.65 at the depth $z = z_{rad}$. Below this depth the temperature $q_m(z - z_{rad})/k$ must be added to the temperature at the base of the assumed heat producing layer. It follows that:

$$T = \frac{S z_{\text{rad}}^2}{2k} + \frac{q_m z}{k} \quad \text{in the region:} \quad z > z_{\text{rad}} \quad . \tag{3.66}$$

If you do not understand what we did in the last lines, draw a little sketch that illustrates every written sentence. Equations 3.65 and 3.66 are those that England and Thompson (1984) used for their classic model explaining regional metamorphism (s. sect. 6.2.1). If we insert reasonable values for the parameters, then we get temperatures at the base of the crust between 500 °C and 600 °C. We also get a depth for the base of the lithosphere (the depth of the 1 200 °C isotherm) around 100 to 150 km. Both corresponds to a large number of observations from the stable continental shields and the equation provides a good model description of continental geotherms.

Exponential Heat Production. A much more elegant model assumption for the distribution of the heat production in the crust is the assumption that there is a continuous exponential drop off in radioactive heat production with depth (model *c* in Fig. 3.18). This model has the great advantage that there is no discontinuity in the heat production in the crust and we do therefore not need several equations to describe a single geotherm as we did above. A continuous distribution of radioactivity with depth also appears intuitively more appropriate. We assume that:

$$S_{(z)} = S_0 e^{\left(-\frac{z}{h_r}\right)} \quad . \tag{3.67}$$

The variable h_r is called the *characteristic drop off* or *skin depth* of heat production. According to eq. 3.67, the heat production at depth $z = h_r$ is only the 1/e part of the heat production at the surface S_0. Our new starting equation is now:

$$k\frac{d^2T}{dz^2} = -S_0 e^{\left(-\frac{z}{h_r}\right)} \quad . \tag{3.68}$$

The integration of this equation is a bit harder than those of the previous section but it still only involves the integration of simple exponential functions (s. Table C.2). A first integration gives:

$$k\frac{dT}{dz} = h_r S_0 e^{\left(-\frac{z}{h_r}\right)} + C_1 \quad . \tag{3.69}$$

Note that we used the "product rule" for this integration (s. appendix C, Table C.1, C.2). Assuming the same boundary condition that we used in the last section, the constant of integration is:

$$C_1 = -h_r S_0 e^{\left(-\frac{z_c}{h_r}\right)} + q_m \quad .$$

After inserting this constant into eq. 3.69 and a second integration we get:

$$kT = -h_r^2 S_0 e^{\left(-\frac{z}{h_r}\right)} - z h_r S_0 e^{\left(-\frac{z_c}{h_r}\right)} + q_m z + C_2 \quad . \tag{3.70}$$

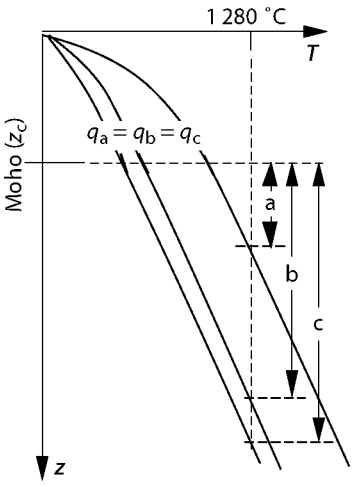


Figure 3.20. This illustration shows how the thickness of the mantle part of a thermally defined lithosphere is automatically determined by the condition of a constant mantle heat flow at the Moho. All three geotherms on this figure have the same thermal gradient at the Moho and therefore the same heat flow through the Moho. However, the mantle parts of the lithosphere (thickness shown by double arrows) is very different for the three examples

The second constant must be $C_2 = h_r^2 S_0$ so that the condition $T = 0$ at the surface ($z = 0$) is fulfilled. Fig. 3.19b shows a geotherm calculated with eq. 3.70 after inserting this integration constant and using reasonable values for all parameters. We see that the geotherm has a realistic shape. Eq.3.70 is a good model description of stable continental geotherms.

How do Geotherms Continue at Larger Depth? In the previous sections we have used a known mantle heat flow as the lower boundary condition for our integration of the steady state heat flow equation. Our calculations were therefore confined to the description of the crust. The thickness of the mantle part of the lithosphere was implicitly determined by the boundary conditions (Fig. 3.20). The depth of the base of the lithosphere is thermally defined by the temperature $T_l \approx 1\,200\,°C$, so we only need to find the depth where our geotherm reaches this temperature to determine the thickness of the mantle part of the lithosphere. With a thermal conductivity of $k = 3$, and a mantle heat flow at the Moho of 0.03 $W\,m^{-2}$, the steady state thermal gradient is $10\,°C\,km^{-1}$ at the Moho. As we assumed no radioactive heat production in the mantle part of the lithosphere, this gradient will be constant in the remainder of the mantle lithosphere. If the Moho-temperature is 500 °C then this gradient implies a thickness of the mantle part of the lithosphere of 70 km (if we define the lithospheric base thermally by the depth where the geotherm intersects the 1 200 °C isotherm).

This is quite a reasonable value for the thickness of the mantle lithosphere. Nevertheless, we have only implied this thickness of the mantle part of the lithosphere whereas the equations of the last sections were only designed to describe the crust. Because there is many reasons why we may want to prescribe the thickness of the mantle lithosphere as well (for example because we know it from considerations of surface elevation or lateral buoyancy forces)

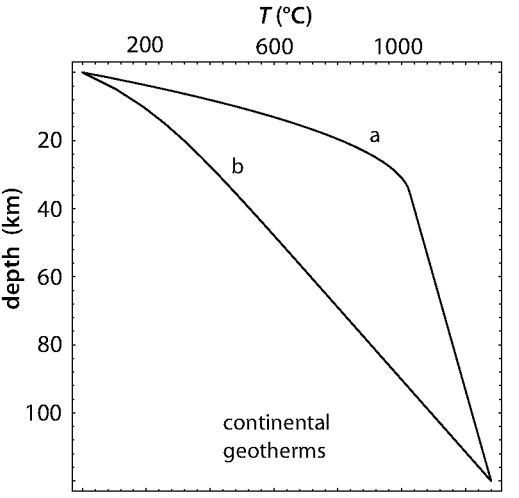


Figure 3.21. Examples of continental geotherms calculated with a lower boundary condition of a fixed temperature at the base of the lithosphere. Geotherm *a* was calculated assuming constant heat production in the crust and no heat production in the mantle lithosphere. Geotherm *b* was calculated for a continuous, exponentially decreasing heat production using eq. 3.74. The temperature T_l is assumed to be 1 280 °C; all other parameters are the same as in Fig. 3.19

a lower boundary condition at the base of the lithosphere is often more useful. In the next section we discuss such alternative lower boundary conditions.

3.4.4 Geotherms with Fixed Basal Boundary Condition

If we define the lithosphere thermally, we implicitly state that we know the temperature at its base. An obvious choice for a lower boundary condition may therefore be: $T = T_l$ at the depth $z = z_l$. This choice allows us to describe temperatures in the entire lithosphere. However, we have to pay for this advantage by having to deal with various discontinuities of the parameters at the Moho, for example density. This complicates the integration of eq. 3.55.

Constant Heat Production. In a model where we assume constant heat production rate in the crust and no heat production in the mantle part of the lithosphere, density *and* heat production are discontinuous at the Moho. This complicates the integration of eq. 3.55 dramatically. We will not present the equations here and refer the interested reader to the original works of Sandiford and Powell (1990) or Zhou and Sandiford (1992). However, for comparison with the thermal model of England and Thompson (1984) we show an example of a geotherm calculated with these assumptions as curve *a* in Fig. 3.21. We see that this model results in unrealistically high temperatures if we assume the surface heat production rate to be representative for the whole crust.

Exponential Heat Production. If we assume a continuous heat production in the whole lithosphere that decreases exponentially with depth, then we can derive from eq. 3.68 an elegant and simple description of stable continental geotherms. After two integrations we get:

$$kT = -h_r^2 S_0 e^{\left(-\frac{z}{h_r}\right)} + C_1 z + C_2 \quad . \tag{3.71}$$

Both constants of integration can only be evaluated after this second integration. The second integration constant C_2 is fairly easy to determine if we assume again that $T = 0$ at the surface where $z = 0$. At $z = 0$ the exponential term in eq. 3.71 goes to 1 so that C_2 must be:

$$C_2 = h_r^2 S_0 \quad . \tag{3.72}$$

The lower boundary condition of $T = T_l$ at the depth $z = z_l$ can be evaluated by rearranging eq. 3.71:

$$C_1 = \frac{kT_l}{z_l} + \frac{h_r^2 S_0 e^{\left(-\frac{z_l}{h_r}\right)}}{z_l} - \frac{C_2}{z_l} \quad . \tag{3.73}$$

After inserting both constants into eq. 3.71 we get:

$$T = \frac{zT_l}{z_l} + \frac{h_r^2 S_0}{k}\left(\left(1 - e^{\left(-\frac{z}{h_r}\right)}\right) - \left(1 - e^{\left(-\frac{z_l}{h_r}\right)}\right)\frac{z}{z_l}\right) \quad . \tag{3.74}$$

Curve *b* in Fig. 3.21 is an example of a geotherm calculated with this relationship. Eq. 3.74 provides a realistic and useful description of stable continental geotherms and has been presented and used by a number of authors (Zhou and Sandiford 1992; Stüwe and Sandiford 1995; Mancktelow and Grasemann 1997: eq. 13).

More General Formulations. Using a lower boundary condition where we explicitly prescribe the thickness of the mantle part of the lithosphere (as we did in the previous section) is extremely useful to explore the influence of thickness variations of crust and mantle lithosphere on the temperatures in the crust. In order to do this more efficiently, it is useful to introduce two new parameters: the vertical thickening (or thinning) strain of the crust and that of the lithosphere. We call these parameters f_c and f_l and will discuss them in some detail in sect. 4.2.3 (s. a. sect. 5.1)(Sandiford and Powell 1990). A value of $f_c = 2$ means that the crust is twice as thick as in the reference state (Sandiford and Powell 1990; Zhou and Sandiford 1992). Using these parameters, eq. 3.74 can be generalized. All we need to do is multiply the reference crustal and lithospheric thicknesses z_c and z_l with their respective thickening strains. We also need to be careful with the thickness of the skin depth of the heat production which also changes with crustal thickening or thinning. Eq. 3.67 becomes:

$$S_{(z)} = S_0 e^{\left(-\frac{z}{h_r f_c}\right)} \quad . \tag{3.75}$$

If we substitute of these generalized formulations for the thicknesses of crust, lithosphere and skin depth into eq. 3.68 and integrate it subject to the same boundary conditions we used for eq. 3.74, we arrive at:

$$T = \frac{zT_l}{f_l z_l} + \frac{f_c^2 h_r^2 S_0}{k}\left(\left(1 - e^{\left(-\frac{z}{f_c h_r}\right)}\right) - \left(1 - e^{\left(-\frac{z_l f_l}{f_c h_r}\right)}\right)\frac{z}{f_l z_l}\right) \quad . \tag{3.76}$$

This equation is the most general and most elegant form of a geotherm equation that can be used to calculate temperatures in the entire lithosphere for any thickening geometry of our choice. We only need to keep in mind that the temperatures we caluclate are only *potential temperatures* which means that they may not be reached during an orogenic cycle. In the next section we will use this equation to calculate some important temperatures.

• *Moho Temperature from eq. 3.76.* For many thermal and mechanical considerations the Moho-temperature is a meaningful parameter that can be used to characterize the thermal structure of the entire lithosphere (sect. 6.2.2). If we want to calculate this temperature for a series of crustal and lithospheric thicknesses, we must evaluate eq. 3.76 at $z = z_c$ for a series of f_c and f_l. Figure 3.22 shows an f_c-f_l-diagram of Moho-temperature. It shows that the Moho-temperature does not change very much for homogeneous thickening of the entire lithosphere (which would appear on this figure as a diagonal path from $f_c = f_l = 1$ towards $f_c = f_l = 2$). This is because the heating effect of the increased thickness of the heat producing crust is almost balanced by the cooling effect of the thickened mantle part of the lithosphere. We have indicated this effect already in the discussion of Fig. 2.18a. However, the strong curvature of the contours on Fig. 3.22 shows that in very thin crusts ($f_c << 1$), the Moho-temperature depends largely on the thickness of the mantle part of the lithosphere. Also, in very *thick* crusts ($f_c >> 1$), the Moho-temperature depends mostly on crustal thickness. This is because there the Moho-temperature is largely determined by the radioactivity in the crust. Small changes in crustal thickness will lead to quite significant temperature changes, while the thickness of the mantle part of the lithosphere is comparably insignificant.

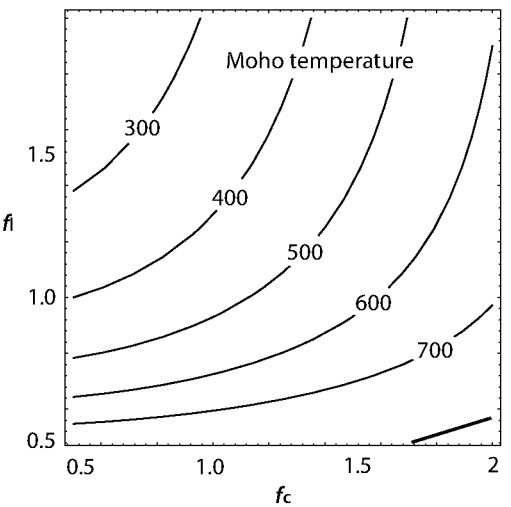


Figure 3.22. Moho-temperatures of continental lithosphere for different crustal thickening strains (expressed by f_c) and for different total thickening strains of the lithosphere (expressed by f_l). The diagram was calculated with eq. 3.76 assuming $z = z_c$. The assumption of the parameters are the same as in Fig. 3.21. The thick line in the bottom right hand corner of the diagram marks the limit of the allowed part of parameter space. It is explained in more detail in the context of Fig. 4.7

• *Surface Heat flow from eq. 3.76.* The surface heat flow q_s is one of the few important thermal parameters of the lithosphere that can be measured directly. It is therefore a much used parameter to define thermal features in the lithosphere (e.g. Zhou and Sandiford 1992). Within the models discussed above, heat flow is simply given by the derivative of the geotherm equations with respect to depth and divided by the thermal conductivity. The *surface* heat flow q_s can then be found by evaluating these derivatives at the depth $z = 0$. For a boundary condition at the base of the lithosphere (and exponentially decreasing heat production with depth) we get from from eq. 3.76:

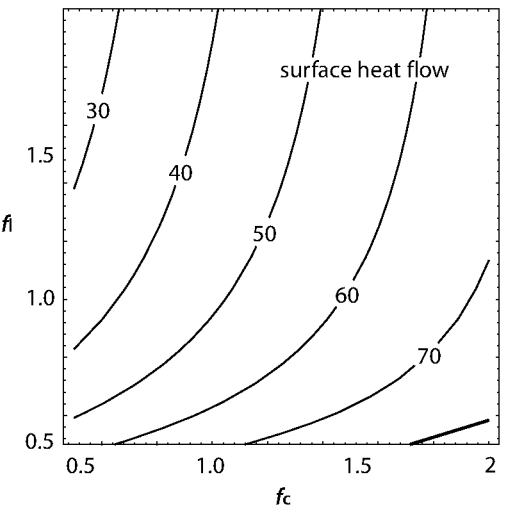


Figure 3.23. The surface heat flow (contoured in 10^{-3}W m−2) for a range of crustal thicknesses (expressed by the vertical thickening strain f_c) and for a range of total thicknesses of the lithosphere (expressed by the vertical thickening strain f_l). The diagram was calculated with eq. 3.77. The assumptions for all parameters are the same as in Fig. 3.21, curve *b*

$$q_s = k\frac{T_l}{f_l z_l} + S_0 f_c h_r \left(1 - \frac{f_c h_r}{f_l z_l}\left(1 - e^{\left(-\frac{f_l z_l}{f_c h_r}\right)}\right)\right) \tag{3.77}$$

Figure 3.23 shows an f_c-f_l-diagram, which is contoured for q_s. We can see that the surface heat flow depends much more on the crustal thickness than the Moho-temperature does (compare Fig. 3.22).

3.5 Heat in the Oceanic Lithosphere

Oceanic lithosphere contains practically no radioactive elements. Thus, one could think that it is simple to describe stable oceanic geotherms. In analogy to continental geotherms we might want to formulate the geotherm equation as:

$$k\frac{d^2T}{dz^2} = 0 \quad . \tag{3.78}$$

After one integration we get:

$$k\frac{\mathrm{d}T}{\mathrm{d}z} = C_1 \quad .$$

Using the boundary conditions that are well-known to us from sect. 3.4.3 with: $q = q_\mathrm{m}$ at the depth $z = z_\mathrm{c}$, we get:

$$kT = q_\mathrm{m} z + C_2 \quad .$$

If we also assume that $T = 0$ at the surface $z = 0$, then $C_2 = 0$ and we can write:

$$T = z\frac{q_\mathrm{m}}{k} \quad , \tag{3.79}$$

... if the same boundary conditions as in sect. 3.4.3 are used. However, eq. 3.79 is not a very good model to describe oceanic lithosphere. A simple consideration of the time scale of conductive equilibration will show us why: oceanic lithosphere is produced at the mid-oceanic ridges and it gets its thickness only by its increasing age. The oldest oceanic lithosphere is about 150 my old (Fig. 2.4). However, in sect. 3.1.4 we showed that the characteristic time scale of equilibration for thermally stabilized lithosphere is of the order of 150 my or more! We can conclude that oceanic lithosphere is *not* thermally stabilized. The assumption underlying eq. 3.78 is wrong. There is no thermally stabilized oceanic lithosphere! We can not assume that $\mathrm{d}T / \mathrm{d}t = 0$ and we must solve the time dependent diffusion equation (eq. 3.6).

3.5.1 Aging Oceanic Lithosphere

The oceanic crust, that is produced from partial mantle melts at the mid-oceanic ridges is only of the order of 5–8 km thick. That is, it is much thinner than the continental crust. At the mid-oceanic ridge the thickness of the entire oceanic lithosphere is that of the crust (Fig. 3.24). The high potential energy of the ridges forces this crust to move away from the ridge. As the oceanic crust ages and moves further and further away from the mid-oceanic ridge, the asthenosphere cools and becomes part of the oceanic mantle lithosphere. It is often said that the mantle successively "freezes" onto the base of the oceanic lithosphere as it ages. While this describes the process quite intuitively, it is somewhat incorrect as the asthenosphere itself is not molten. Regardless, the process of the successive cooling of the aging oceanic lithosphere can be described with the diffusion equation using simple initial and boundary conditions. Indeed, the description of oceanic lithosphere with these boundary conditions has become one of the most successful models of plate tectonic theory (s. a. Sclater et al. 1980). It is called the *half space cooling model* (s. sect. 3.6.1).

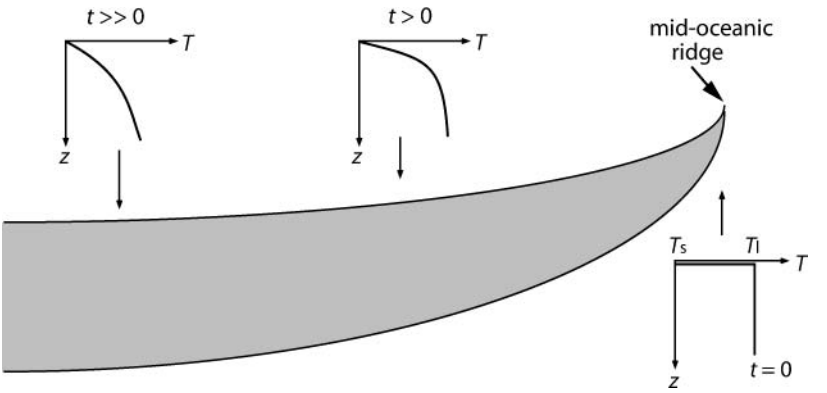


Figure 3.24. Thickness and thermal profile of oceanic lithosphere at a series of points. The oceanic crust is not drawn separately. On the scale of this sketch it would appear as a very narrow band of constant thickness near the upper boundary of the gray shaded region

The Half Space Cooling Model. As any other problem in the theory of heat conduction, the half space cooling model relies on the integration of eq. 3.6, using a set of boundary and initial conditions. These conditions are provided by geological observation: The temperature at the surface of mid-oceanic ridges is that of the water temperature. For simplicity, we assume that it is $T_s = 0$. Below the ridge, the mantle temperature is almost constant – convection equalizes all temperature gradients. Thus, we can write a very simple initial condition describing the thermal profile below mid-oceanic ridges:

- $T = T_s$ at the depth $z = 0$ and:
- $T = T_l$ in all depths $z > 0$ at time $t = 0$.

This initial condition is illustrated in T-z-diagram on the bottom right corner of Fig. 3.24. For the upper boundary condition it is obvious to assume that the temperature at the ocean floor remains constant. As there is effectively no lower boundary, we assume that it lies at infinity and that the temperature there is $T = T_l$. We can write this as follows:

- $T = T_s$ at $z = 0$ for all $t > 0$ and:
- $T = T_l$ at $z = \infty$ for all $t > 0$.

(Fig. 3.24). The solution of the heat conduction equation for these boundary conditions is:

$$T = T_s + (T_l - T_s)\mathrm{erf}\left(\frac{z}{\sqrt{4\kappa t}}\right) \quad . \tag{3.80}$$

This solution is already a bit familiar to us from section 3.1.3 and we discuss this solution in some more detail in sect. 3.6.1 (s. a. sect. 3.1.3). Fig. 3.25a

shows temperature profiles through oceanic lithosphere of different ages, that were calculated with eq. 3.80. The curves correspond to the two sketches of thermal profiles in the middle and on the left of Fig. 3.24. Fig. 3.25b shows the depth of a series of isotherms as a function of age.

Surface Heat Flow: The Test for the Model. Temperature profiles calculated with this model for the cooling oceanic lithosphere can not be tested directly, as we cannot drill deep enough into the oceanic lithosphere. Our observations are confined to parameters which we can measure near the surface. One of these parameters is easy to measure and very useful to infer the thermal profile: the surface heat flow (Pollack et al. 1993) (Fig. 3.1). The surface heat flow is the product of thermal conductivity and the thermal gradient at $z = 0$. This can be calculated from eq. 3.80 and can be compared with measured data in the oceans. To obtain surface heat flow we must differentiate eq. 3.80 with respect to depth and evaluate it at $z = 0$. From eq. 3.80 this is:

$$q_s = k(T_l - T_s)\frac{\mathrm{d}\left(\mathrm{erf}\left(\frac{z}{\sqrt{4\kappa t}}\right)\right)}{\mathrm{d}z}_{,z=0} \quad . \tag{3.81}$$

As the error function itself is an integral (see eq. 3.15), it is easy to differentiate eq. 3.80 (sect. 3.1.3). We get:

$$q_s = k(T_l - T_s)\sqrt{\frac{1}{\pi\kappa t}} \quad . \tag{3.82}$$

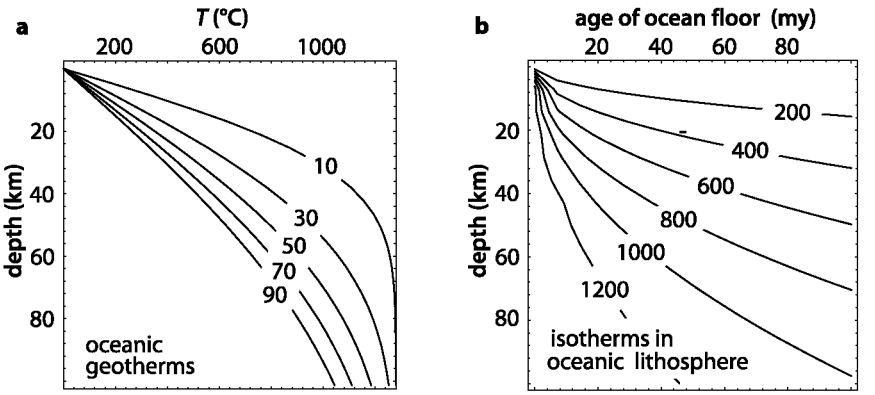


Figure 3.25. a Temperature T versus depth profiles through oceanic lithosphere at a number of different ages labeled in my. **b** The depth of isotherms (in °C) in oceanic lithosphere as a function of age between 0 and 100 my. The curves on both figures were calculated with eq. 3.80 assuming $T_l = 1\,280\,°C$. The age can be converted into distance from the mid-oceanic ridge by using $x = u/t$ where x is the distance from the ridge and u is the rifting rate. Compare the curves also with Fig. 3.40

This equation can be generalized for the description of different oceanic plates with different rifting rates. For this, we express the rifting rate u as $u = x/t$. There, x is the distance from the mid-oceanic ridge and t is the age. If we replace t in eq. 3.82 by x/u, we get:

$$q_s = k(T_l - T_s)\sqrt{\frac{u}{\pi\kappa x}} \quad . \tag{3.83}$$

Eq. 3.83 shows us that the surface heat flow as a function of distance from the mid-oceanic ridge is a square root function. Fig. 3.26 shows the surface heat flow in oceanic lithosphere as calculated with eq. 3.83. The heat flow data of Sclater et al. (1980) show that these curves correspond well with heat flow measured in the deep oceans. In sect. 4.4.1 we will show that the half space cooling model is not only a good description for the temperatures and heat flow in oceanic lithosphere, but can also be used to describe the water depth of the oceans. It can even be used to calculate the magnitude of the ridge push force (sect. 5.3.2). The relationship between all these parameters that are described with the half space cooling model is called the *age-depth-heat flow relationship* of oceanic lithosphere. This age-depth-heat flow relationship corresponds fantastically well with our observations up to an age of the oceanic lithosphere of 50 – 80 my. The age-depth-heat flow relationship is generally accepted as one of the greatest successes of plate tectonic theory.

Alternative Models for the Aging Oceanic Lithosphere. The half space cooling model is the most famous model for the description of oceanic lithosphere, but there is several reasons why it may not be a perfect description:

– The half space cooling model assumes implicitly that the heat flow at the base of the lithosphere changes through time. It is not clear that this should be so.

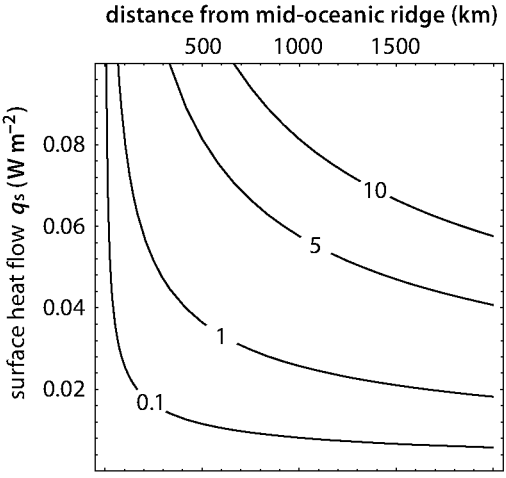


Figure 3.26. The surface heat flow of oceanic lithosphere as a function of age and therefore as a function of distance from the mid-oceanic ridge as calculated with eq. 3.83. Contours are for different rifting rate labeled in cm y^{-1}

– The model fails to describe the water depth and the surface heat flow of oceanic lithosphere beyond an age of about 80 my.

Moreover, various recent studies have shown that the increase in water depth and changes in heat flow with distance from the ridge deviate a bit from the half space cooling model and that there is a relationship between seafloor subsidence rate and height of the ridge (Dumoulin et al. 2001). One possible alternative model is to assume that the mantle heat flow through the base of the lithosphere is kept constant by small scale convection (Doin and Fleitout 1996). This assumption leads to a description which corresponds much better with the long term evolution of oceanic lithosphere than the half space cooling model. This idea is know by the name of *CHABLIS-model*. This name is an acronym for: **C***onstant* **H***eat flow* **A***pplied to* **B***ottom of* **L***ithospheric* **I**s*otherm* . Some authors have also argued that the observed seafloor depth and heat flow can be better explained if small amounts of radiogenic heat production of the thin oceanic crust are considered (Hillier and Watts 2005).

3.5.2 Subduction Zones

The description of the kinematics, thermal evolution and dynamics of subduction zones is a fundamentally two-dimensional problem. It is the first problem in this book for which we require more than one spatial coordinate to characterize the essence of the problem (Fig. 3.27). Many problems related to subduction zones concern the accretionary wedge that forms near the surface between the surface of the subducting slab and the upper plate. Dynamic and kinematic models for accretionary wedges will be discussed in sect. 6.2.3 and also in sect. 5.3.2. Here we discuss some general aspects about the deep thermal structure of subduction zone environments.

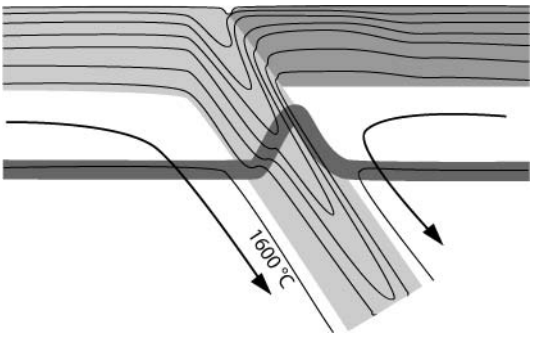


Figure 3.27. Schematic illustration of the temperature distribution in subduction zones. the subducted lithosphere is shaded light, the upper plate dark. The thick dark line that follows the 1 600 °C-isotherm outside the subduction zone is the Clapeyron-curve. It marks the olivine-spinel phase transition

Isotherms in Subduction Zones. Fig. 3.27 shows, schematically, the shape of isotherms in subduction zones. In the subducting slab, the isotherms will be bent and subducted with the slab. The further they are subducted, the more they merge to the center of the slab as both surfaces of the subducting slab equilibrate with the surrounding mantle temperatures. A thermal steady state will be reached when the curvature of the isotherms is large enough so that the rate of thermal equilibration is balanced by the subducting velocity (s. Fig. 3.3; s. Molnar and England 1995). In this stage, *diffusion* (which leads to the decay of the high curvature of the temperature profile in the tip of the subducting slab) will be balanced by *advection* (which moves the isotherms to larger depths). A steady state is reached that is very similar to the balance discussed in the second comparison on page 3.2 and also equivalent to the steady state that landforms between incising drainages may reach (discussed in Fig. 4.37). The time that is needed by subduction zones to reach this thermal steady state depends on the thickness of the plate and on the subduction rate. It can be estimated with the Peclet number (sect. 3.3.4).

At a temperature of about 1 600 °C, which is in about 400 km depth, olivine reacts to form spinel. The depth of this phase transition is called the *Clapeyron-Curve*. This reaction is *exothermic* with about $1.7 \cdot 10^5$ J kg^{-1}. Thus, the isotherms in this depth have a kink. The positive slope of the Clapeyron curve in P-T-space causes that the Clapeyron curve is somewhat higher within the subducting slab than it is outside. At a depth of 650 km (about 1 700 °C) there is another kink in the geotherm, caused by the phase transition from spinel to oxide (not illustrated on Fig. 3.27). The qualitative

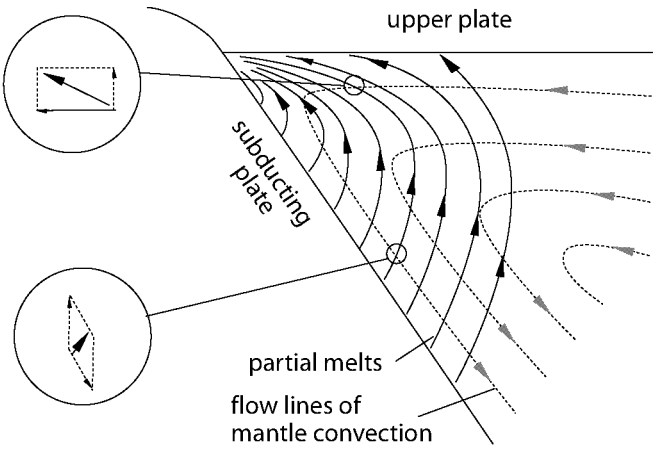


Figure 3.28. The motion of melts in and above the Benioff zone according to Spiegelman and McKenzie (1987). The dashed lines show the convective motion in the asthenosphere, the continuous lines are the motion of the partial melts. The enlarged sections show how the velocity field of the partial melts is given by the sum of the upward velocity of the melt and the motion in the mantle wedge

direction of this kink is opposite to that of the Clapeyron curve as the spinel-oxide phase transition is *endothermic.*

Fig. 3.27 shows schematically that the isotherms within the upper plate are closer to the surface near the subduction zone than they are in the far field. This is because of the dehydration of the subducting plate and the consequential rise of partial melts and other hot fluids. This leads typically to high temperature metamorphism in the rocks of the upper plate and ultimately to the development of magmatic arcs (see next section). This is in contrast to the very *low* temperatures that occur in the subducting plate up to very large depths. This coupled occurrence of low-pressure - high-temperature and high-pressure - low-temperature metamorphism was recognized by Miyashiro (1973) as one of the characteristic features of metamorphic terrains in subduction zone environments. He called this a *paired metamorphic belt.*

Island Arcs and Subduction Zones. An interesting observation in the upper plate of subduction zones is that there is volcanic arcs that always form a narrow line that is exactly where the seismically active surface between the subducting slab and the upper plate is about 150 km deep (Isacks and Barazangi 1977). In subduction zones that have a dip of 45° this implies a horizontal distance of the arc from the trench of 100–150 km. If the subduction angle is steeper, then this distance is shorter and vice versa. This observation is true for the distance of the Aleute-volcanoes to the Aleute Trench, for the distance of the Indonesian volcanoes from the Java Trench and many other volcanic arcs around the globe. This observation is not trivial to explain. The volcanics that erupt from these volcanoes are derived from partial melts in the mantle wedge that melted during fluid infiltration of fluids that were derived by dehydration of sediments on the surface of the subducting slab in the Benioff-zone. This zone stretches for several hundreds of kilometers along the surface of the subducting slab and is definitely much wider than the width of the volcanic arcs on the surface. Some authors have suggested that there are important pressure sensitive dehydration reactions that occur in exactly 150 km depth, but there is little petrological evidence for this.

An alternative explanation was suggested by Spiegelman and McKenzie (1987) (Fig. 3.28). Their model describes the motion of partial melts through the mantle wedge as the sum of two vector fields:

1. The motion of the asthenosphere in the mantle wedge. This motion follows the wedge and is illustrated in Fig. 3.28 by the dashed lines.
2. The motion of the partial melts. Partial melt is produced continuously along the surface of the subducting plate and moves vertically upwards.

The sum of the two velocity fields results in curved paths that converge at the tip of the mantle wedge (Fig. 3.28). This elegant model is a beautiful example for a successful model description of fluid flow in deforming rocks.

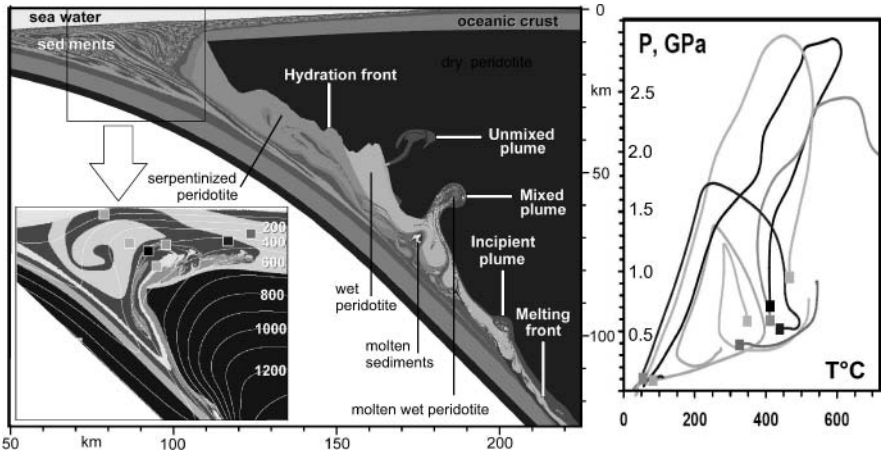


Figure 3.29. Integrated thermomechanical model of Gerya and Yuen (2003) to describe subduction related processes. The shown model also considers metamorphic processes, for example dehydration reactions and is set up to investigate the development of mixed and unmixed plumes in the mantle wedge in response to slab dehydration (Gerya pers. comm. 2006). Different gray shades are different layers. The inset at left shows more detail in the accretionary wedge but is actually from a different model run. The *P-T* diagram at right shows *P-T* paths of different rocks in the wedge as indicated by the symbols in the inset at left. Note that crustal rocks can easily reach 2.5 GPa by being dragged down along the surface of the subducted slab. Because they are then rapidly exhumed within the same wedge, they have not found time to heat up and remain in the eclogite and blueschist facies (s. Fig. 7.1)

***P-T* Paths in Subduction Zones.** Although the model shown in Fig. 3.28 is extremely elegant, a range of observations and new modeling results have made it somewhat redundant. Geologists have noted that arc volcanoes are not as narrow as thought by Isaacks and Barazangi (1977) and our recent understanding of dehydration processes on subducted slabs have indicated that the temperature range of dehydration may be small enough to cause some focusing of fluids without having to appeal to the model of Fig. 3.28. One of the most sophisticated models that have recently been used to describe such processes is the model of Gerya and Yuen (2003) (Fig. 3.29).

3.6 Thermal Evolution of Intrusions

Intrusion of magmatic rocks into higher levels in the crust is an important geodynamic process that can be responsible for a large range of thermal, chemical and mechanical changes in the crust. Intrusive rocks, as well as their contact aureoles, are familiar to us from field observations. Thus, their geodynamic interpretations can often be tested directly with structural and petrological data. The process of intrusion itself is a very efficient mechanism

for the transport of heat. Thus, most intrusions do not cool very much on their intrusive path and their temperature may be used to infer the temperature of rocks at the depth of their origin. There are two important reasons, why the quantitative description of the thermal evolution of intrusions is quite simple:

- In comparison to the duration of a contact metamorphic event or the duration of an orogenic cycle, the rate of intrusion is very rapid. Thus, for the thermal modeling of intrusions it is possible to assume that their emplacement was *infinitely* rapid, compared to the time of the subsequent thermal equilibration. This is what is called an *instantaneous heating model*. The thermal equilibration of intrusions with their surroundings can therefore be described with the heat conduction equation (eq. 3.6), assuming the intrusion geometry as an "initial condition".
- Most intrusions are small if compared to the size of their surroundings, for example the distance to the surface or to the base of the lithosphere. Thus, the boundary conditions that are needed to solve the heat conduction equation can often be assumed to lie at infinity in comparison to the scale of the problem.

With these two assumptions, it is possible to solve the heat conduction equation. The solutions may then be used for the analytical description of the thermal evolution of intrusions. For simple intrusion geometries, for example dikes, the description is very similar to description of the thermal evolution of oceanic lithosphere (sect. 3.5.1). However, before we use such a model, we need formulate two more simplifying assumptions which we will make initially:

- The latent heat of fusion - which actually plays an important role for the thermal energy budget of intrusions - will be neglected. Thus we will analyze in the first instance none of the processes discussed in sect. 3.2.
- The thermal conductivity is assumed to the constant in space. Thus we will also not consider any of the problems discussed in sect. 3.1.1.

With these assumptions, it is possible to integrate eq. 3.6. We begin with some simple examples.

3.6.1 Step-shaped Temperature Distributions

The most simple of all model examples describing the cooling of rocks in the direct vicinity of intrusions is given by the thermal equilibration of step-shaped temperature profiles in one dimension. This example is illustrated in Fig. 3.30 and is one of the most useful examples for the understanding of the cooling history of intrusions. We interpret the temperatures on the two sides of the step as the intrusion- and the host rock temperatures; T_i and

T_b, respectively. The step itself is the intrusion contact. If we choose a one-dimensional coordinate system in which the origin $z = 0$ is exactly at the contact of the model intrusion, then the initial and boundary conditions of this equilibration problem may be described by:

- Initial condition: $T = T_i$ for all $z > 0$ and $T = T_b$ for all $z < 0$ at $t = 0$.
- Boundary conditions: $T = T_b$ at $z = -\infty$ and $T = T_i$ at $z = \infty$ for all $t > 0$.

You may have noticed that there is *two* boundary conditions that are located a very long distance from the contact *inside* the intrusion and far away from the contact in the host rock (at $z = +\infty$ and $z = -\infty$). We need *two* boundary conditions because the equation that is to be solved (eq. 3.6) is a partial differential equation of the *second* order (s. sect. B.1.1). Integration of eq. 3.6 using these boundary and initial conditions gives:

$$T = T_b + \frac{(T_i - T_b)}{2}\left(1 + \text{erf}\left(\frac{z}{\sqrt{4\kappa t}}\right)\right) \quad . \tag{3.84}$$

We will not discuss how eq. 3.84 was derived (s. sect. 3.1.3) but when you compare this equation to eq. 3.80 you will see that it is very similar and differs from the most simple form of the half space cooling model only by some shifting and scaling of the error function. Because of the choice of coordinate system we have made to formulate this problem (Fig. 3.30), this solution looks very simple. In another coordinate system in which the coordinate origin is located at a distance l from the temperature step, the initial condition must be reformulated to: $T = T_i$ for all $z > l$ and $T = T_b$ all $z < l$ at $t = 0$. The boundary conditions remain the same. The solution gets the form:

$$T = T_b + \frac{(T_i - T_b)}{2}\left(1 + \text{erf}\left(\frac{z - l}{\sqrt{4\kappa t}}\right)\right) \quad . \tag{3.85}$$

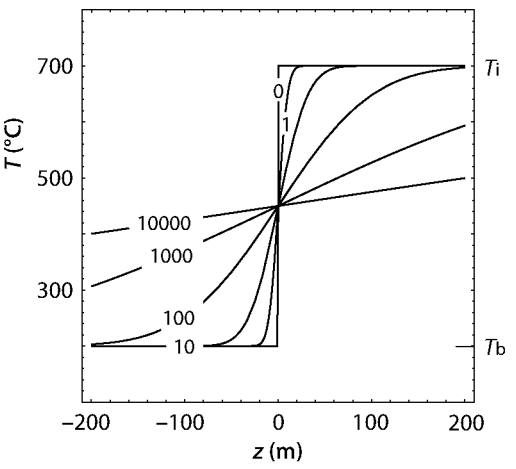


Figure 3.30. Thermal equilibration of an initially step-shaped temperature distribution. The curves were calculated with eq. 3.84 for $\kappa = 10^{-6}\ \text{m}^2\,\text{s}^{-1}$, $T_i = 700\,^\circ\text{C}$ and $T_b = 200\,^\circ\text{C}$. The different curves are temperature profiles at different times (in years) after the intrusion event

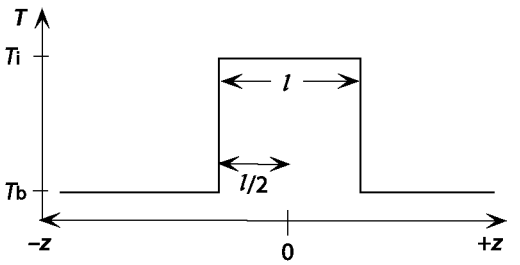


Figure 3.31. Schematic illustration of the initial condition and the variables of the dike cooling problem of eq. 3.88

Again, in comparison to eq. 3.85 you can see that this solution only shifts the temperature profile to the right place. On Fig. 3.30 it may be seen that the thermal evolution on both sides of the mean temperature between T_i and T_b develops symmetrically. This is to be expected as the initial and boundary conditions are also symmetric.

• *Cooling of half spaces.* In the example of eq. 3.84, the temperature at $z = 0$ stays constant in time. It has the value $T_\mathrm{b} + (T_\mathrm{i} - T_\mathrm{b})/2$. Thus, this problem is very similar to the description of the cooling of semi-infinite half spaces (sect. 3.5.1). This thermal problem is very important in the earth sciences and may be described by the following initial and boundary conditions:

– Initial condition: $T = T_\mathrm{b}$ at all $z > 0$ and $T = T_\mathrm{i}$ at $z = 0$ at time $t = 0$.
– Boundary conditions: $T = T_\mathrm{i}$ at $z = 0$ and $T = T_\mathrm{b}$ at $z = \infty$ for all $t > 0$.

These conditions are very similar to those of the last problem. Thus, the corresponding solution is also similar to eq. 3.84:

$$T = T_\mathrm{b} + (T_\mathrm{i} - T_\mathrm{b}) \left(1 - \mathrm{erf}\left(\frac{z}{\sqrt{4\kappa t}}\right)\right) \quad . \tag{3.86}$$

We have met this equation in a slightly different form already in sect. 3.5.1. The result of eq. 3.80 and eq. 3.86 can be simplified if it is expressed as the dimensionless temperature $\theta = (T - T_\mathrm{b})/(T_\mathrm{i} - T_\mathrm{b})$ (sect. 1.2). Then, using the complementary error function, eq. 3.86 simplifies to:

$$\theta = \mathrm{erfc}\left(\frac{z}{\sqrt{4\kappa t}}\right) \quad . \tag{3.87}$$

This simplification is shown here to illustrate that cooling curves of this problem have the shape of an error function. However, in the remainder of this section we will not use dimensionless temperatures. We begin with some geologically relevant examples that may be described with this solution.

3.6.2 One-dimensional Intrusions

One of the simplest but also most important applications of the equations introduced in the last section is the description of the cooling history of

intrusions (Jaeger 1964). As the solutions shown above are one-dimensional, their application is particularly relevant to the description of the thermal evolution of dikes that are narrow compared with their lateral extent. When using the solutions described above to describe the cooling history of dikes, it is implied that the dike extends "infinitely" in the two spatial directions normal to the coordinate described in the cooling problem. In contrast to the previous sections, we only need to be careful to consider both surfaces of the dike. For a coordinate system with its origin in the center of a dike with the thickness l, the initial conditions may be described by: $T = T_\mathrm{i}$ for $-(l/2) < z < (l/2)$ and $T = T_\mathrm{b}$ for $(l/2) < z < -(l/2)$ (Fig. 3.31). The boundary conditions remain the same as for the step problem. With these conditions, a solution of eq. 3.6 may be found to be:

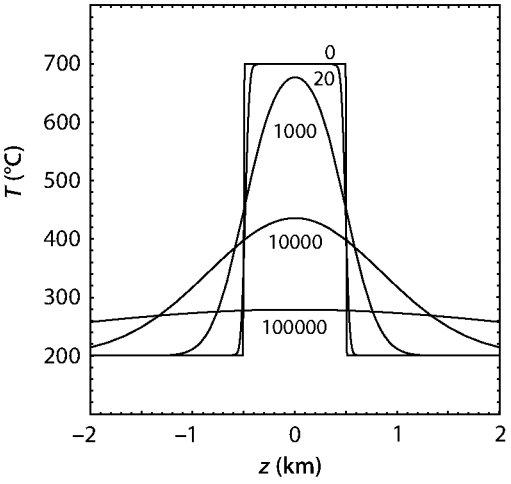


Figure 3.32. Thermal equilibration of one-dimensional intrusions, for example magmatic dikes of large lateral extent (calculated with eq. 3.88 and labeled in years after initial intrusion). All parameters are the same as in Fig. 3.30. Cooling curves of rocks from a range of distance from the dike center are shown in Fig. 3.33a

$$T = T_\mathrm{b} + \frac{(T_\mathrm{i} - T_\mathrm{b})}{2}\left(\mathrm{erf}\left(\frac{0.5l - z}{\sqrt{4\kappa t}}\right) + \mathrm{erf}\left(\frac{0.5l + z}{\sqrt{4\kappa t}}\right)\right) \quad . \tag{3.88}$$

It may be easily seen, that the solution is made up of descriptions for two opposing step-shaped temperature profiles at $z = -l/2$ and $z = l/2$. Fig. 3.32 shows the thermal evolution described by eq. 3.88. As the diffusion equation is a linear differential equation, the diffusive equilibration of just about any one-dimensional geometry may be described by the summation of solutions for various initial conditions.

In contrast to Fig. 3.30, the temperature at the intrusion contact departs from the temperature $(T_\mathrm{i} + T_\mathrm{b})/2$ after some time in Fig. 3.32. The contact of the dike begins to cool. This is because the dike contact at $z = +l/2$ begins to follow the thermal effects of the temperature step at $z = -l/2$. Correspondingly, the other dike contact at $z = -l/2$ cools, because it "feels" the cooling at $z = +l/2$.

Cooling History of Simple Intrusions. In the following paragraphs we will use eq. 3.88 to infer some characteristic features of contact metamorphism. Firstly, eq. 3.88 shows us that – in the absence of other thermal processes – the maximum temperature that may be reached by contact metamorphism is much lower than the intrusion temperature: Only at the very contact of the intrusion the contact metamorphic temperatures may reach the half way mark between the initial host rock and intrusion temperature. We can conclude that field observations of contact metamorphic haloes documenting haloes of considerable width and temperature imply that thermal processes other than conductive equilibration have played a role in their formation (s. sect. 3.6.4).

• *Cooling curves.* In order to interpret heating and cooling curves of rocks in the contact metamorphic environment, it is useful to plot eq. 3.88 in a temperature-time diagram (Fig. 3.33a). This figure illustrates that rocks located at different distances from the intrusion may experience very different cooling curves. For example, it may be seen that some rocks cool, while others heat up, or that rocks cool with different rates. In fact, near the contact of the intrusion, cooling curves have extremely complicated shapes including more than one maximum in the cooling rate (e. g. the 490-m-curve in Fig. 3.33a). Spend some time and think through why these different shapes come about. As simple as the model is, it teaches us much about the equilibration of contact metamorphic aureoles: Many metamorphic processes, for example grain growth or cation diffusion, are strongly dependent on both temperature and cooling rate (e. g. Dodson 1973). The interpretation of these curves is therefore extremely important (s. sect. 7.2).

• *Cooling rates.* The cooling rate s for a chosen point near the intrusion is described by the time derivative of eq. 3.88. As the error function itself is an integral, it is not too difficult to find this derivative, although we will not explain it in detail here. It is:

$$s = \frac{\mathrm{d}T}{\mathrm{d}t} = \frac{(T_\mathrm{i} - T_\mathrm{b})}{4t\sqrt{\pi\kappa t}} \left(\frac{z - 0.5l}{\mathrm{e}^{((0.5l-z)^2/4\kappa t)}} - \frac{z + 0.5l}{\mathrm{e}^{((0.5l+z)^2/4\kappa t)}} \right) \tag{3.89}$$

(s. sect. 3.1.3, 3.5.1). Cooling rates as a function of time as calculated with this equation are shown in Fig. 3.33b. They correspond directly to the curves in Fig. 3.33a.

For many petrological questions the cooling rate at a given *temperature* is much more important than the cooling rate at a given *time*. For this, a *parametric* plot of temperature against cooling rate is useful. *Parametric* plots are diagrams in which two independent functions of the same variable (here: time) are plotted against each other. Thus, the parametric plot of T against s shown in Fig. 3.34 is a combination of Figs. 3.33a and 3.33b. The time dependence of temperature or cooling rate can not be illustrated on this figure. Thus, Fig. 3.34 may appear a bit confusing at first view. Nevertheless,

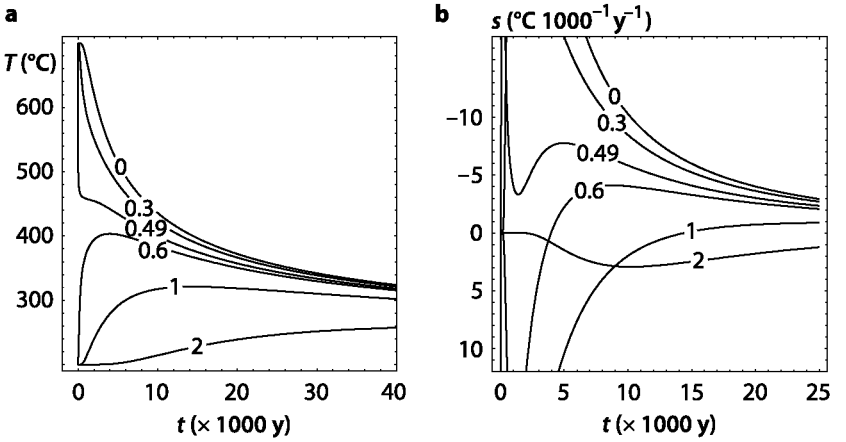


Figure 3.33. a Temperature-time paths (cooling curves) for a series of rocks within and within the contact aureole of a 1 km thick magmatic dike ($l = 1$ km) shown up to 40 000 years after intrusion (all constants are the same as in Fig. 3.32). The figure was calculated with eq. 3.88. The curves are labeled for distance from the center of the intrusion in km. As the thickness is $l = 1$ km, the first three curves are within the magma and the others in the country rock. **b** Cooling rates for the same points as shown in **a** plotted against time. Curves are calculated with eq. 3.89

such diagrams are crucial for a meaningful interpretation of petrological and geochronological data.

• *Contact Metamorphic Peak.* Aside from cooling curves or cooling rates, there is even more important information on the thermal evolution of intrusions that may be extracted from eq. 3.88. For example, the *time* of the contact metamorphic thermal peak $t_{T_{\max}}$ for the model of eq. 3.88 may also be found analytically. At the thermal peak the rate of temperature change is zero: $s|_{t=T_{\max}} = 0$ (read: s at $t = T_{\max}$). Thus, this time is given by setting eq. 3.89 to zero and solving for time. We get:

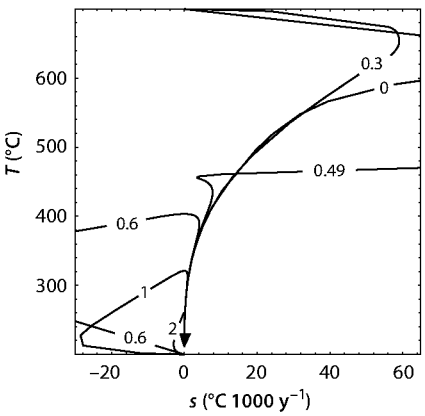


Figure 3.34. Parametric plot of cooling rate against temperature. The diagram was constructed from Figs. 3.33a and 3.33b. Although the diagram may not appear intuitive at first, it is simply a combination of the curves from Fig. 3.33a,b and is extremely useful for the interpretation of the equilibration of mineral parageneses (sect. 7.2)

$$t_{T_{max}} = -\frac{lz}{2\kappa \ln\left(\frac{z-0.5l}{z+0.5l}\right)} \quad . \tag{3.90}$$

From this, we can also get the thermal peak temperature as a function of distance from the intrusion. We get this by substituting the time obtained from eq. 3.90 into eq. 3.88 and solving that for temperature (Fig. 3.34; Fig. 3.35). With this diagram we can make some fundamental predictions about the nature of contact metamorphism:

1. The contact metamorphic peak temperature drops rapidly with *increasing* distance from the heat source.
2. The time of peak contact metamorphism increases rapidly with *increasing* distance from the heat source and with *decreasing* metamorphic grade. This predicts that – if contact metamorphism occurred – low grade metamorphic rocks should experience their metamorphic peak later than high grade metamorphic rocks (Den Tex 1963).

These predictions help to infer heating mechanisms of metamorphic terrains. For example, during regional metamorphism the relationships between grade and timing of metamorphism are reversed (sect. 6.3.3 and sect. 7.4.1). In the chapter on *P-T-t*-paths we will discuss further implications of the timing relationships of various cooling curves.

More Complicated One-dimensional Geometries. One of the largest drawbacks of the model discussed in the last section (eq. 3.88 and its derived relationships) is that it predicts much narrower contact metamorphic aureoles than those that are generally observed around intrusions. One of the reasons for this may lie in the geometry of the heat source. Other causes will be discussed in sect. 3.6.4.

• *Dike swarms.* In terrains that are penetrated by many intrusions, the mean contact metamorphic temperature may be much higher than that would be observed around a single intrusion. This may be described schematically by

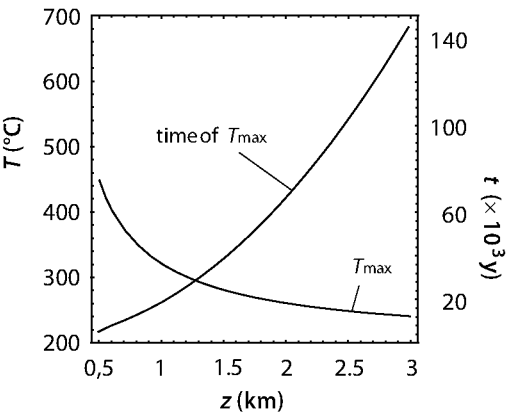


Figure 3.35. Contact metamorphic peak temperature and the time of the contact metamorphic temperature peak of the simple one-dimensional intrusion from Figs. 3.31 and Fig. 3.32. Calculated by substituting eq. 3.90, into eq. 3.88. The thickness of the intrusion l is 1 km, $T_i = 700\,°C$, $T_b = 200\,°C$ and $\kappa = 10^{-6}\ m^2\,s^{-1}$

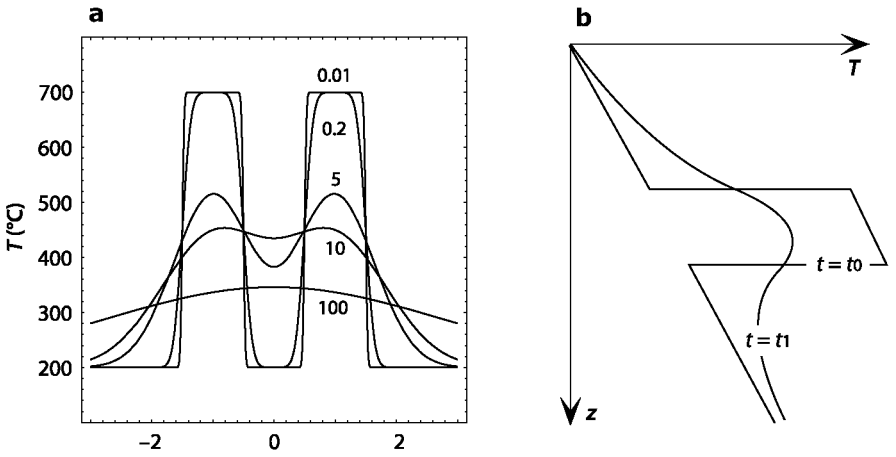


Figure 3.36. Two examples of complicated one dimensional intrusion geometries. **a** Contact metamorphism between two neighboring intrusions. The figure was calculated with eq. 3.91 using $z_1 = -1\,000$, $z_2 = 1\,000$ and $l_1 = l_2 = 1\,000$. Curves are shown in thousands of years (e. g. the line labeled for 0.2 corresponds to 200 years). Note that the contact metamorphic aureole *between* the intrusions is much wider than on their outside. **b** Schematic illustration of the diffusive equilibration of a step-shaped temperature profile (for example a one-dimensional intrusion like a sill) superimposed on a linear geotherm. Temperature profiles are shown at two different time steps t_0 and t_1. As the diffusion equation is a linear differential equation, the temperatures of eq. 3.88 can simply be added to the geotherm equation (in this case a straight line)

the combination of a series of temperature steps. If there is N intrusions of the thicknesses l_n, that intrude at the depths z_n, then this can be described by the summation of $2N$ steps in the temperature distribution. The solution is:

$$\theta = \frac{1}{2}\sum_{n=1}^{N}\left(\mathrm{erf}\left(\frac{z-(z_n-0.5l_n)}{\sqrt{4\kappa t}}\right)+\mathrm{erf}\left(\frac{(z_n+0.5l_n)-z}{\sqrt{4\kappa t}}\right)+...\right) \quad (3.91)$$

where θ is again the normalized temperature $\theta = (T-T_\mathrm{b})/(T_\mathrm{i}-T_\mathrm{b})$. Fig. 3.36a shows an example of two intrusions calculated with this equation. It may be seen that the contact metamorphic halo between the intrusions is much wider and of a higher temperature than on their outside. Because of this observation, Barton and Hanson (1989) suggested that multiple intrusion may be the principle heat source for low-pressure high-temperature metamorphism (s. sect. 6.3.3). Fig. 3.36b shows another schematic example for a one-dimensional problem that may be solved by the summation of a series of one-dimensional model geometries (s. p. 58).

• *Spherical intrusions.* The thermal evolution of spherical intrusions is also a one-dimensional problem in polar coordinates. The equation we need to solve

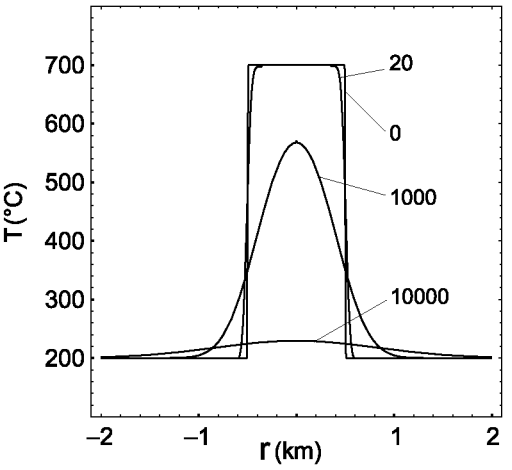


Figure 3.37. Cooling history of a spherical intrusion. For easy comparison, all chosen parameters and the shown time steps (labeled in years) are the same as those in Fig. 3.32. Calculated with eq. 3.92.

is eq. 3.12. If we want to compare the thermal evolution of spherical intrusions with that described by eq. 3.88, then we formulate the following boundary conditions: $T = T_\mathrm{b}$ at $r = \infty$ and $r = -\infty$, and the initial condition $T = T_\mathrm{i}$ in the region $-R < z < R$ and $T = T_\mathrm{b}$ in the region $-R > z > R$ at $t = 0$, where R is the radius of the intrusion and is analogous to $l/2$ in the Cartesian example discussed in eq. 3.88. r is the distance from the origin. The solution of eq. 3.12 under these conditions is:

$$T = T_\mathrm{b} + \frac{(T_\mathrm{i} - T_\mathrm{b})}{2}\left(\mathrm{erf}\left(\frac{R-r}{\sqrt{4\kappa t}}\right) + \mathrm{erf}\left(\frac{R+r}{\sqrt{4\kappa t}}\right)\right)$$
$$-\frac{(T_\mathrm{i} - T_\mathrm{b})}{r}\sqrt{\kappa t/\pi}\left(\mathrm{e}^{-\left(\frac{(R-r)^2}{4\kappa t}\right)} - \mathrm{e}^{-\left(\frac{(R+r)^2}{4\kappa t}\right)}\right) \quad . \tag{3.92}$$

Temperature profiles across cooling spheres at different times are shown in Fig. 3.37. They may be directly compared with those in Fig. 3.32. It may be seen that spheres cool much faster than dikes, which is intuitively clear as they have a much larger ratio of surface to volume in comparison to one dimensional steps in Cartesian coordinates.

3.6.3 Two-dimensional Intrusions

The description of two-dimensional thermal problems is – for most boundary conditions – not much harder than one-dimensional problems because heat conduction in several spatial dimensions can be described as the sum of conduction in the individual directional components (s. eqs. 3.9 to 3.10). In general it can be said that two-dimensional heat conduction problems may be described by the product of the one-dimensional solutions if: 1. the initial conditions may be expressed as the product of two functions $f(z)$ and $f(y)$

and 2. the boundary conditions are given by a constant temperature or constant heat flow. Solutions of the two-dimensional heat conduction equation with z and y as the spatial coordinates can therefore be expressed as:

$T =$ solution in z-direction $\times$ solution in y-direction

For example, the cooling history of a *corner* is described by the product of the cooling of two initial step-shaped temperature profiles as we discussed them in eq. 3.86:

$$T = T_b + (T_i - T_b)\text{erf}\left(\frac{z}{\sqrt{4\kappa t}}\right)\text{erf}\left(\frac{y}{\sqrt{4\kappa t}}\right) \quad . \tag{3.93}$$

The diffusive equilibration of *squares* may be used to describe the cooling history of a rectangular hot region. The solution for this can be derived directly from eq. 3.88:

$$T = T_b + \frac{(T_i - T_b)}{2}\left(\text{erf}\left(\frac{0.5l - z}{\sqrt{4\kappa t}}\right) + \text{erf}\left(\frac{0.5l + z}{\sqrt{4\kappa t}}\right)\right)$$
$$\times \left(\text{erf}\left(\frac{0.5l - y}{\sqrt{4\kappa t}}\right) + \text{erf}\left(\frac{0.5l + y}{\sqrt{4\kappa t}}\right)\right) \quad . \tag{3.94}$$

This solution may be used to describe the cooling history of a rectangular hot region (Fig. 3.38) and longer expansions of the same solution can be used to describe the cooling of any two dimensional shape of an instantaneously emplaced heat source (Fig. 3.39). However, it also finds a series of important applications in the fields of geomorphology (sect. 4.5) and petrology (sect. 7.2). In Chapter 4.5 we will see that weathering of granites can be described with the same solution.

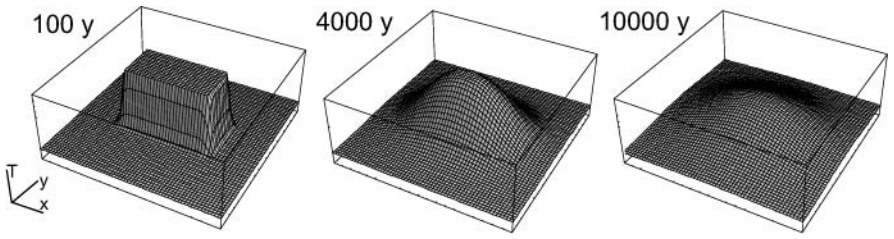


Figure 3.38. Three dimensional illustration of the cooling of a two-dimensional intrusion (2 times 1 km in size) of 700 °C intruding 300 °C hot rocks. Calculated with eq. 3.94. Temperatures are shown 100, 4 000 and 10 000 years after initial intrusion

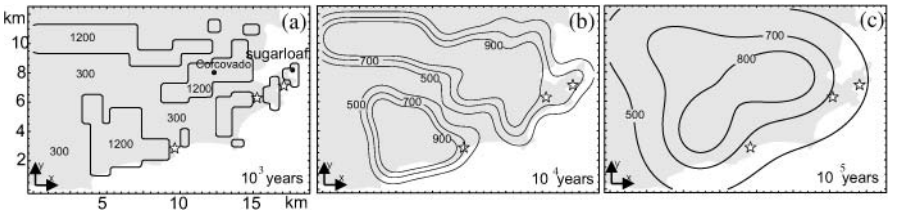


Figure 3.39. Temperatures around a series of intrusions with complicated shapes Modeled with a series of equations like eq. 3.94 after Kühn et al. (2004)

3.6.4 Modeling Realistic Intrusions

A series of observations in contact metamorphic aureoles of intrusions show that these are much wider and of a higher temperature than those we have predicted in the last section even as in the two dimensional examples shown. There is two important reasons for this:

- All problems we have discussed so far have been "instantaneous cooling" problems. This means, we have assumed that the cooling history commences at the time of intrusion. This need not be the case. In fact, in dikes through which magma is fed into a pluton, this would be highly unlikely. We need to describe some contact aureoles with a model where the temperature is fixed at the intrusion contact.
- So far we have neglected the latent heat of fusion as part of the cooling history. This latent heat of fusion amounts to about 320 kJ per kg of rock or roughly $8.64 \cdot 10^8$ J m^{-3}. During crystallization of intrusions this heat is added to the thermal energy budget available to cause temperature change and causes buffering of the cooling history.

In the following we discuss some simple model tools to describe both processes.

Fixed Boundary Conditions. Intrusion near the surface, where the temperature is constant, or intrusions through which magma flows to keep them at constant temperature must be modeled assuming a fixed temperature at the model boundary. If only one of the boundaries is fixed in temperature, then such problems may be described as a *half space problem* (sect. 3.6.1), as we have done when describing the evolution of oceanic lithosphere (see also Fig. 3.40). However, if both boundaries of a one-dimensional problem are fixed in temperature, then none of the solutions we discussed so far can be used. Under fixed boundaries the integration of eq. 3.6 is quite difficult and the solutions are not as simple as those we have discussed in sect. 3.6.2 and 3.6.3. Eq. 3.6 may only be solved by a Fourier transform (s. sect. B.4). Such solutions contain infinite summations. In their most general form, boundary and initial conditions of diffusion problems with fixed boundaries are given by:

- Initial condition: In the region $0 < z < l$ the temperature is given by $T = f_1(z)$ at time $t = 0$.
- Boundary conditions: At times $t > 0$ the temperature at $z = 0$ is given by $T = f_2(t)$ and at $z = l$ it is given by $T = f_3(t)$.

The function $f(z)$ can be used to describe the shape of a cooling body and the functions f_2 and f_3 can describe a large number of thermal processes at the model boundaries. The fact that f_2 and f_3 are functions and not fixed values is also a sort of "fixed boundary" (s. sect. B.2.4). In other words, fixed boundary conditions need not be a fixed value of temperature, but they need to be defined at all times by external parameters. Eq. 3.6 can only be solved using Fourier series and such solutions therefore contain infinite summations and trigonometric functions. However, for many special cases of the space and time dependent functions $f_1(z)$, $f_2(t)$ and $f_3(t)$ Fourier series solutions are relatively easy to derive and can be looked up in the literature (e. g. Carslaw and Jaeger 1959).

The Stefan Problem. The latent heat of reaction is an important part of the heat budget of high grade metamorphic terrains when phase transitions occur (see sect. 3.2.3). As we need about 1 000 Joules to heat one kg of rock by one degree ($c_p = 1\,000\ \mathrm{J\,kg^{-1}\,K^{-1}}$), the latent heat of fusion in enough to heat a rock by about 320 °C (because $L = 320\ \mathrm{kJ\ kg^{-1}}$). An intrusion of $T_\mathrm{i} = 700\,^\circ\mathrm{C}$, that intrudes host rocks of $T_\mathrm{b} = 200\,^\circ\mathrm{C}$, is $\Delta T = 500\,^\circ\mathrm{C}$ hotter than its surroundings. This corresponds to $\Delta T c_p = 500\,000\ \mathrm{J\,kg^{-1}}$ additional energy that is brought into the rock by this temperature difference. However, the total *heat content* of the intrusion (including its latent heat) that is brought into the rock is $\Delta T c_p + L = 820\,000\ \mathrm{J\,kg^{-1}}$. The excess energy is therefore about 1.64 times as large as the excess temperature.

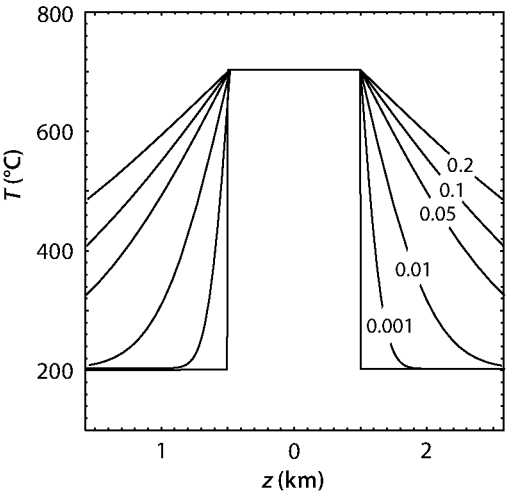


Figure 3.40. Temperature profiles around a dike which is kept at constant temperature by the flow of magma. The curves were calculated with eq. 3.86 (curves are labeled in my). Compare this figure with Fig. 3.25 and Fig. 3.30

This means that we have underestimated the cooling history in the previous sections substantially (s. p. 123).

If we want to describe the cooling history properly (rather than being satisfied with the ball park estimate above) we need to consider where and when this crystallization heat is added to the energy budget. To illustrate this, it is useful to imagine the processes involved in the freezing of a lake. During cooling of the air below the freezing point, at first the lakes surface will freeze. The crystallization heat that is freed during this process buffers the further freezing process. During further cooling of the surface, the subsequent thickening of the ice layer will slow down, as the frozen layer insulates the water to the outside and the latent heat of crystallization freed at the ice-water interface remains contained in the water. For this reason it is rare to find pack ice on the polar oceans that is thicker than about 2 m. In fact, it was the observation of ice on the polar oceans that lead Stefan (1891) to describe the problem that now bears his name.

For the one-dimensional case and if the magma of a cooling intrusion crystallizes at a single eutectic temperature, there is an analytical solution that can be used to describe its thermal evolution under consideration of the latent heat of fusion. This is the solution found be Stefan (1891) for the freezing of water. However, most rocks crystallize in divariant reaction over a large temperature interval between a solidus and a liquidus temperature, rather than at a single temperature. Then, numerical solutions of the heat flow equation must be used to consider the effects of latent heat (s. sect. 3.2.3). Regardless, the solution of Stefan (1891) gives important insights into the thermal processes involved. It solves the heat conduction equation under consideration of the latent heat crystallization at the rock- magma interface for the geometry described by:

– $T = T_\mathrm{b}$ at all $z > 0$ and $T = T_\mathrm{i}$ at $z < 0$ at time $t = 0$

and boundary conditions at infinity. It is also assumed that the magma crystallizes at temperature $T = T_\mathrm{i}$. The solution that describes the temperatures outside the crystallising interface is given by:

$$T = T_\mathrm{b} + (T_\mathrm{i} - T_\mathrm{b}) \left(\frac{\mathrm{erfc}\left(\frac{z}{\sqrt{4\kappa t}}\right)}{1 + \mathrm{erf}(\lambda))} \right) \quad . \tag{3.95}$$

In this equation, λ is given by the function:

$$\frac{L\sqrt{\pi}}{c_p(T_\mathrm{i} - T_\mathrm{b})} = \frac{\mathrm{e}^{-\lambda^2}}{\lambda(1 + \mathrm{erf}(\lambda))} \tag{3.96}$$

The derivation of this equation is complicated and of no relevance here. Eq. 3.96 may be solved iteratively or its solutions can be looked up in tables. Values for λ can then be inserted into eq. 3.95. This equation describes the temperature profile around a crystallizing dike margin. Fig. 3.41 shows

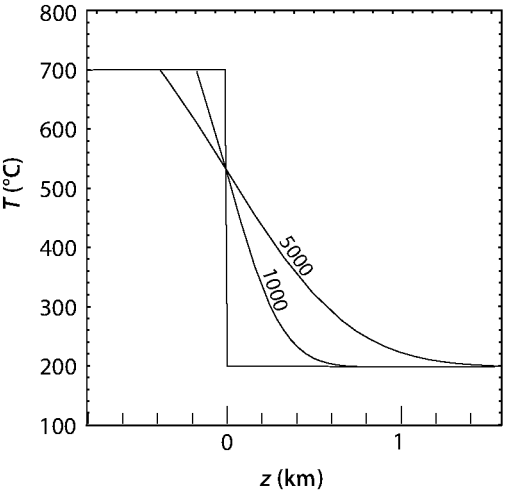


Figure 3.41. Temperatures in the contact aureole of a crystallizing interface between magma and host rock after 1 000 and 5 000 years, as calculated with eq. 3.95. Note that the contact metamorphic aureole is wider and of higher temperature than when only heat conduction is considered (Fig. 3.32). All parameters assumed here correspond to those used for Fig. 3.32 with the only difference being that latent heat is considered here

some curves calculated with eq. 3.95. The thickness of the dike is no part of this solution. The position $z = 0$ is the location of the dike margin at the onset of crystallization. The solution may be used up to the time where the crystallization interfaces of the opposite walls of the dike meet at its center. Thereafter numerical solutions must be used to describe the subsequent cooling history.

Heat Content of Intrusions and Metamorphic Terrains. If we recall eq. 3.3, there is a simple relationship between heat and temperature. The relating proportionality constants are the heat capacity c_p and density ρ. In fact, all problems we have described using temperature, could have also been formulated in terms of heat using:

$$\frac{\partial H}{\partial t} = \frac{\partial T}{\partial t} \rho c_p \quad . \tag{3.97}$$

Instead of going through many calculated examples here, we only want to state that the heat content of an intrusion or a metamorphic terrain can be viewed – in one dimension – as the area underneath a $T - z$ curve (Fig.3.42). In essence, this is what eq. 3.3 and eq. 3.97 state (some more detail is given in the first edition of this book). In other words, the heat content of a dike of thickness l and temperature T_i relative to its surroundings of temperature T_b is given in $\mathrm{J\,m^{-2}}$ by: $(T_\mathrm{i} - T_\mathrm{b}) l \rho c_p$. Using typical values of $\rho = 2\,700\ \mathrm{kg\,m^{-3}}$ and $c_p = 1\,000\ \mathrm{J\,K^{-1}\,kg^{-1}}$, the intrusion of Fig. 3.32 has a heat content of $H = 1.89 \cdot 10^{12}\ \mathrm{J\,m^{-2}}$. This is the heat content per square meter of dike surface.

In high grade metamorphic terrains containing syn-metamorphic intrusives it is often discussed if the volume of the intrusions is sufficient to contribute significantly to the metamorphism. In other words, it is discussed if the metamorphism is *contact metamorphism* in the widest sense (e. g. Problem 3.14).

In order to do this estimate properly, the heat content of the intrusives must be compared with the heat content of the terrain. If the specific heat capacities of the intrusives and the metamorphic host rocks are the same, then the comparison of energy contents can also be made as a comparison of the temperatures. However, we must consider the latent heat of fusion that is part of the heat of the intrusives, but not of the host rocks. As simple calculation shows that:

$$T_{\max} = T_{\mathrm{b}} + \left(T_{\mathrm{i}} - T_{\mathrm{b}} + \frac{L}{c_p} \right) \frac{V_{\text{intrusives}}}{V_{\text{terrain}}} \quad . \tag{3.98}$$

There, T_{b} and T_{i} are the temperature of the host rock before metamorphism and that of the intrusion, respectively. $V_{\text{intrusives}}$ is the volume of the intrusives and V_{terrain} is the volume of the entire metamorphic terrain. $T_{\max}$ is the maximum temperature that can be reached by contact metamorphism.

If the *aerial* proportion of intrusives to host rock are representative for the *volumetric* proportion of intrusives in the terrain, then the volumes of eq. 3.98 may be replaced by areas. Using $T_{\mathrm{i}} = 700\,^{\circ}\mathrm{C}$, $T_{\mathrm{b}} = 300\,^{\circ}\mathrm{C}$, $L = 320\,000\ \mathrm{J\,kg^{-1}}$ and $c_p = 1\,000\ \mathrm{J\,kg^{-1}\,K^{-1}}$, eq. 3.98 shows the following: only about 55 % of the terrain must consist of syn-metamorphic granites in order to heat the entire terrain to 700 °C, even if the intrusion temperature itself was only 700 °C. If the intrusives are 1 200 °C hot mafic magmas, then only 30 % of the terrain must be intrusives in order to heat the terrain to 700 °C.

• *Using heat content as a boundary condition.* In numerical calculations of thermal evolutions on grids of finite extent it is often not possible to assume boundary conditions at infinity. Then, a consideration of the heat content may come in handy as a boundary condition. For example, the boundary conditions for eq. 3.88 were assumed at infinity there, but may also be formulated in terms of the heat content of the intrusion. As no heat can be lost from the system if it cools by conduction only, the area underneath the curves in Fig. 3.32 must stay constant between $z = +\infty$ and $z = -\infty$. This is schematically shown on Fig. 3.42. During cooling of the intrusion, the area A must always be as large as the sum of $2B + 2C$. When solving the heat flow equation numerically on grids of finite extent, for example between the two straight lines on Fig. 3.42, problems are often easier to handle this way than they are if the temperature is assumed to be constant at infinity. In this case the heat flow at the model boundary (given by the angle α) could be adjusted so that the areas C have the correct size. From Fig. 3.42 it may be seen that $A = 2B + 2C$ and $\tan(\alpha) = \Delta z / \Delta T$. From this, the thermal gradient at the model boundary is given by:

$$\alpha = \mathrm{tg}^{-1} \left((A - 2B)/\Delta T^2 \right) \quad . \tag{3.99}$$

This relationship is a useful in many numerical descriptions of diffusion problems with boundary conditions at infinity.

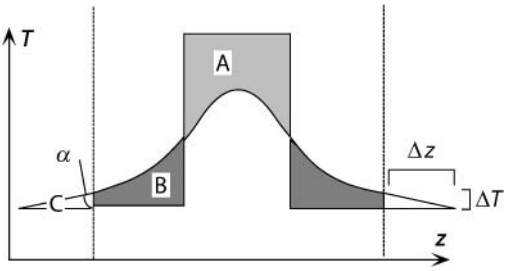


Figure 3.42. Schematic illustration of the heat content of a dike. The sum of the areas of the two dark-shaded regions B, plus the white triangles C must be the same as the light-shaded area A. Then, the heat content of the total system remains constant

3.7 Selected Heat Transfer Problems

In this section we discuss a selection of geologically important heat transfer problems that do not belong directly to any of the past sections but are important to understand geodynamic processes. We discuss mainly problems which are subject to spatially or temporally changing temperatures. Such problems can be described with periodic boundary conditions and have the great advantage that analytical solutions of the heat conduction equation can be found for them. In particular, we have selected three geodynamically relevant sets of problems, which may be described with periodic boundary conditions as well as the temperature distribution around faults. Analytical solutions for these and many others interesting heat transfer problems can be found in the literature (e. g., Carslaw and Jaeger 1959)

3.7.1 Periodic Temperature Fluctuations

The temperatures at the surface of earth are subject to the daily or annually periodically changing temperatures of the atmosphere. Problems where this is relevant, range from understanding the thickness of permafrost soils, to the regulation of temperatures in tunnels and insulation of walls of buildings. Many of these problems can be described with a one-dimensional coordinate system with z as the coordinate normal to the surface and with boundary conditions that describe a periodic fluctuation of the temperature at the surface. This may be written as:

- Initial condition: $T = T_0$ at all z at time $t = 0$.
- Boundary condition: $T = T_0 + \Delta T \cos(ft)$ at $z = 0$ for all $t > 0$, and $T = T_0$ at $z = \infty$ for all $t > 0$.

There, ΔT is half the amplitude of the annual fluctuation, t is time and f is the frequency of the periodic temperature cycle (Fig. 3.43 a). T_0 is the mean temperature over one cycle. The time dependent diffusion equation (eq. 3.6) can be integrated using these assumptions. We will not go through this integration here, but the result is amazingly simple. It is given by:

$$T = T_0 + \Delta T \mathrm{e}^{\left(-z\sqrt{\frac{f}{2\kappa}}\right)} \cos\left(ft - z\sqrt{\frac{f}{2\kappa}}\right) \quad . \tag{3.100}$$

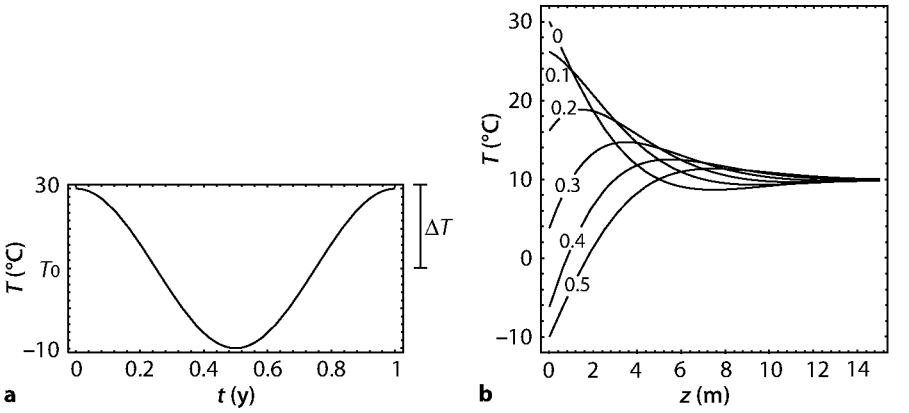


Figure 3.43. The temperature in the upper few meters of the crust as a function of annually changing surface temperature. **a** shows the upper boundary condition: the temperature T as a function of time t at $z = 0$. The annual mean temperature was assumed to be T_0=10 °C. The variation about this mean was assumed to be $\Delta T = 20$ °C. **b** shows six thermal profiles in the ground at six different times through the course of half a year. The curves are labeled for time in years. It may be seen that below depths of about 2 m temperatures never sink below the freezing point

This equation may be used to describe temperature fluctuations at depth as a function of a periodic temperature variation at the surface. It may be seen that this equation contains a trigonometric function and an exponential function. At each time t it describes a cosine function of temperature which decays in amplitude exponentially with depth. At the depth $z = (f/2\kappa)^{-0.5}$ the amplitude of the temperature oscillation is that of the surface divided by e. This depth is often called the *characteristic depth of equilibration* or *skin depth* (s. sect. 3.4.3). Eq. 3.100 is extremely important for many near surface problems, for example temperature profiles in snow, air temperatures in caves and many more (Fig. 3.43b).

3.7.2 Folded Isotherms

A beautiful problem illustrating the relationships between length and time scales of heat conduction and advection (s. sect. 3.1.4, 3.3.4) is given the shape of isotherms during folding. Before we discuss this problem it should be said that – strictly speaking – isotherms can not be folded, as they are not material lines. However, a number of model descriptions use the term "folding" even when talking of isotherms and we use it here as well. Fig. 3.44a shows schematically how isotherms may be folded during deformation of rocks. This process may occur if the axial plane of the folds is not parallel to the isotherms. Whether or not folding of isotherms has a thermal influence on rocks depends on the relationship between the wavelength and amplitude of the fold, on the folding rate and of course on the diffusivity κ. If

the wavelength, the amplitude and the folding rate are large, then isotherms will be folded together with the stratigraphy. If the folding rate is small, then the rate of thermal equilibration is rapid compared with the folding and the isotherms will remain flat. Field observations like the updoming of the Tauern Window in the eastern Alps, together with the updoming of the Alpine metamorphic isograds show that it may be important to estimate the magnitude of this effect. If the estimates show that folding of rocks is rapid enough to fold the isotherms as well, then we should observe that antiforms cool and synforms heat. With the methods of modern petrology it is conceivable that such details of the thermal evolution can be tested (sect. 7.2).

A first estimate of the potential magnitude of an isotherm folding process can be made using the Peclet number (sect. 3.3.4). For a geologically reasonable shortening rate of 1 $\mathrm{cm\,y^{-1}}$ an amplitude of a single antiform of 5 km forms in about 0.5 my. The rate u, with which the material lines are deformed is therefore $10^4\ \mathrm{m\,my^{-1}}$. Using l as the amplitude and $\kappa = 10^{-6}\ \mathrm{m^2\,s^{-1}}$ we get from eq. 3.51, that $Pe \approx 1.5$. This shows that diffusion and advection processes are both relevant for the assumed parameters and that a more detailed investigation of the problem is justified.

A quantitative and very simple model that can be used for the description of this process was developed by Sleep (1979). This model is based on the following assumptions:

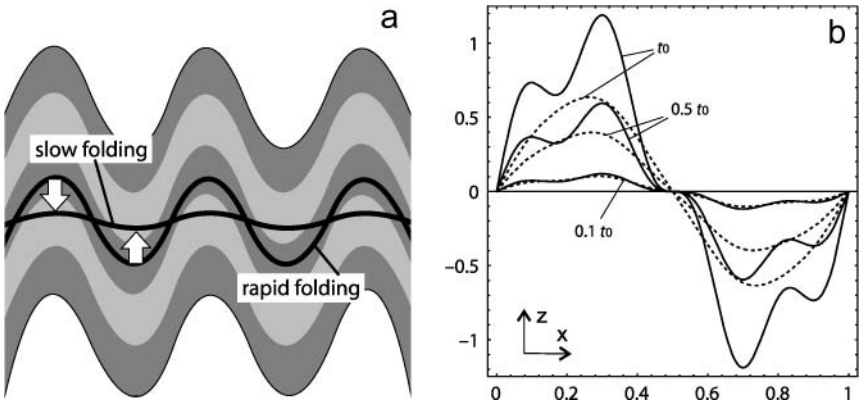


Figure 3.44. Illustration of folded isotherms. **a** Schematic illustration. The light and dark shaded regions are folded strata, the thick lines are isotherms. During *slow* folding, equilibration is faster than folding and isotherms will not be folded with the rock. During *rapid* folding of the rock conductive equilibration can not keep up with the material advection and the isotherms will be folded with the rock. **b** Folding of stratigraphy and isotherms as calculated with the model of Sleep (1979). The continuous lines show the shape of a layer at three different points in time. The folding is characterized by a principal fold with wave length and amplitude of 1, overprinted by a parasitic fold with wavelength and amplitude 0.25. For this model two sets of eq. 3.101 and eq. 3.102 must be summed up. For details see Sleep (1979) or the first edition of this book

1. Before folding, isotherms are parallel to each other and to the surface of earth. The isotherms have a constant distance to each other so that the initial temperature distribution as a function of depth is: $T_{(t=0)} = gz$, where g is the geothermal gradient and z is depth.

2. Folding of rocks occurs by shear folding along axial planes that are perpendicular to the isotherms and a sine-shaped fold is produced that has the form:

$$v = v_0 A\sin\left(\frac{2\pi x}{\lambda}\right) \quad \text{or:} \quad z = tv_0 A\sin\left(\frac{2\pi x}{\lambda}\right) \quad . \tag{3.101}$$

In this equation, v is the displacement rate at each point of the fold, v_0 is the displacement rate of the fold hinge and x is the horizontal coordinate. z is the depth of the folded rock at time t. A is the amplitude of the fold. This assumption describes shear folding at constant volume and does not consider shortening perpendicular to the axial plane of the folds. λ is the wavelength of folding. Using these assumptions, eq. 3.42 may be integrated. According to Sleep (1979) this gives:

$$T = g\left(z - z_0\left(1 - \mathrm{e}^{-t/t_0}\right) A\sin\left(\frac{2\pi x}{\lambda}\right)\right) \quad . \tag{3.102}$$

There, the constants z_0 and t_0 are:

$$z_0 = \frac{v_0\lambda^2}{4\pi^2\kappa} \quad \text{and} \quad t_0 = \frac{\lambda^2}{4\pi^2\kappa} \quad . \tag{3.103}$$

This equation may – of course – also be reformulated to solve for the depth z of a chosen isotherm T. Folding events that last shorter than t_0 will cause a significant deformation of the isotherms. If they last longer, then the additional deformation is negligible. For most field examples of folding, the geometry assumed for the folding process in this model is too simple. However, Sleep (1979) notes that *all* fold geometries that have formed by shear folding can be represented by a summation of sine-functions. Thus, eq. 3.102 could be applied to all sine-shaped components of a random folding geometry and the results could then be summed up. Fig. 3.44b shows an example in which the amplitude and wavelength of two folds, a principal fold and a parasitic fold is considered. There, the amplitude of the overprinting parasitic fold is 1/4 of that of the principal fold.

3.7.3 Isotherms and Surface Topography

An important example of a heat conduction - advection problem concerns the influence of the surface topography on isotherms at depth. Rocks inside mountains are thermally insulated, while rocks nearer the surface of an incising valley are cooled by the surface. As a consequence, isotherms follow the earth's surface it in a damped form. Just how the distance of a given

isotherm from the surface varies with amplitude and wavelength of the topography is of large importance for the interpretation of low temperature geochronological data in mountainous regions, for the design of ventilation systems in tunnels and more (Fig. 3.45) (Braun 2002; 2006). In this section we discuss some models that can be used to estimate the magnitude of this effect.

The Upper Boundary: The Topography. For simplicity we assume that the surface topography may be described by a sine-function with the wavelength λ and the amplitude $h_0/2$ where we interpret the wavelength λ as the distance between two parallel valleys and h_0 as the maximum elevation of the peaks above the valleys. Using the coordinate system illustrated in Fig. 3.46a,b, the elevation h at any point of the topography is described by:

$$z_{(T=0)} = -h = -h_0 \frac{1}{2}\left(1 + \cos\left(\frac{2\pi x}{\lambda}\right)\right) \tag{3.104}$$

Using such a simple function to describe topography allows us to evaluate the magnitude of the thermal effects as a function of two simple parameters of topography: the wavelength and the amplitude.

We also assume that the temperature along the curve described by eq. 3.104 is the surface temperature $T_s = 0$ and neglect any atmospheric temperature gradient or seasonal variation. However, even for these simplified assumptions, integration of the two-dimensional diffusion- or diffusion-advection equation (eq. 3.6 or 3.42) under this boundary condition is very difficult (s. sect. 3.6.3). A common way to surround this problem is by substituting this boundary condition of *constant* temperature at a *variable* spatial position, by a boundary condition of *variable* temperature at a *constant* elevation, for example at $z = 0$. This would be described by:

$$T(x)_{(z=0)} = \Delta T \frac{1}{2}\left(1 + \cos\left(\frac{2\pi x}{\lambda}\right)\right) \tag{3.105}$$

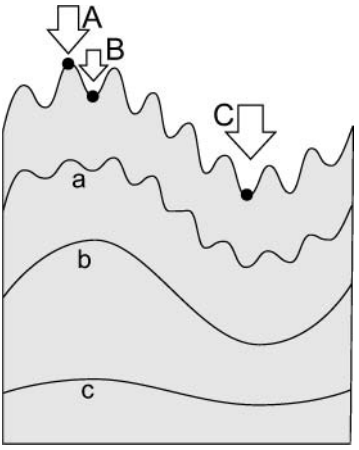


Figure 3.45. Schematic illustration of isotherms underneath topography. (a), (b) and (c) show three different isotherms at depth. Note that the topographic perturbation of isotherms decreases with depth in proportion to the wavelength of the topography. Using a geochronological system that closes at isotherm (b), a comparison of samples from A and B (vertical age profiling) could be used to determine the erosion rate, while a comparison of samples from A and C may be used to study the landform evolution. Using age elevation relationships at A and B with an isotopic system that closes at isotherm (a) would result in an overestimate of the erosion rate (Braun 2006; Stüwe et al. 1994).

where $\Delta T = h_0 g$ and g is the geothermal gradient in the absence of topography. This assumption implies that the thermal gradient inside the mountains is linear. ΔT corresponds to h_0 in the proper formulation (s. Fig. 3.46). This approximation is good if the wavelength of the topography is large compared to the amplitude because then the lateral cooling through the sides of the valley can be neglected. Note that this approximation of the topography is actually quite a correct description if the surface temperature on a flat shield *does* vary laterally, for example because of the presence of lakes. Using these assumptions, we can discern three different types of scenarios described by different solutions of the diffusion – advection equation:

Topography Without Erosion. If there is no erosion, there is no advection towards the surface. As a consequence, the topographic perturbation effect on isotherms is substantially smaller than it would be in an eroding terrain. To estimate it we need to solve the two dimensional diffusion equation (eq. 3.9) subject to the boundary conditions of eq. 3.105. The solution is:

$$T_{(x,z)} = T(x)_{(z=0)} \times \mathrm{e}^{-2\pi z/\lambda} \quad . \tag{3.106}$$

We can see from this solution a fundamental result (shown in Figs. 3.46b): The perturbation of isotherms decreases exponentially with depth and in proportion to the wavelength of the topography. In other words: at a depth $\lambda/2\pi$ the amplitude of the isotherm is a mere $\mathrm{e}^{-1} \approx 0.3$ of the amplitude of the surface topography. Lets use the Alps and an isotherm relevant for

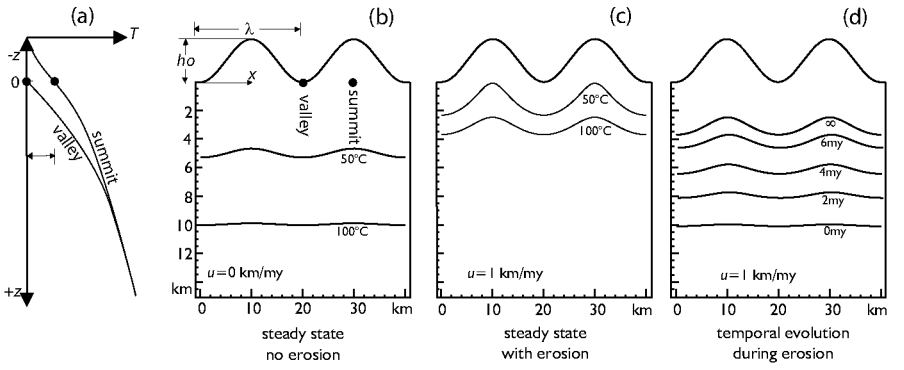


Figure 3.46. Isotherms underneath regions of high topographic relief. **b**, **c** and **d** show two-dimensional profiles through a mountainous topography. The two isotherms in **b** are for a non-eroding topography calculated with eq. 3.105 and adding a linear thermal gradient to the solution to place the different isotherms at the correct depths. **c** shows a thermal steady state case for an eroding topography. In **d** the time dependent evolution underneath an eroding topography is shown for a single isotherm, in this case 100 °C. The two black dots in **a** and **b** are at equal depth, but they have a different temperature. Note that in the chosen coordinate system the surface is located at negative values for z, but (according to eq. 3.104) at positive values for h (s. Fig. 4.3)

fission track analysis ($\approx$ 100°C corresponding to a depth of $\approx$ 3 km) as an example: The Alps have a topographic amplitude of about 3 km and a series of topographic wavelengths from about $\lambda \approx 2$ km in the most rugged regions to $\lambda \approx 200$ km from the northern to the southern Molasse basin. Inserting these numbers into the exponential term of eq. 3.106 shows that the narrow wavelengths are just about invisible for the 100°C isotherm, while 90% of the longest wavelength is preserved at 3 km depth. This caused Brown (1991) to conclude the interpretation of age – elevation profiles from apatite fission tack data may be done without topographic correction.

Eroding Topography. During erosion material is advected towards the surface, isotherms are compressed into the topography and the amplitude of a given isotherm is substantially larger than when no erosion occurs. To estimate the perturbation effect quantitatively we need to solve a two dimensional form of the diffusion – advection equation (eq. 3.42). Eqs. 3.45, 3.46 and 3.47 are three examples for geotherms during erosion but without consideration of topography. These equations may be expanded into two dimensions and modified to account for the variable boundary at the top surface. Solutions typically show the same fundamental relationship discussed in connection with eq. 3.106, namely that the effect decreases exponentially with depth and in proportion to the wavelength of the topography. However, depending on the erosion rate, the advection processes may be strong enough to perturb isotherms of geological relevance. Stüwe et al. (1994) found a semi-analytical solution of the two-dimensional diffusion-advection equation to describe this problem (Fig. 3.46c and 3.45). They concluded that at erosion rates above

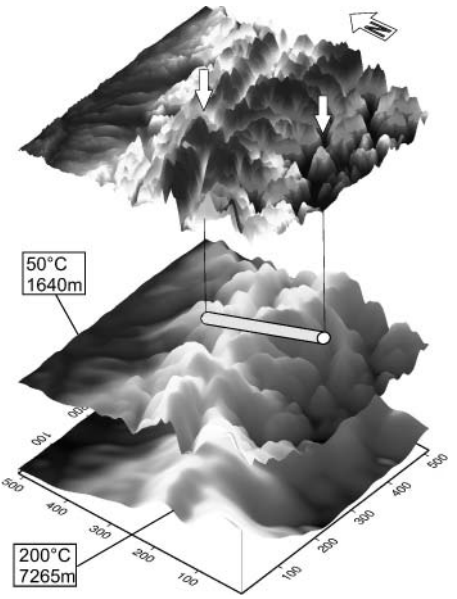


Figure 3.47. Example of a three dimensional conduction-advection model to consider topographic perturbation effects on topography (Hergarten and Stüwe in prep). For this example, the digital elevation model of the Gotthard region was interpolated onto a three dimensional grid to consider thermal effects important for ventilation in the longest road tunnel on earth: the Gotthard base tunnel. Below the topography, two isotherms are shown (labeled for temperature and depth). Assumed erosion rate was 1 mm per year. North and south entrance of the Gotthard tunnel are shown by the white arrows

500 m my^{-1} it becomes important to consider the topographic effects on the interpretation of apatite fission track results.

Asymmetric Advection, Three-dimensionality and Time Dependence. Several other processes not considered in the discussion above may be of interest when estimating topographic corrections on isotherms at depth. These include radiogenic heat production, time dependent effects, atmospheric temperature gradients, convective heat transfer by fluids or seasonal temperature variation and asymmetric advection due to variable erosion rate. To account for such processes properly, it is usually necessary to use numerical solutions of the diffusion – advection equation. Then, all these processes can be considered in a much more straight forward manner. A nice examples of the use of a three dimensional model is presented by Craw et al. (2005) and another one is shown in Fig. 3.47. Several three dimensional models are currently in use to describe these effects. Mancktelow and Grasemann (1997) investigated the time dependent effects how this steady state is reached (Fig. 3.46d). However, as the Peclet number of most topographies is small, it is usually not necessary to investigate the time dependent evolution of isotherms. Asymmetric erosion due to differential rain fall on different sides of a mountain range was considered by Stüwe and Hintermüller (2000) and also discussed in the first edition of this book. With the advent of a series of new thermochronological methods (e.g. House et al. 1998; 2000) enough detail of low temperature cooling curves is starting to be resolved to justify careful modeling of all these processes.

3.7.4 Temperature Distribution Around Faults

The thermal evolution of rocks around faults is a typical two-dimensional problem in which all three heat transfer mechanisms may play a role: *diffusion* in the foot and hanging wall of the fault, *advection* of heat by the relative motion of the two sides of the fault and *production* of friction heat in the fault itself (s. Fowler and Nisbet 1982). In the following analysis we only discuss diffusion and advection. For the importance of mechanical heat production, the interested reader is referred to the now classic discussions by Molnar and England (1990a), Graham and England (1976) and Pavlis (1986), sect. 3.2.2 and a wealth of modern literature on the subject.

Fig. 3.48 shows a vertical cross section through a package of rock that is transected by a fault (in the shown orientation it is a *normal* fault). The normal fault is inclined with 60° to the left and the initial isotherms are inclined with 20° to the right. The displacement along the fault (10 km in this case) opposes the hot rocks in the foot wall with the relatively cold rocks in the hanging wall. As a consequence, the isotherms are stretched near the fault. The lateral temperature gradient in the vicinity of the fault is *decreased* by the fault displacement (Fowler and Nisbet 1982). If the fault were a reverse fault of the same angle, then the situation would be reversed: the foot wall would be cooled, the hanging wall would be heated and the

isotherms would be *compressed.* The heating of rocks by reverse faulting is one of several processes that have been made responsible for the formation of inverted metamorphic gradients (s. discussion by England and Molnar 1993).

• *Estimating the thermal influence.* In order to estimate the thermal influence of a fault zone on its surroundings, we can employ two simple tools which we have discussed in previous sections: The thermal time constant (eq. 3.17) and the Peclet number (eq. 3.51). In Fig. 3.48a,b and c, the rate of material advection u (displacement rate) is 1, 10 and 20 km my^{-1}, respectively. From eq. 3.51 we can estimate the length scale l where both diffusion and advection influence the thermal structure (i.e. $Pe = 1$) by (Fig. 3.16):

$$l = \frac{\kappa}{u} \quad . \tag{3.107}$$

With $\kappa = 10^{-6}$ m^2 s^{-1}, this gives l= 30, 3 and 1.5 km, respectively. A comparison with Figs. 3.48a,b and c shows that the region over which isotherms are curved corresponds indeed to these length scales. This suggests that a more detailed description with sophisticated numerical models is not necessary to understand the first order effects.

• *Temperature-time evolution during exhumation in the vicinity of faults.* In many regions of active and ancient mountain belts it is observed that displacement along fundamental structures leads to different rates of exhumation of the foot wall and the hanging wall. This may lead to a complicated thermal evolution of rocks as there are two competing thermal processes:

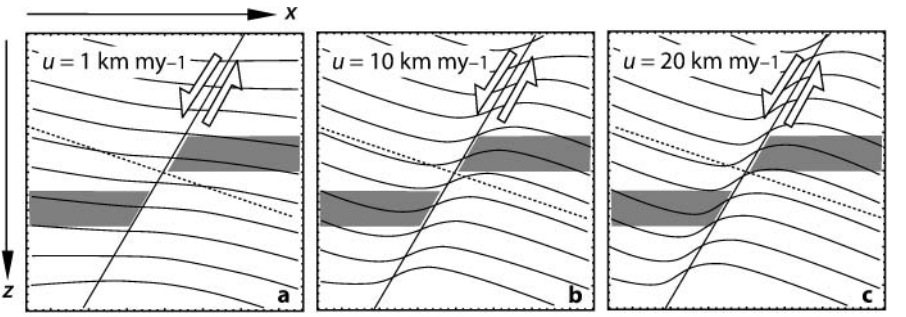


Figure 3.48. Isotherms in a crustal cross section around a normal fault that is inclined with 60 degrees to the left. The shown area is 50 km by 50 km in size. The figures are labeled for the rate of normal displacement u. **a**, **b** and **c** show the temperatures after 10 my, 1 my and 0.5 my. Thus, the displacement is the same in all three figures. The gray shaded region indicates schematically a lithological layer. The isotherms are shown every 50 °C. The isotherms were inclined with 20 degrees to the right before the fault became active (dashed line). The boundary conditions on all four sides are given by constant heat flow. This implies that the crustal section shown is surrounded on all sides by matter and that the diagram can be rotated arbitrarily. The diagram was calculated with a numerical solution of a two-dimensional form of eq. 3.41. For an analytical solution of related problems see e. g. Voorhoeve and Houseman (1988)

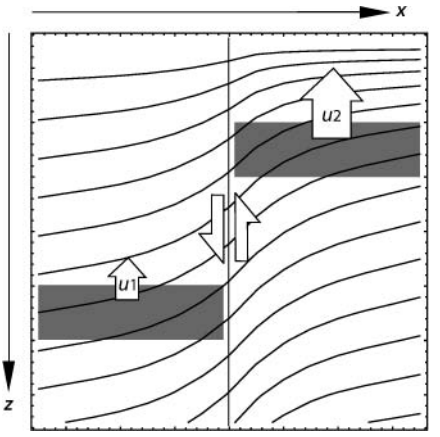


Figure 3.49. Isotherms in a vertical cross section through the crust with a vertical fault. Both sides of the fault exhume with different rates u_1 and u_2. The shown section is 50 km by 50 km. The boundary condition at the top boundary is given by a constant temperature. The boundary conditions on all other sides are given by constant flow of heat. In contrast to Fig. 3.48 all isotherms are preserved, because of the fixed top boundary

1. The heating and cooling of the two respective sides of the fault.
2. The cooling of rocks with proximity to the surface.

Fig. 3.49 illustrates this with a vertical cross section through the crust. This figure differs from Fig. 3.48 in that the upper boundary (the earth's surface) is now defined by a boundary condition of constant temperature. Thus, in contrast to Fig. 3.48, no isotherms intersect the surface. The crustal section shown is divided into two blocks separated by a vertical fault. The two blocks exhume with two different rates, u_1 and u_2.

In order to understand the thermal evolution of rocks near the fault, consider rocks in the slower exhuming block (left block on Fig. 3.49) near the fault. There, the *cooling* influence of the surface is opposed by the *heating* influence of the block on the right hand side. Because of this, it may happen, that rocks that cool during exhumation experience a late stage heating event caused by the other side of the fault. An example of such a thermal evolution was documented by Grasemann and Mancktelow (1993) at the Simplon-line in the central Alps.

3.8 Problems

Problem 3.1. *Converting different units of energy (p. 51)*:
In nuclear reactions, mass is converted to energy. How long can a 60-W-light globe be lit with 1 g of mass assuming that this mass may converted completely into energy? Remember: energy = mass × speed of light^2. The speed of light is $\approx 300\,000$ km s^{-1}. A related problem is found in Problem 5.3.

Problem 3.2. *Converting different units of energy (p. 53)*:
What is the conversion factor between hfu (1 hfu $= 10^{-6}$ cal cm^{-2} s^{-1}) and the SI-units W m^{-2}.

Problem 3.3. *Understanding heat refraction qualitatively (p. 56)*:
A spherical iron ore body of 10 km diameter (with extremely high thermal conductivity) lies in the middle of a 30 km thick crust. Draw a cross section through the crust and sketch schematically some isotherms. Discuss the thermal consequences that such a geometry may have for the surrounding rocks.

Problem 3.4. *Understanding heat refraction quantitatively (p. 56)*:
Calculate the temperature at 10 km depth in the crust using the following assumptions. The crust is made up of schists with a conductivity of $k = 2\ \mathrm{J\,s^{-1}\,m^{-1}\,K^{-1}}$. These schists are intruded by a 2 km thick sill that has a conductivity of $k = 4\ \mathrm{J\,s^{-1}\,m^{-1}\,K^{-1}}$. The upper contact of the sill is in 5 km depth. The thermal gradient at the surface is $20\,^{\circ}\mathrm{C\,km^{-1}}$ and the temperature at the surface is $0\,^{\circ}\mathrm{C}$. The temperature profile is in steady state (there is no exchange of heat between the layers) and there is no heat production in the crust (i.e. the different sections of the geotherm are linear). You can use eq. 3.7.

Problem 3.5. *Using thermal time constant (p. 62)*:
Two continental plates collide and deform a 35 km thick crust. The deformation rate $\dot{\epsilon}$ is a) $10^{-12}\ \mathrm{s^{-1}}$ and b) $10^{-16}\ \mathrm{s^{-1}}$. During and after deformation, the thermal structure of the crust re-equilibrates by diffusion. For the given deformation rates, estimate whether the equilibration of the crust is faster, slower or of similar rate as the deformation? The time scale of the thermal equilibration may be estimated with the thermal time constant (eq. 3.17). What consequences may your results of a) and b) have for structures and parageneses that may be observed in a thin section?

Problem 3.6. *The importance of radiogenic heat production (p. 66)*:
A roughly spherical radioactive ore body of 10 km diameter produces about $S_{\mathrm{rad}} \approx 100$ micro Watts of heat per cubic meter. Estimate how hot the center of the body will get after about $t = 10^5$ years. Use eq. 3.21 but before you do, make an argument why it may be realistic to neglect heat conduction. Use eq. 3.18 and estimates for the necessary parameter values as discussed in the text, for example $\kappa = 10^{-6}\mathrm{m^2 s^{-1}}$, c_p=1 000 J $\mathrm{kg^{-1}K^{-1}}$ and $\rho = 2\,700\mathrm{kg\ m^{-3}}$.

Problem 3.7. *The importance of mechanical heat production (p. 68)*:
a) What is the mechanical heat production rate of a 5 km wide shear zone which deforms at a rate of i) $\dot{\epsilon} = 10^{-13}\ \mathrm{s^{-1}}$ or: ii) $\dot{\epsilon} = 10^{-15}\ \mathrm{s^{-1}}$? Assume that the deviatoric stress that the shear zone material supports is between 30–300 MPa. Give minimum and maximum values using both strain rates and both shear strengths using eq. 3.25. b) How warm could the shear zone possibly get if deformation lasts for 1 my? ($c_p = 1\,000\ \mathrm{J\,kg^{-1}\,K^{-1}}$; $\rho = 2\,700\ \mathrm{kg\,m^{-3}}$). c) Which parameters control if (and how much) the shear zone heats up during this process? (Another problem related to mechanical heat production is Problem 5.3)

Problem 3.8. *Understanding heat of reaction (p. 76)*:
How much mass is converted to energy when burning 5 kg of wood?

Problem 3.9. *The importance of latent heat of fusion (p. 78)*:
A high grade metamorphic rock contains 30 % partial melts. All of this partial melt was formed by a single melting reaction at a fixed temperature. The rock cools conductively from its metamorphic peak (which was much higher than this melting temperature) with a constant cooling rate of $100\,^{\circ}\mathrm{C\,my^{-1}}$. Estimate how long the rock will be buffered to a constant temperature when this melt crystallizes? Give the result in my. The latent heat of fusion is $320\,000\ \mathrm{J\,kg^{-1}}$, the rock has a density of $\rho = 2\,700\ \mathrm{kg\,m^{-3}}$ and a specific heat capacity of $c_p = 1\,000\ \mathrm{J\,kg^{-1}\,K^{-1}}$. Discuss the potential effect of your result on geothermometry that may be planned for this rock.

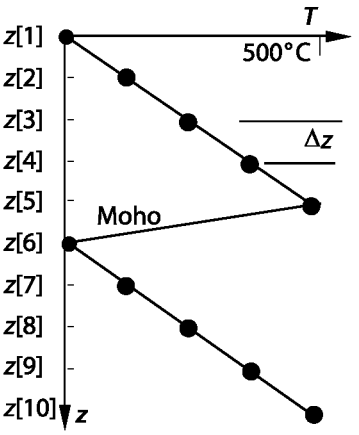
Problem 3.10. *Understanding the Peclet number (p. 86)*:
A regional metamorphic event occurred over the whole of a 30 km thick crust. A mountain belt at the surface eroded at the same time and exhumed the metamorphic rocks during this process. Estimate whether the regional thermal evolution can be described by only considering heat conduction (that caused the regional metamorphic event) or if heat advection (due to erosion) must also be considered. Use erosion rates of a) 100 m $\mathrm{my^{-1}}$; b) 1 000 m $\mathrm{my^{-1}}$; c) 5 000 m $\mathrm{my^{-1}}$ and eq. 3.51.

Problem 3.11. *Contribution of radioactivity to heat flow (p. 92)*:
Use eq. 3.61 to estimate how the surface heat flow changes if the radiogenically caused heat flow doubles and the mantle heat flow is decreased by 50%. Note that *both* will occur when the lithosphere is doubled in thickness.

Problem 3.12. *Cooling of oceanic lithosphere (p. 101)*:
The temperature distribution in oceanic lithosphere may be described with the *half space cooling model* (eq. 3.80). a) Calculate the depth of the 1 000 °C-isotherm for an 80 my old oceanic lithosphere. Assume the temperature of the asthenosphere is $T_1 = 1\,200\,^{\circ}\mathrm{C}$ and the temperature at the surface is $T_s = 0\,^{\circ}\mathrm{C}$. The diffusivity κ is $10^{-6}\ \mathrm{m^2\,s^{-1}}$. Use eq. 3.80 and Fig. 3.6 or the approximation in Table C.9 to solve the error function. b) Draw a temperature profile through 10 my old oceanic lithosphere with the same assumptions.

Problem 3.13. *Qualitative thermal evolution of intrusions (p. 112 – 116)*:
a) Estimate the total duration of cooling of a 50 m wide dike with $\kappa = 10^{-6}\ \mathrm{m^2\,s^{-1}}$. Use eq. 3.18. b) Assume that the dike has intruded with 700 °C into host rocks that are 300 °C hot. What is the maximum contact metamorphic temperature? c) How much additional heat does the dike bring into the rock it intrudes? Use eq. 3.3 and eq. 3.97 and $\rho = 2\,700\ \mathrm{kg\,m^{-3}}$, $c_p = 1\,000\ \mathrm{J\,kg^{-1}\,K^{-1}}$. d) Draw a qualitative temperature profile across the dike at 40 years after intrusion. Help yourself for this with the result from a).

Figure 3.50. Illustration for Problem 3.15



Problem 3.14. *Inferring metamorphic heat sources (p. 123)*:
Estimate if the following metamorphic terrain could have been heated by contact metamorphism. The terrain has reached a peak temperature of 600 °C. About 10% of the area of the terrain are syn-metamorphic mafic intrusions that had an intrusion temperature of 1 100 °C. Another 30% of the area of the terrain are syn-metamorphic granitoids that had an intrusion temperature of 700 °C. The peak metamorphic pressure was 5 kbar, which corresponds to a depth of 18.5 km. Before metamorphism the terrain was at the same depth and had a temperature corresponding to a stable geothermal gradient of 16.2 °C km^{-1}. The density of the rocks is ρ=2 700 kg m^{-3} and the specific heat capacity is c_p= 1 000 J kg^{-1} K^{-1}. Answer the question graphically and algebraically with and without consideration of the latent heat of fusion of the magmas (L = 320 000 J kg^{-1}).

Problem 3.15. *Inverted isograds and numerical solutions of the heat flow equation (sect. 3.1.1, B.2)*:
Calculate the thermal evolution above and below a thrust that has doubled the entire crust of z_c = 40 km. Assume that the thrusting rate was much faster than the rate of thermal equilibration. Thus, we can assume a "saw tooth" geotherm as our initial condition (Fig. 3.50). The initial geotherm is defined as follows: In the region $0 < z < z_c$ it is given by $T = T_{Moho}(z/z_c)$; in the region $z_c < z < 2z_c$ it is given by $T = T_{Moho}((z - z_c - \Delta z)/z_c)$. ($T_{Moho}$ = 500 °C and z_c = 40 km). The distance between discrete points for your calculation is Δz = 10 km. Use eq. B.16 and eq. B.18 in order to approximate eq. 3.6. For the mathematical stability of your solution you have to make sure that the constant $R = (\kappa \Delta t)/(\Delta z^2)$ is smaller than 0.25. This condition gives you the maximum time step Δt that you can use. κ is 10^{-6} m^2 s^{-1}.